Analytical Modeling of Buried Pipeline Response to Permanent Earthquake Displacements

By

T. D. O'Rourke and C. H. Trautmann

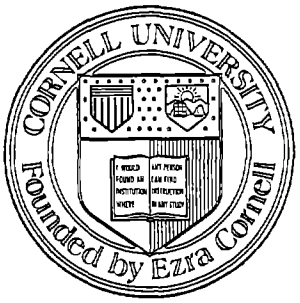

School of Civil and Environmental Engineering
Cornell University
Ithaca, New York

REPORT TO

National Science Foundation
Division of Problem-Focused Research
Earthquake Hazards Mitigation Program
Grant Number PFR-7823096

July 1980

GEOTECHNICAL ENGINEERING REPORT 80-4

ANALYTICAL MODELING OF BURIED PIPELINE RESPONSE TO PERMANENT EARTHQUAKE DISPLACEMENTS

by

T. D. O'Rourke and C. H. Trautmann

Sponsored by The National Science Foundation
Division of Problem-Focused Research
Earthquake Hazards Mitigation Program

Grant Number PFR-7823096

School of Civil and Environmental Engineering
Cornell University
Ithaca, New York

July, 1980

ABSTRACT

This report examines the performance of continuous and jointed, buried pipelines subjected to permanent differential ground movements caused by earthquakes. Records of pipeline damage are summarized for several different earthquakes with special attention to the 1971 San Fernando Earthquake. Observations of damage along the Sylmar segment of the San Fernando fault zone show that pipelines with rubber gasket joints performed substantially better than those with cement-caulked joints and that lines of Mannesman steel were more heavily damaged than lines composed of cast iron or other types of steel.

The behavior of various types of pipeline coupling is studied, and an assessment is made of their vulnerability to differential ground movement. The results of finite element modeling of jointed pipeline response to strike-slip faulting are summarized.

The report shows that the most important parameter affecting pipeline response to strike-slip faulting is the angle of pipeline/fault intersection. Pipeline performance is represented as a plot of the total fault offset to cause failure versus the angle of pipeline/fault intersection. For pipelines with flexible, gasketed couplings, this relationship is derived from two distinct curves: one determined by bending failure of the pipe and the other by axial pull-out at a coupling. In all cases, the optimum orientation of the pipeline relative to the fault occurs at the transition point between failure by bending and coupling pull-out.

The long-term records of maintenance for buried pipelines in areas of fault creep are examined. A hyperbolic function is found to adequately represent the distribution of strike-slip displacement relative to the fault centerline for some areas of fault creep.

Intentionally Blank

ACKNOWLEDGEMENTS

The research described in this report was sponsored by the National Science Foundation under Grant No. PFR-7823096, for which William Hakala was the program manager.

Many people contributed information that was used either directly or indirectly in the report. Our appreciation is extended to these people, who include O. W. Steinhardt, A. E. Johnson, R. A. Morris, and R. L. Dirks of the Pacific Gas and Electric Company; J. D. McNorgan and J. M. Lange of the Southern California Gas Company; R. O. Burford, T. L. Youd, M. G. Bonilla, and S. S. Schultz of the U.S. Geological Survey, and T. Berry of the City of Hollister, California. Special thanks is given to R. S. Bryant of the Los Angeles Department of Water and Power for his contributions of information and insight.

Special recognition is extended to Wil Sawbridge and Tina Foote who drafted the figures and typed the manuscript, respectively.

Intentionally Blank

TABLE OF CONTENTS

TABLE OF CONTENTS
(con't.)

LIST OF TABLES

LIST OF FIGURES

LIST OF FIGURES
(con't.)

LIST OF SYMBOLS

a,b	Constants associated with hyperbolic functions
C_a	Adhesive shear strength between lead and cast iron
d	Fault displacement
d'	Relative horizontal displacement of soil normal to longitudinal axis of buried pipe
d_c	Critical fault displacement to cause pipeline failure
d_{cb}	Critical fault displacement to cause pipeline failure by bending
d_h	Horizontal component of fault movement
d_L	Depth of lead caulking in a bell-and-spigot joint
d_r	Reverse slip component of fault movement
d_s	Strike slip component of fault movement
d_{ult}	Relative horizontal displacement to cause ultimate soil pressure against buried pipe
D	Pipe diameter
E	Young's modulus
E_s	Secant modulus
E_t	Initial tangent modulus
f_N	Normal force
K	Curvature
K_c	Critical curvature to cause pipeline leakage
L	Distance from fault centerline
M_c	Moment causing leakage at a pipe joint
M_p	Moment in pipeline

LIST OF SYMBOLS
(con't.)

N_q	Brinch Hansen bearing capacity factor
P	Axial pipe force
q	Horizontal pressure against buried pipe
q_u	Ultimate horizontal soil pressure against buried pipe
S	Pipe elongation
S_L	Axial joint slip
t	Pipe thickness
y	Distance from neutral axis
z	Depth of pipe invert
Z	Depth to pipe springline
β	Angle of pipeline/fault intersection
ε	Strain
ε_f	Failure strain
γ	Soil unit weight
θ	Joint rotation
σ	Stress
σ_a	Adhesive stress per unit distance of pipe circumference between lead and cast iron
σ_f	Failure stress for cast iron

CHAPTER 1

INTRODUCTION

1.1 Background

During an earthquake, permanent differential movements can be caused by faulting, soil liquefaction, slope instability, seismic compaction, and local lurching and squeezing of the ground. Buried pipelines can be damaged either by permanent movements of this type or by seismic ground waves. The amount of damage associated with each form of displacement depends, in part, on the characteristics of the earthquake. For example, the 1972 Managua earthquake caused surficial displacement along four prominent strike-slip faults through the downtown area of the Nicaraguan capital (11). Nearly all water mains crossing the faults ruptured, causing a major portion of the total damage sustained by the city water distribution system (13). In a similar fashion, surface faults and landslides caused by the 1971 San Fernando earthquake ruptured water, gas, and sewage lines (6, 47, 79) with high concentrations of pipeline damage along the Sylmar segment of the San Fernando fault. By way of contrast, most of the pipeline damage during the 1969 San Rosa earthquake was related to seismic wave propagation (77).

Overall, it is not particularly meaningful to assign average proportions of damage to either permanent movement or seismic shaking. The two forms of displacement often are interrelated so that a clear distinction cannot be made between damage caused by one or the other. Nevertheless, it is important to recognize that permanent differential movements may accompany any earthquake and that the movements can assume a variety of patterns depending on local soil conditions and the presence of faults.

Table 1.1 summarizes the permanent ground movement phenomena and associated pipeline damage reported for ten North American earthquakes. The earthquakes were selected principally on the basis of location within or close to the United States. The table emphasizes the substantial impact of permanent ground movement on lifelines, even for earthquakes where no surficial faulting was observed. For earthquakes with significant surface faulting, pipeline damage has been especially severe as is evidenced by observations reported for the 1906 San Francisco, 1931 Managua, 1952 Kern County, 1971 San Fernando, and 1972 Managua earthquakes.

Perhaps the Managua earthquakes best illustrate the danger associated with differential ground movements. Managua, Nicaragua, was partially destroyed by the 1931 earthquake, primarily by fault movements beneath buildings and by fires that burned out of control because the principal city water main had been ruptured at a fault crossing (28,84). Approximately forty-one years later, Managua was severely damaged by the earthquake of December 23, 1972. Again, a significant part of the damage was caused by surface faulting (11), and the water supply system was totally disrupted, most notably by faults (11,13). Although four strike-slip faults were observed during the 1972 Managua earthquake, no movement was detected along the 1931 fault scarp. In addition, only two of the four surface faults had been recognized prior to the earthquake. The failure to anticipate the specific locations of surface faulting places a severe limitation on mitigation techniques and suggests that, for Managua, lifeline risk should be assessed on the basis of strike-slip displacement as a system-wide parameter.

Especially in the distribution systems, many pipelines are sufficiently flexible to deform as the ground deforms (52,63). In some cases, therefore, analyses can be simplified by assuming a one to one correspondence between pipeline and soil movement. Notable exceptions occur when the pipelines are either structurally

Table 1.1 Summary of permanent ground movement and related pipeline damage for selected earthquakes.

Earthquake	Magnitude/ Intensity	Faults	Landslides	Liquefaction/ Seismic Compaction	Reported Pipeline/Conduit Damage	Remarks	Reference(s)
San Francisco, 1906	Magnitude = 8.3 Intensity = XI	Up to 6.4 m of right lateral strike slip on San Andreas fault; max throw = 0.9 m. Smaller displacements on subparallel faults. Width of fault disturbance generally from 1 to 15 m, up to 125 m Length of fault = 435 km Fault appeared as 1)trench, 2) low ridge, and 3) series of en echelon cracks.	Extensive slope failure, including, 1)rotational slumps, 2) earth flows, 3) rock avalanches. Many additional slides occurred the following year when rainfall infiltrated ground cracks.	Three major zones of liquefaction - induced lateral spreading in San Francisco causing substantial damage to buried utilities.	Wrought iron water pipe (0.76 diameter) fractured at nine fault crossings. Extensive damage to gas and water lines in liquefaction areas of San Francisco. Gas line breaks and lack of water from broken water mains led to fire destruction of much of San Francisco.	Much pipeline damage attributed to lateral spreading and ground cracks; fault damage generally low because of population density. Many previously faulted areas now are highly populated.	18, 25, 49, 97
Managua, Nicaragua 1931	Not reported	One main strike slip fault; lateral displ. not measured; max throw 10.2 cm; max. length mapped 2.5 km; max width of zone of faulting = 150 m.	Landslides primarily along steep natural slopes.	No liquefaction or seismic compaction reported.	Principal cast iron water main pulled apart at fault line. Welded steel pipe (0.3 m diameter) ruptured by landslide. Most house connections in water distribution network were broken.	Extensive destruction attributed to surface faulting. Water main ruptures contributed significantly to fire damage.	24, 84
Imperial Valley 1940	Magnitude = 7.1 Intensity = X	Maximum 2.1 m of right lateral strike-slip displacement mapped for 60 km. Fault developed dip slip component south of U.S. - Mexico border. Maximum throw about 1.2 m.	Area characterized by low topography - no landslides reported.	Numerous sand boils and spouts produced in Colorado River delta area.	Many irrigation pipes ruptured Extensive damage to the All-American Irrigation Canal.	Area was largely agricultural with relatively low population density.	67, 89
Kern County 1952	Magnitude = 7.2 Intensity = VII-XI	Reverse oblique surface faulting; length of fault = 64 km; width of fault zone = 1/2 to 1 km; max. throw = 1.2 m; max. left lateral slip = 0.8 m. Fault displacement occurred as pressure ridges, en echelon fractures, and tension cracks.	Extensive landslides in in the form of rock falls, avalanches, shallow soil flow, and movements up to several feet along old deep, massive slides.	Mud volcanoes and extensive cracking in water saturated terraces along creek beds.	Pipeline ruptures with compression and extension at fault crossings. Oil pipeline ruptured along western extension of surface faulting. Gas transmission line (0.8 m diameter) severely deformed at fault crossing: tension, bending and torsional distortions observed.	No surficial faulting in deep alluvium of San Joaquin Valley although substantial movement along fault trace on either side.	12, 22 67, 78
San Francisco 1957	Magnitude = 5.3 Intensity = VI	No observed surface displacements on faults.	Shallow landslides along sea cliffs; 100 m-wide slide in artificial fill induced by liquefaction.	Landslide caused by liquefaction; seismic compaction indicated by differential settlement at San Francisco Airport and settlement near water tanks.	Pipeline breaks at San Francisco Airport from differential settlement. Pipeline separations caused by fill settling around water tanks.	Many pipeline breaks at rigid or semi-rigid connections with structures.	7, 17 76, 87

Table 1.1 (con't.)

Hebgen Lake Montana 1959	Magnitude = 7.1 Intensity = X	Several steeply inclined normal faults; max. throw = 1.5 to 6 m. Surface ruptures include scarps, scarplets, moletracks, and monoclinal warping.	Widespread landslides, rock falls, and slumping of sediments.	Liquefaction phenomena include sand spouts and sinkholes.	Maximum damage confined to areas adjacent to two major faults where water supply lines were ruptured, pipes broken and a culvert collapsed.	Area 69 km long and 23 km wide subsided as much as 0.6 m. Widespread formation of grabens next to faults.	29,32 56,92 93
Alaska 1964	Magnitude = 8.5 Intensity = XI-XII	Two faults on Montaque Island in Prince William Sound; max. throw = 7 m; length = 300 km.	Extensive slope failures: 1. Rock avalanches in glaciated areas. 2. Near horizontal spreading of saturated soils. 3. Subaqueous sliding on lake shores and sea costs. 4. Large translatory slides in sensitive clay.	Extensive liquefaction of saturated, granular soils, causing ground cracking and sliding.	Over 200 breaks in gas and 100 breaks in water distribution systems at Anchorage. Gas lines within fault zones ruptured at ground cracks. Three major petroleum transmission lines were undamaged except for one circumferential crack.	Most pipeline damage due to landslides and ground cracking.	26,27 34,50 53
Borrego Mountain 1968	Magnitude = 6.4 Intensity = VII-IX	Three main strike slip surface faults; max right lateral displ. = 38 cm; max. throw = 23 cm in isolated locations.	Widely distributed slides in dry surficial deposits; widespread slumping of soil mostly within 3 to 5 km of main surface faults.	Sand boils as evidence of liquefaction; widespread seismic compaction.	Pipe ruptured at fault crossing; cracked concrete canal lining from slumping along canal embankments.	Earthquake caused 1-2.5 cm displacment on the Imperial, Superstitition Hills and San Andreas faults at distances of 70, 45 and 50 km, respectively, from epicenter.	1, 2, 16
San Fernando 1971	Magnitude = 6.4 Intensity = XI	Reverse oblique fault dipping 70° north. Most movement distributed across zone 50 to 100 m wide. Max. combined disp. = 1.9 m; Max. throw = 1.39 m. Length of faulting = 1.5 km. Movement on many small faults continued for days after the main shock.	Many landslides including slumps and rockslides in nearby foothills of San Gabriel Mtns. and extensive slumping around upper and lower Van Norman Reservoirs. Sliding was predominatly in bedrock, alluvial soils, and fills. Deep slumping generally absent.	Estimated $30 million damage to various utilities. Liquefaction-induced lateral spreading near Juvenile Hall. Sand boils observed at several locations.	Extensive pipeline damage, especially in areas of active faulting. 113 gas line breaks, 52 breaks in one 41 cm diameter gas transmission line, 9 breaks in one 66 cm diameter gas transmission line. Overall, 17,000 customers lost gas service because of the earthquake. 38 km of sewer pipe required replacement. Damage concentrated at pipe joints; flexible joints (rubber gasket) behaved significantly better than rigid joints (cement caulked) in water distribution system.	Earthquake caused extensive pipeline damage by faulting, landsliding, and liquefaction. 25 to 50% of pipeline damage occurred within the fault zones, which represented only 0.5% of the area affected by strong ground shaking.	6,36 44,47 54,57 61,69 70,73 74,79 83,85 95,96 98
Managua, Nicaragua 1972	Magnitude = 5.6	Four main, strike slip surface faults; max. left lateral displ. = 38.1 cm; max. throw = 10.2 cm; max length mapped = 5.9 km; max width of zone of faulting = 2.5 km.	Landslides primarily along steep natural slopes and steep granular embankments.	No obvious movement related to liquefaction. No reported seismic compaction.	Extensive damage to water distribution system with many pipelines ruptured at fault crossings. Substantial damage to asbestos-cement pipe and cast iron pipelines with lead joints. Severe strain on electric transmission line caused by landslide.	Extensive destruction attributed to surface faulting. Lack of liquefaction effects, in part, due to low water table and short duration of shaking.	11, 13 19,51

restrained, such as at connections with other pipe or buildings, or subjected to locally severe changes in movement that might occur at a fault or along the boundaries of a landslip. A key to understanding pipeline performance, therefore, is the characterization of typical ground movement patterns and the identification of areas where abrupt changes in displacement occur.

The limit to which a pipeline can sustain differential movement generally depends on the stress/strain behavior of the pipe material, the rotation and pull-out capacity of the couplings, and characteristics of the line such as susceptibility to corrosion, state of repair, and method of installation. Limits of this sort are likely to be valid for pipelines deformed by vibrations as well as for those deformed by permanent movement. Consequently, studies of pipeline performance under permanent, differential movement can provide useful information for studies of dynamic performance.

Several investigations have been devoted to the behavior of continuous, ductile pipelines subject to strike-slip faulting (45,46,59). These studies have shown the close relationship between pipeline performance and key variables such as the angle of pipeline/fault intersection and the frictional resistance along the longitudinal axis of the pipe. Studies of this nature are lacking for pipelines typical of water and gas distribution systems where many different types of line construction result in a wide range of behavior.

The capacity to withstand differential ground movement is closely related to the type and location of couplings. A variety of couplings have been used in practice with the result that current pipeline systems contain lines that differ substantially in their ability to accommodate ground movements. Strategies for replacement and repair as well as protective designs should be based on understanding how different types of couplings affect buried pipeline behavior.

Numerical techniques are well suited for modeling the complex conditions of soil/structure interaction that affect buried, articulated pipelines. In particular, the finite element method can simulate stress/strain properties of the pipe material, pull-out and rotation constraints at the couplings, and the passive pressure and frictional effects of the soil as an aggregate system. This type of analysis can point out the dominant failure modes for various line configurations and provide a quantitative scale of vulnerability among the combinations of pipe material and coupling type commonly used in water and gas distribution systems.

1.2 Objectives

There are two principal objectives of the report:

1. To summarize field observations of various pipelines that have been subjected to permanent differential movements from earthquakes.

2. To summarize the results of finite element modeling for buried pipelines deformed by strike-slip faulting. In particular, the summary emphasizes the role of couplings in the response of pipelines to differential ground movement. The effects of various parameters are examined; they include the type of coupling, coupling location, angle of intersection between the pipeline and fault, relative stiffness between the pipe and surrounding soil, and distribution of the fault displacement.

Because earthquakes can be regarded as large-scale tests, the study concentrates on field observations of pipeline performance. These observations are used to point out pipeline elements that are most susceptible to damage and as a background for assessing the results of the numerical modeling.

1.3 Scope

The report is composed of five chapters, of which the first presents background information and introductory comments. The second chapter discusses the observations of ground movement and pipeline repair for the 1971 San Fernando earthquake, concentrating on pipeline response to surface rupture along the Sylmar segment of the San Fernando fault. The third chapter deals with the properties of cast iron and the special characteristics of various types of coupling. The fourth chapter summarizes the results of the finite element simulation of buried pipeline response to strike-slip faulting. Conclusions and recommendations are presented in the fifth chapter.

CHAPTER 2

PIPELINE RESPONSE TO GROUND FAILURE DURING THE 1971 SAN FERNANDO EARTHQUAKE

2.1 Background

A survey of damage caused by the 1971 San Fernando earthquake shows that, in comparison to surface structures, pipeline systems are particularly vulnerable to local differential movement. The area of surface fault displacement caused by the earthquake was approximately one-half of one percent of the area affected by strong ground shaking (39). Consequently, fault displacement contributed only a small portion of the total damage sustained by surface structures. In contrast, approximately 25 to 50 percent of all pipeline breaks in the area of strong ground shaking occurred at or near fault crossings (60). After examining the earthquake effects in detail, Youd (96) concludes that strong ductile pipelines withstood ground shaking, but were unable to withstand the large permanent ground deformations generated by faulting and ground failures. In addition, the earthquake triggered over 1000 landslides (79). Block movements of soil along the northwest rim of the Upper Van Norman Reservoir and an extensive, tongue-like spreading of soil along the reservoir's eastern shore (96) caused severe damage to water and gas transmission lines (54, 74, 83).

Because the most detailed records from the earthquake are associated with areas of surface faulting, this chapter emphasizes pipeline damage caused by fault movement. Nevertheless, it should be recognized that faults and landslides commonly show similar patterns of movement. Particularly along their margins with more stable ground, landslides frequently concentrate displacements into zones that resemble normal and strike-slip faulting.

2.2 Ground Movement Patterns

The surface faulting associated with the 1971 San Fernando earthquake occurred mainly on a left lateral thrust fault, which has been designated by the U.S. Geological Survey (USGS) as the San Fernando fault zone (91). Of the four individual segments of the fault (95), the Sylmar segment intercepted the largest portion of the water and gas distribution system.

Figures 2.1 and 2.2 each show a plan view of the Sylmar segment of the San Fernando fault zone. Although the Sylmar segment was roughly 1.8 mi. (2.9 km) long in the east-west direction, the figures show only about one mi. (1.6 km) of the segment that was located in the City of Los Angeles along its eastern end. This zone extends from the boundary between the cities of San Fernando and Los Angeles, slightly west of Cometa Ave., to an area slightly east of Chippewa St. Attention is focused on this portion to take advantage of the observations and repair records of the Los Angeles Department of Water and Power, which are available only for this section of the fault segment.

The ground displacements on the Sylmar segment occurred within a zone ranging from 150 to 350 ft (46 to 107 m) in width (91). The broad boundaries of this zone are shown by the dashed lines in each figure. Most of the lateral movement and roughly half of the vertical displacements occurred within a zone 150 ft (46 m) wide along the southern edge of the fault (44,91,95). This zone is shown by the ruled area in each figure.

The ground north of the Sylmar segment was thrust upward and left laterally (to the west) along ruptures dipping 70° to the north (91). The general sense of this displacement is indicated in Figure 2.3, which is an oblique view of the block movement. The maximum strike and reverse-slip components of fault movement were 6.2 and 4.9 ft (1.9 and 1.5 m) respectively (91). As

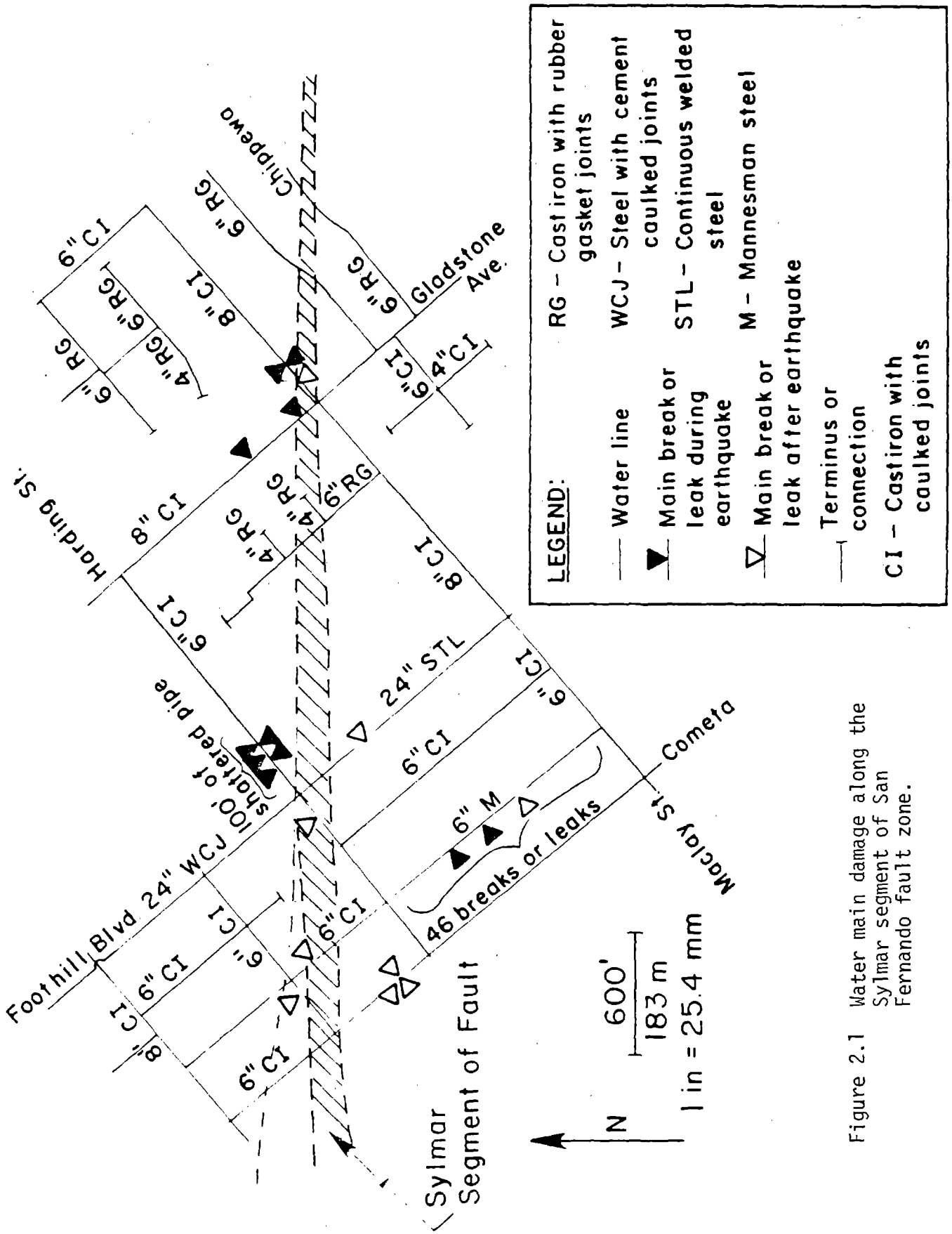

Figure 2.1 Water main damage along the Sylmar segment of San Fernando fault zone.

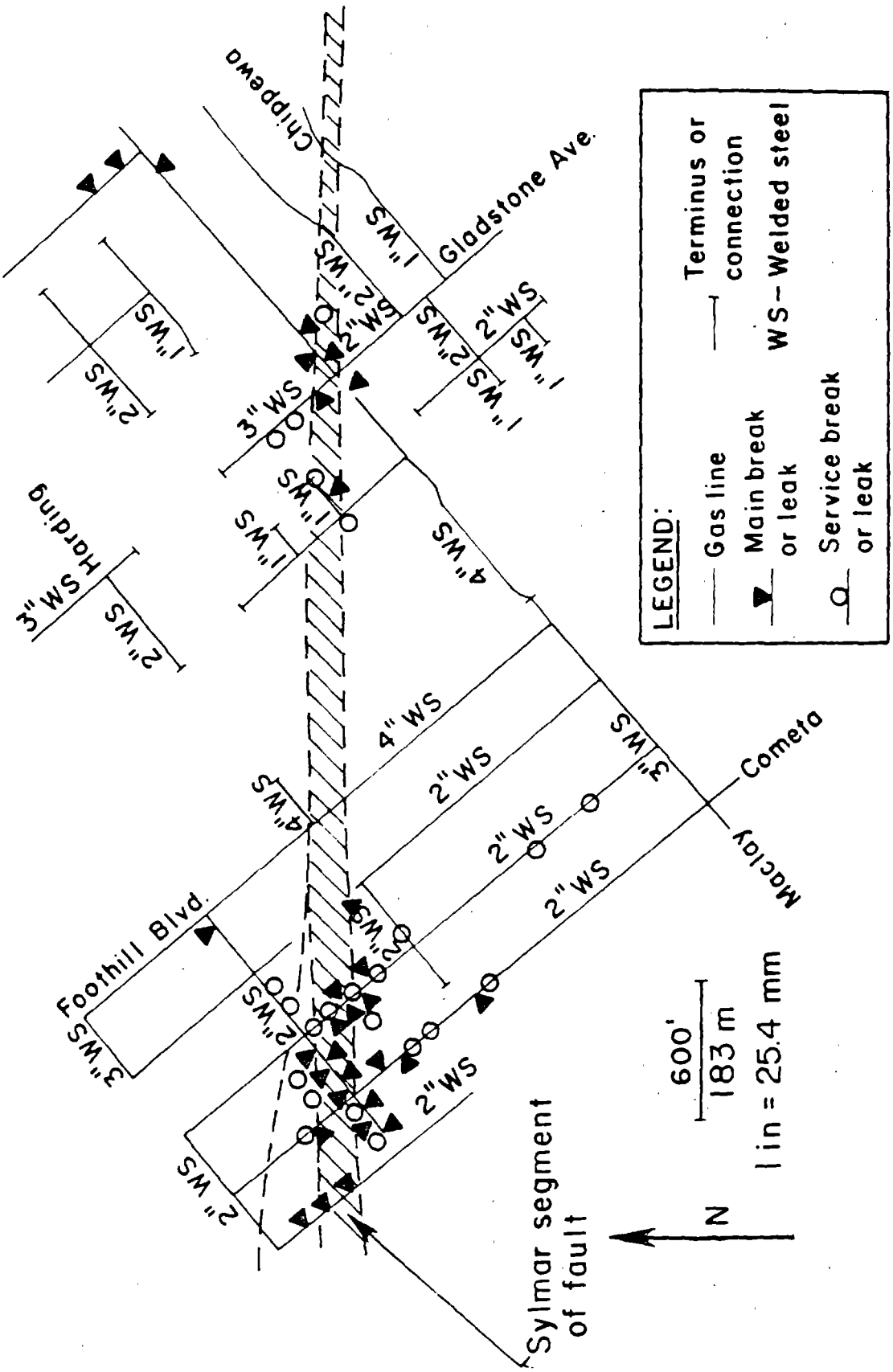

Figure 2.2 Gas main damage along the Sylmar segment of San Fernando fault zone.

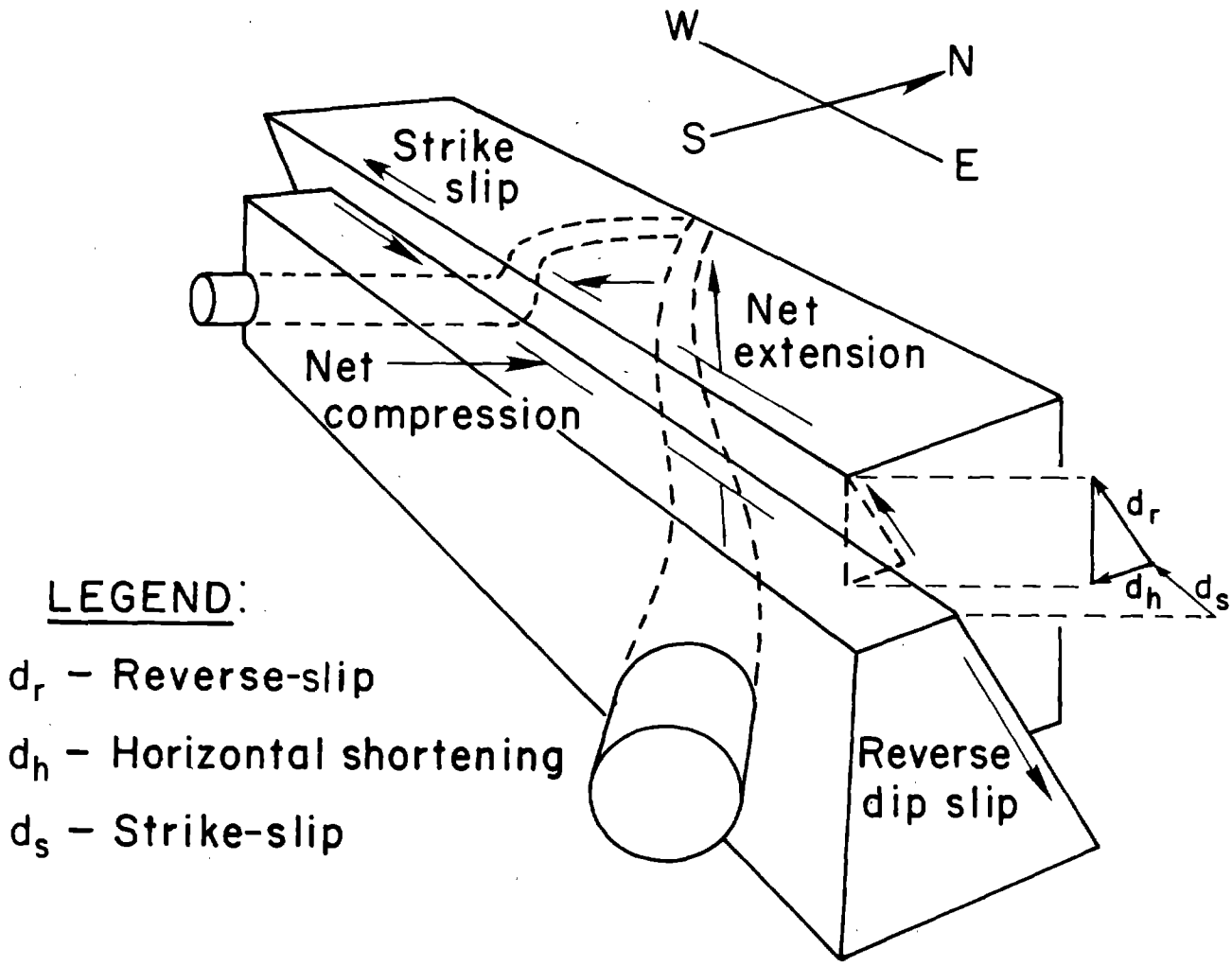

Figure 2.3 Block diagram of San Fernando fault motion.

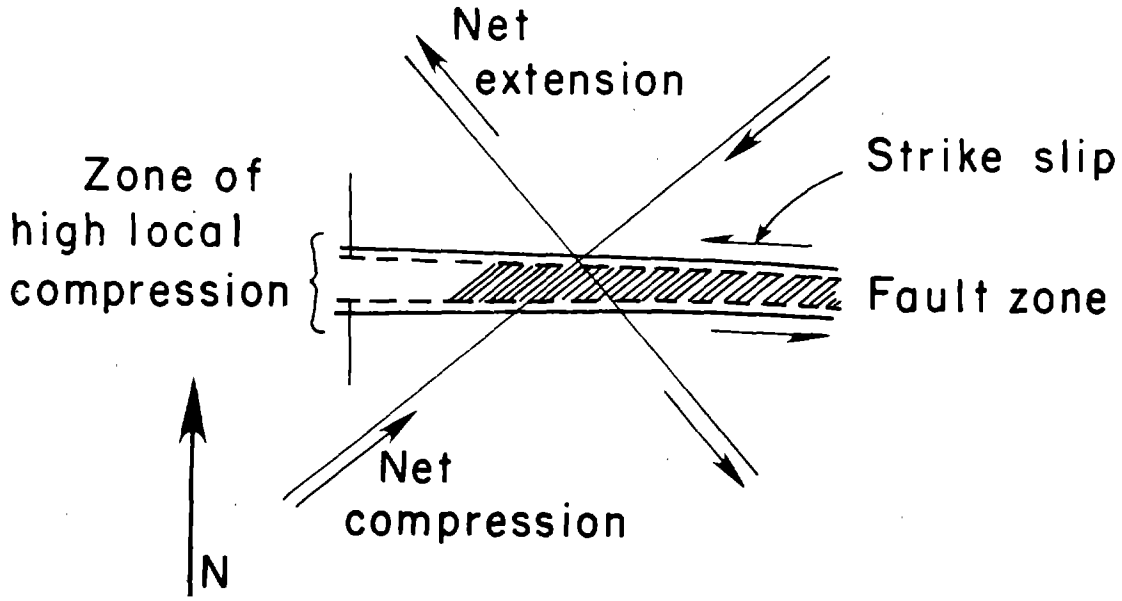

Figure 2.4 Relative ground displacements associated with San Fernando faulting.

illustrated in the figure, the strike-slip component of movement promoted a net compression of the northeast-trending lines and a net extension of the northwest-trending lines. Overall, the pattern of pipeline damage was consistent with the general patterns of tensile and compressive ground strains shown by Slemmons (71), Friedman et al. (30), and Stearns (82) to be characteristic of reverse-slip faulting.

The distribution of movement within the fault zone was complex. Frequently, large displacements were concentrated along individual scarps. At Cometa Ave. near the western end of the zone, a 30 ft (9 m) wide shear zone showed a total of 1.5 ft (0.5 m) vertical offset and 6 ft (1.8 m) left lateral offset (91). The maximum displacements across individual breaks in the fault zone were often substantially less than these. Toward the east, the displacement across the zone diminished. Horizontal shortening across the zone was consistently between 1.8 and 2.5 ft (0.6 and 0.8 m) (91).

The nature of the ground movements within the actual fault zone differed dramatically from those outside the zone, as shown in Figure 2.4. Within the zone, both northwest and northeast-trending lines were compressed, as indicated by the buckling of pipelines at all orientations and by the offsets of pavement slabs (44,74,83,91). Some northwest-trending lines that failed by compression within this zone also failed by tension immediately north of the zone (91).

The mechanics of the ground deformation within the zone are as yet unknown, but it is significant for the analysis of pipeline behavior to recognize that high angle thrust faults can generate permanent compressive ground movements in all directions, even though the faulting may show a significant component of strike-slip movement.

2.3 Pipeline Damage

Most pipelines in the San Fernando area were buried primarily in alluvial sands and gravels at depths between 2.5 and 5.0 ft (0.8 and 1.5 m). The operating pressures for the gas and water distribution lines were approximately 60 and 150 psi (0.4 and 1.0 MPa), respectively.

Superimposed on Figures 2.1 and 2.2 are maps of the water and gas distribution systems within 1000 ft (305 m) of either side of the fault. Also marked are pipeline leaks or breaks that were repaired shortly after the earthquake. Owing to the continuing high frequency of water main damage, Figure 2.1 includes repairs over a four year period following the earthquake.

All the cast iron water mains with cement-caulked joints that crossed the fault in the area under consideration were damaged. Most of the mains were composed of 18 ft (5.5 m) lengths of gray, cast iron pipe joined at cement-caulked, bell-and-spigot couplings. Both northwest and northeast trending lines ruptured, but damage was most prominent along northeast trending lines where compressive ground deformations were largest. The most striking damage occurred along the northeast-trending Harding St. where 100 ft (30 m) of cast iron line were shattered.

In contrast to the lines with cement-caulked couplings, cast iron mains with rubber gasket joints showed no damage in the area under consideration. These pipelines were composed of 18 ft (5.5 m) lengths of gray, cast iron pipe joined by rubber gasket, or push-on, couplings. Most of these pipelines crossed the fault in the vicinity of Maclay Ave. and Chippewa St. In the same area, four repairs were required at cement-caulked couplings.

Although locally severe concentrations of ground movement were observed between Cometa Ave. and Foothill Blvd., there are no records of water main repair

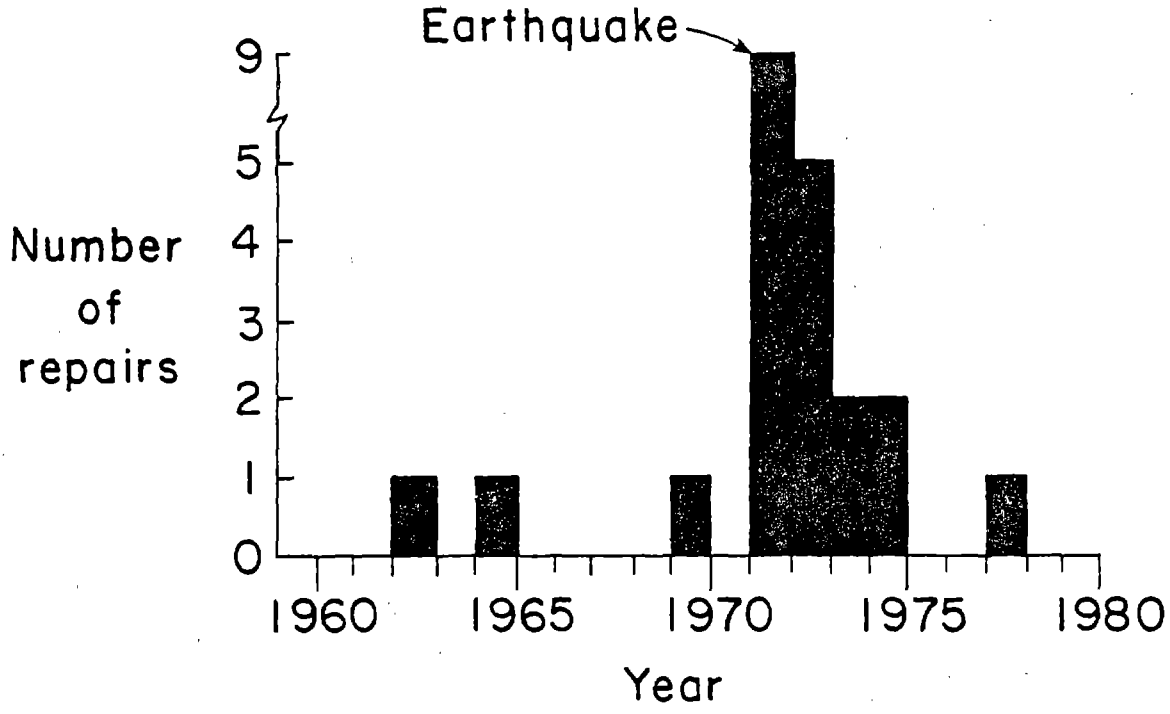

a) repairs to lines within 1000 ft of the fault

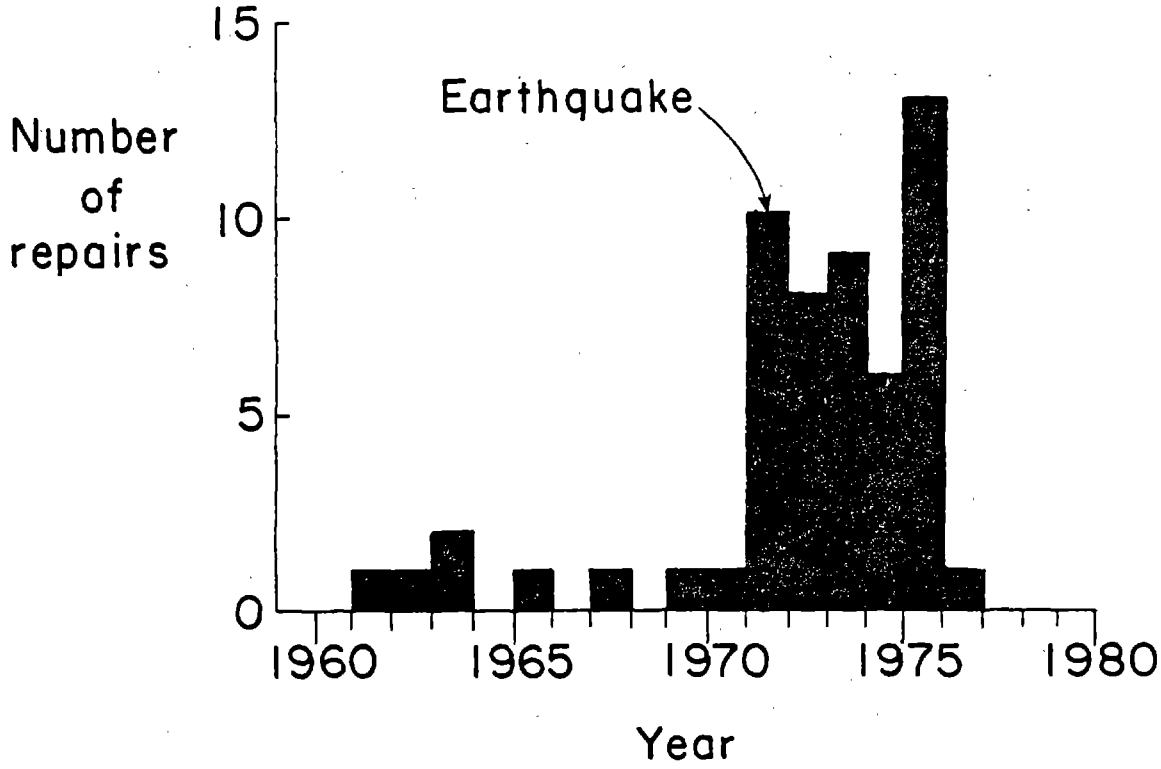

b) repairs to Mannesman line

Figure 2.5 Frequency of repair to water mains.

in this vicinity immediately after the earthquake except for the shattered line on Harding St. It is difficult to explain the absence of damage in the water mains immediately adjacent to the extensive gas main ruptures at this location.

The cement-caulked, cast iron mains required continuous repair in this area for several years after the earthquake. The long-term damage occurred principally as broken connections between service lines and mains. The long term effects of the earthquake are illustrated in Figure 2.5a which shows the annual repairs to water mains with 1000 ft (305 m) of the fault segment for a 20 year period. Although time-dependent movements on the Sylmar fault segment were measured after the earthquake (58,85), these contributed less than one percent of the total vertical component of slip measured shortly after the earthquake. The long term damage most likely is the result of residual strains incurred during the earthquake and of gradual movements in the pipes and ground as the site was reconstructed.

One line, composed of Mannesman steel, is not included among the pipelines from which the figure is derived because repair records indicate an anomalously high level of damage that would be misleading if included as part of the general record of repairs. Figure 2.5b shows the annual repairs for this section of Mannesman steel pipe, which was located south of the fault near the western end of the Sylmar segment. The Mannesman line was repaired at least 45 times following the earthquake until the line was replaced in 1975.

The seismic vulnerability of the line can be gauged from its repair history before the earthquake. The yearly frequency of repair on a unit length basis for the Mannesman line was approximately 20 times higher than that of the other lines shown in Figure 2.1. This behavior corroborates previous experience. Damage to corrosion-prone pipe has been reported for U.S. earthquakes as early as the 1952 Kern County earthquake. More recently, Isenberg (40,41) has reported

relatively high levels of damage for corroded pipe in response to seismic shaking in the southern portion of the San Fernando Valley.

Table 2.1 summarizes reported instances of seismic damage to corrosion-prone mains for five U.S. earthquakes. In each instance, a significant portion of the system damage was attributed to lines affected by corrosion. Elements especially vulnerable to corrosion-related damage are threaded connections in galvanized steel and lines composed of Mannesman or Matheson steel pipe. Most lines with Mannesman and Matheson pipe were installed during the 1920's or early 1930's. Experience has shown them to be subject to internal corrosion, which frequently is exhibited at the pipe surface in the form of corrosion pits or rust spots.

As shown in Figure 2.2, the gas distribution system in the area under consideration was composed of welded steel pipelines. Individual pipe lengths were approximately 40 ft (12 m). Service laterals, typically 3/4 to 1 in (19 to 25 mm) in diameter, were connected to the distribution mains through welded service tees.

Damage occurred at similar levels of intensity on both northwest and northeast-trending lines. Ruptures occurred mostly by buckling and twisting of the mains, although in many locations, service tees were sheared at their connections with the mains. Damage was most extensive in the western portion of the fault segment where differential ground movements were largest.

On acetylene-welded lines, ruptures often coincided with the welds. Trends of this sort could not be distinguished for electric-arc-welded lines.

2.4 Summary

In summary, the information on pipeline damage along the Sylmar segment of the San Fernando fault zone shows four significant features:

Table 2.1 Summary of earthquake damage to corrosion-prone pipe.

Earthquake	Type of Pipe Affected	Damage Description	References
1952 Kern County	Steel and cast iron pipe	Leaks at rust holes in steel pipe, cracks in moderately graphitized cast iron pipe.	(37)
1957 San Francisco	Not specified	Four leaks for San Francisco water distribution system in corrosion-weakened pipe.	(76)
1965 Puget Sound	Galvanized steel service laterals and steel mains.	Failure of service laterals at exposed, threaded portions of pipe; leaks at rust spots in steel mains.	(40)
1969 Santa Rosa	Steel pipe	Leaks at rust holes in steel pipe.	(77)
1971 San Fernando	Welded steel pipe Mannesman pipe Matheson pipe	Leaks at rust holes and corroded areas of pipe.	(40,41)

1. Pipelines with rubber gasket joints performed substantially better than those with cement-caulked joints. In the area under study there were no leaks on rubber gasket mains during or immediately after the earthquake, whereas there were several repairs at cement-caulked couplings on lines in the immediate vicinity of those with rubber gasket couplings.

2. Adjacent to the fault zone, northeast trending lines were compressed and northwest trending lines were extended. The alternating modes of tension and compression were primarily a function of pipeline orientation relative to the left lateral slip along the fault. Nevertheless, within the zone of largest ground movement, all lines were placed under compression regardless of orientation.

3. Lines made of Mannesman steel were highly susceptible to internal corrosion and were more heavily damaged than lines composed of cast iron or other types of steel.

4. Damage to water mains continued for several years after the earthquake, mainly in the form of ruptured connections between mains and service lines.

CHAPTER 3

STRENGTH AND PERFORMANCE CHARACTERISTICS OF PIPELINE COMPONENTS

3.1 Selection of Components

The two principal components of all pipelines are the individual pipe sections and the couplings that connect them. The behavior of the pipe sections will depend on the stress/strain properties of the pipe material, cross-sectional geometry of the pipe, and section length. The behavior of the couplings will depend on their slip and rotation characteristics.

Pipes can be composed of either brittle or ductile material. Brittle materials include gray cast iron, concrete, and clay; ductile materials include steel, ductile iron, and some types of plastic. Although the performance of the pipeline will be closely related to the pipe material, the capacity to sustain differential ground movements will also be dependent on the type and location of the couplings.

This study concentrates on gray cast iron pipe with special emphasis on the changes in pipeline performance associated with various types of coupling. Gray cast iron was selected for several reasons. Because it is a brittle material, its stress/strain relationship can be modeled in a relatively simple manner. It is significantly more vulnerable to rupture than steel or ductile iron and, therefore, well suited for studying the changes in pipeline performance associated with various types of couplings. Finally, it represents a widely used material for which there is little information regarding soil/structure interaction.

This chapter develops a general stress/strain relationship for gray cast iron on the basis of published tensile test data. In addition, the chapter summarizes strength and performance characteristics of lead-caulked, mechanical,

and Dresser long couplings. The stress/strain relationship and coupling characteristics are used for modeling the behavior of pipeline components in the finite element simulations described in Chapter 4.

3.2 Gray Cast Iron

In tension, gray cast iron exhibits a non-linear stress-strain curve. Figure 3.1 shows a typical stress-strain curve from test data summarized by Johnson (43). As stress is first applied, strain is linearly proportional to stress to approximately one third of the failure stress (72). For this portion of the curve, the modulus is, therefore, constant and equal to the initial tangent modulus. Once the stress level exceeds one third the failure stress, the curve flattens monotonically to failure. This phenomenon has been attributed to the "notch effect", whereby plastic strains accummulate under the influence of void-like flakes in the cast iron (72).

If the load is reduced from any point along the curve, the initial curve is not retraced; instead, the strain decreases proportionally to the decrease in stress with a modulus equal to the initial tangent modulus (62, 3). After several load/unload cycles to the same maximum stress level, cast iron retraces the same stress-strain curve at a slope parallel to the initial tangent modulus (62). The failure strain, therefore, depends greatly on the stress history.

The behavior of gray cast iron will vary depending on whether the pipe was manufactured by sand mold or centrifugal casting. The fabric of centrifugally-cast pipe has smaller concentrations of graphite than that of sand cast pipe and its tensile strength may be as much as 50 percent higher (55). Centrifugal casting was adopted on a large scale by the pipe industry after 1930. Correspondingly, this date often can be used to estimate the pipe material if the year of installation for the line is known.

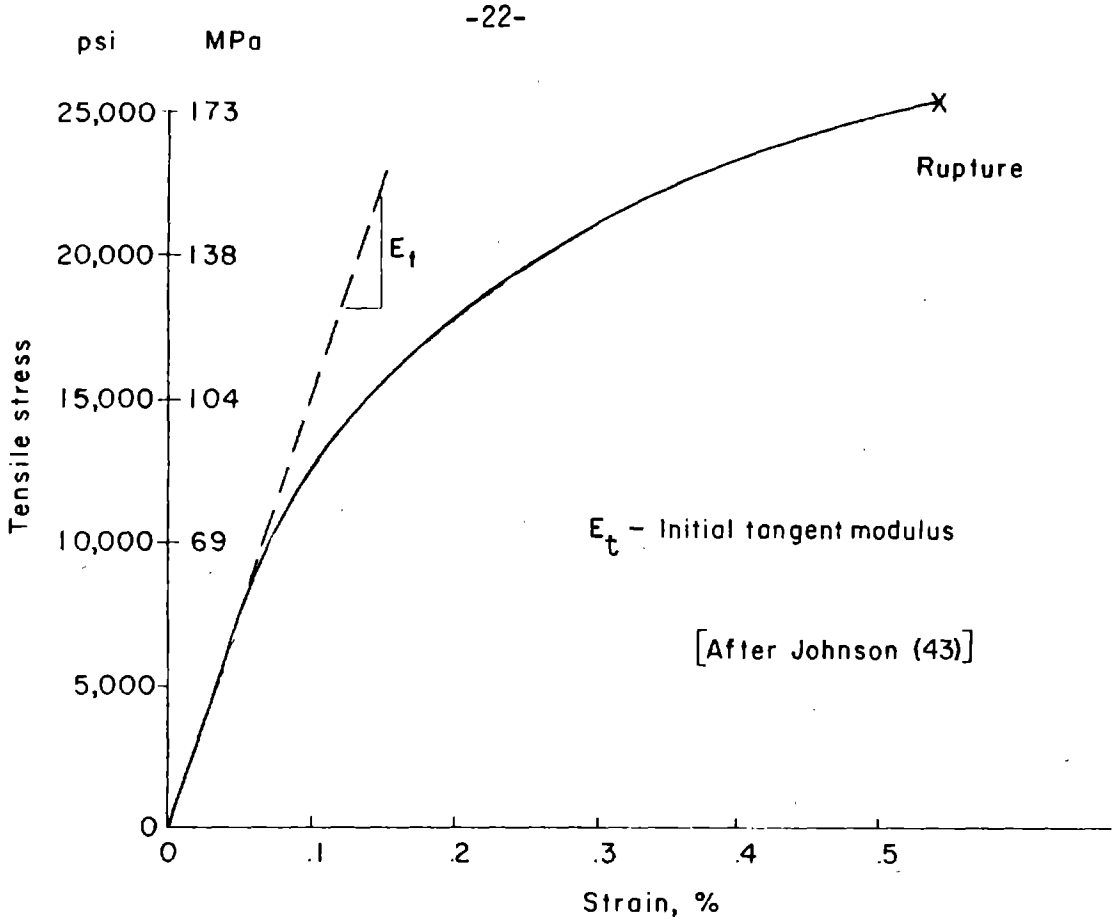

Figure 3.1 Stress-strain curve for cast iron.

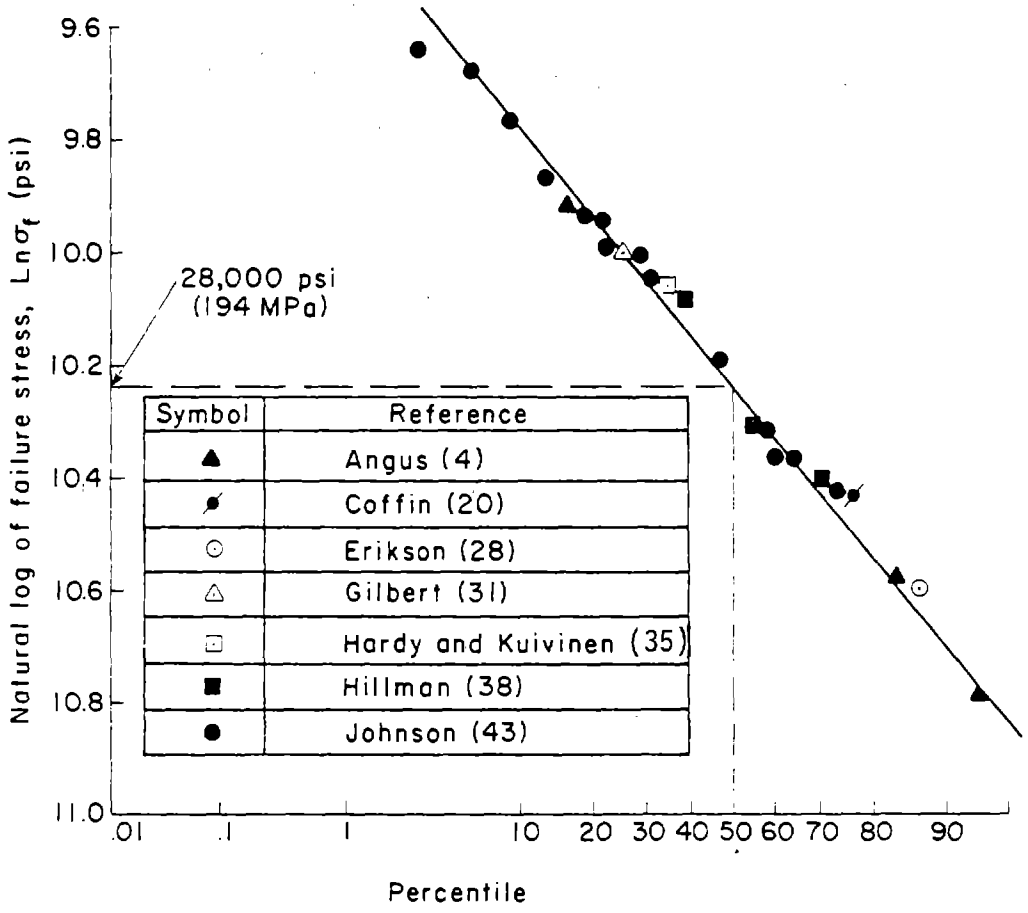

Figure 3.2 Cumulative frequency diagram of tensile strength data for cast iron.

Many factors influence the strength of cast iron in uniaxial tension primarily by affecting the form and quantity of carbon in the iron matrix. One of the most significant factors is the cooling rate which may cause substantial variation in properties even for metal of the same composition, cast from the same ladle (9). A general discussion of the factors affecting cast iron strength can be found in several references, including those by the British Cast Iron Research Association (9) and the American Society for Metals (3).

In order to develop a representative stress/strain curve, test data were gathered from several different sources. Figure 3.2 shows the failure stress, σ_f, for 24 tests plotted on probability paper. A log normal distribution gave a good fit to the data. In a similar fashion, data for both the failure strain, ε_f, and initial tangent modulus, E_t, were analysed. The data for these two parameters were normally distributed.

The mean value of the failure stress, failure strain, and initial tangent modulus are summarized in Figure 3.3. They were used to construct the stress-strain curve shown in the figure. The secant modulus to 80 percent of failure stress is 6.4×10^6 psi (44 GPa).

The curve is strictly valid for virgin extension and therefore is independent of stress history. Straightforward use of the curve assumes that the pipe has experienced relatively low stresses during placement and service and that the pipe is in a corrosion-free environment.

3.3 Lead-Caulked Couplings

A lead-caulked joint is a semi-flexible connection. Under some circumstances, it can accommodate deformation by small rotations and axial slip.

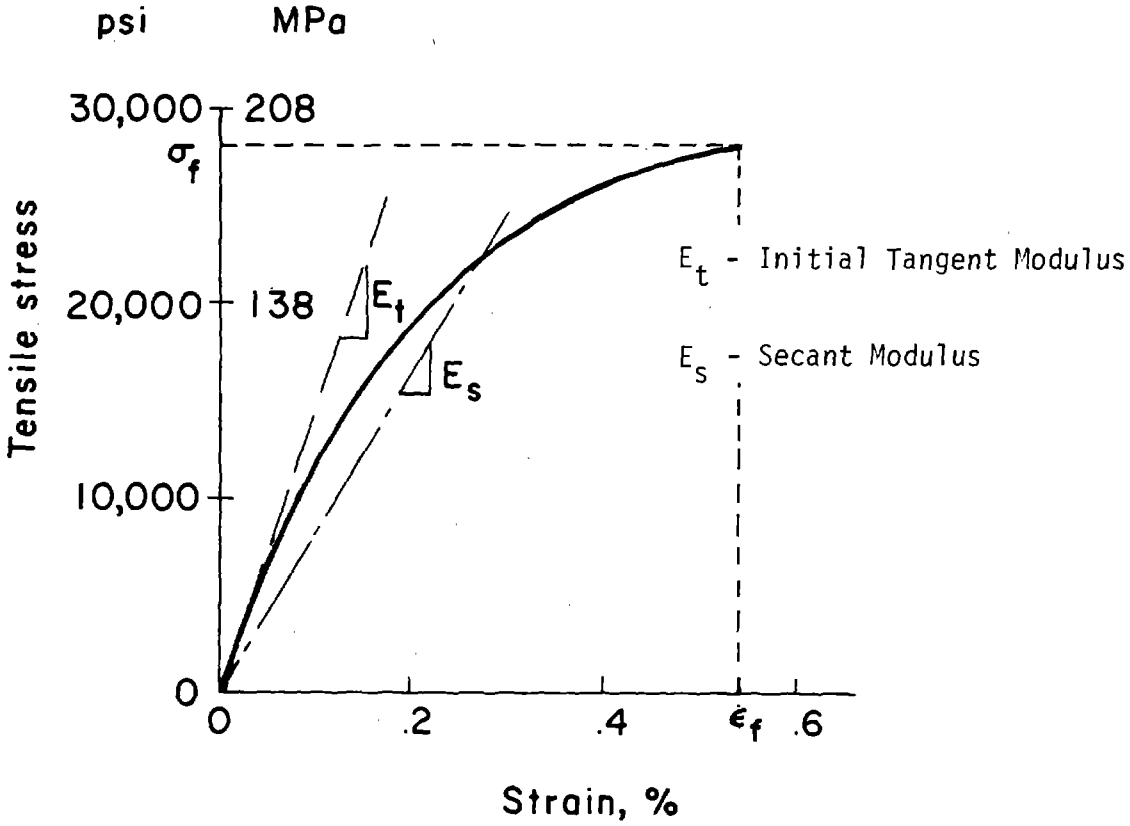

Strength parameter	Mean value	Coefficient of variation
σ_f	28000 psi (194 MPa)	1.35[1]
ϵ_f	0.52%	0.38
E_t	14.5×10^6 psi (10 GPa)	0.36
E_s	6.4×10^6 psi (44 GPa)	----

[1]Failure strength was log-normally distributed. This number is the geometric standard deviation (The bounds obtained by multiplying and dividing the mean by the geometric standard deviation include about two-thirds of the data.)

Figure 3.3 Mean stress-strain curve for cast iron constructed from average values of initial tangent modulus, failure stress, and failure strain.

However, the amount of rotation and slip that can be sustained tend to be highly varied and generally well below the limits of flexible, gasketed couplings.

The construction of lead-caulked joints consists of three principal operations: 1) packing oakum, which is a hemp yarn, into the joint; 2) pouring molten lead into the joint; and 3) ramming and tamping the lead in the joint with a caulking tool.

The behavior of lead joints is complicated by their tendency for self-healing after initial leakage. This phenomenon is well documented (21,52) and is related, in part, to the oakum. In water mains, the wet oakum tends to expand within the annular space between the spigot and bell during deformation, thus helping to close off leakage paths. This type of behavior is not as likely in natural gas mains where the gas typically dries and shrinks the oakum.

Figure 3.4 shows cross-sectional views of a lead-caulked joint subjected to both axial pull-out and pure bending. In both cases, the adhesive strength at the pipe/lead interface, C_a, is critically important because it is the major source of resistance against slip and rotation at the coupling.

To determine the magnitude of adhesion typical for lead-caulked joints, data associated with 24 pull-out tests were analysed. The adhesive strength for each test was calculated by dividing the pull-out force associated with the onset of slip by the circumferential area of the spigot in contact with the lead. For the tests analyzed, the depth of caulked lead, d_L, was typically 2.25 in. (57 mm). Table 3.1 summarizes the pertinent test data and adhesive strength for each test. The adhesive strength is plotted as a function of the nominal pipe diameter in Figure 3.5. The adhesion appears to be independent of diameter.

Figure 3.6 is a histogram showing the distributed frequency of the adhesive strength. The data show a mean value of 252 psi (1.75 MPa) and a standard deviation of 80 psi (0.55 MPa).

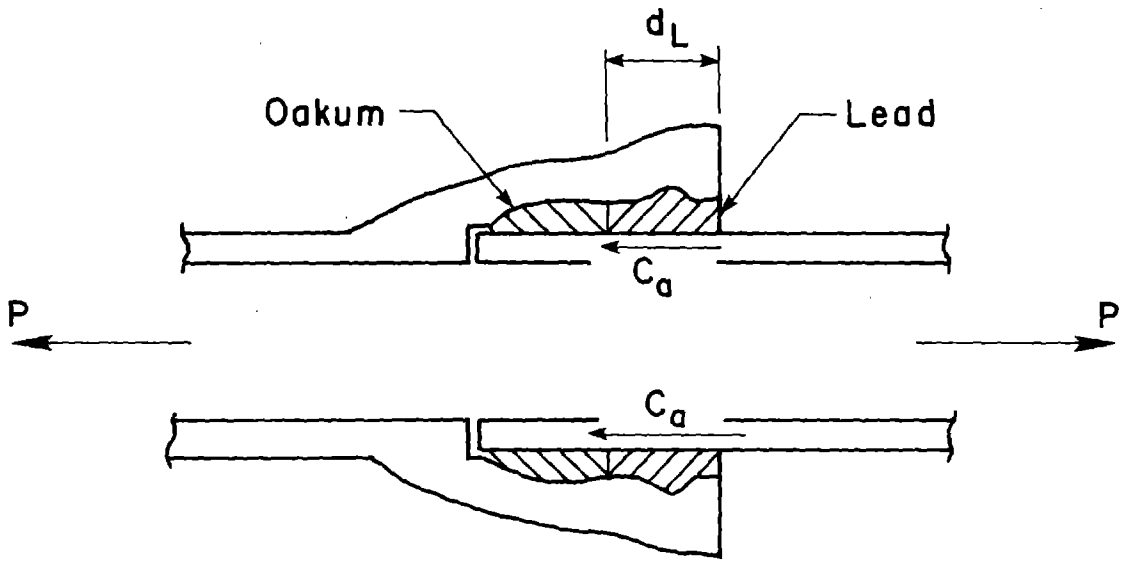

a) Lead - caulked joint subject to pull - out

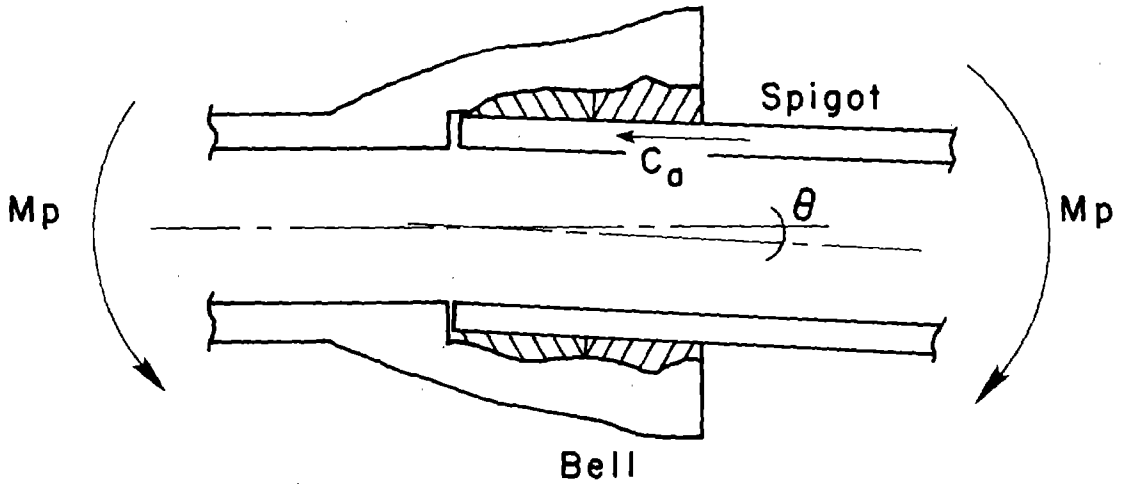

b) Lead - caulked joint subject to bending

Figure 3.4 Cross-sectional view of a lead-caulked joint subjected to a) pull-out, and b) bending.

Table 3.1 Data summary for pull-out tests on lead-caulked couplings.

Nominal diameter in.	Outside diameter in.	Pull-out Force at first slip X 10^3 lbs.	Adhesive Strength C_a, psi	Reference
24	26.3	45.7	246	Prior (64)
60	64.8	121.6	266	ibid
18	19.9	50.4	358	ibid
12	13.5	22.7	238	ibid
36	39.2	51.9	187	ibid
60	64.8	48.1	105	ibid
36	39.2	97.7	353	ibid
48	52	54.3	148	ibid
36	39.2	82.4	298	ibid
18	19.9	43.8	312	ibid
18	19.9	30.8	219	ibid
6	7.1	8.5	169	ibid
12	13.5	20.4	214	ibid
6	7.1	10.6	211	ibid
24	26.3	54.3	292	ibid
20	22.1	39	250	Committee on Cast Iron Pipe Joints (21).
20	22.1	48	307	
20	22.1	52	333	
20	22.1	38	243	ibid
20	22.1	58	371	ibid
20	22.1	62	397	ibid
20	22.1	20	128	ibid
20	22.1	40	256	ibid
20	22.1	25	160	ibid

Note: 1 in = 25.4 mm

1 psi = 7 KP_a

1 lb = 4.4 N

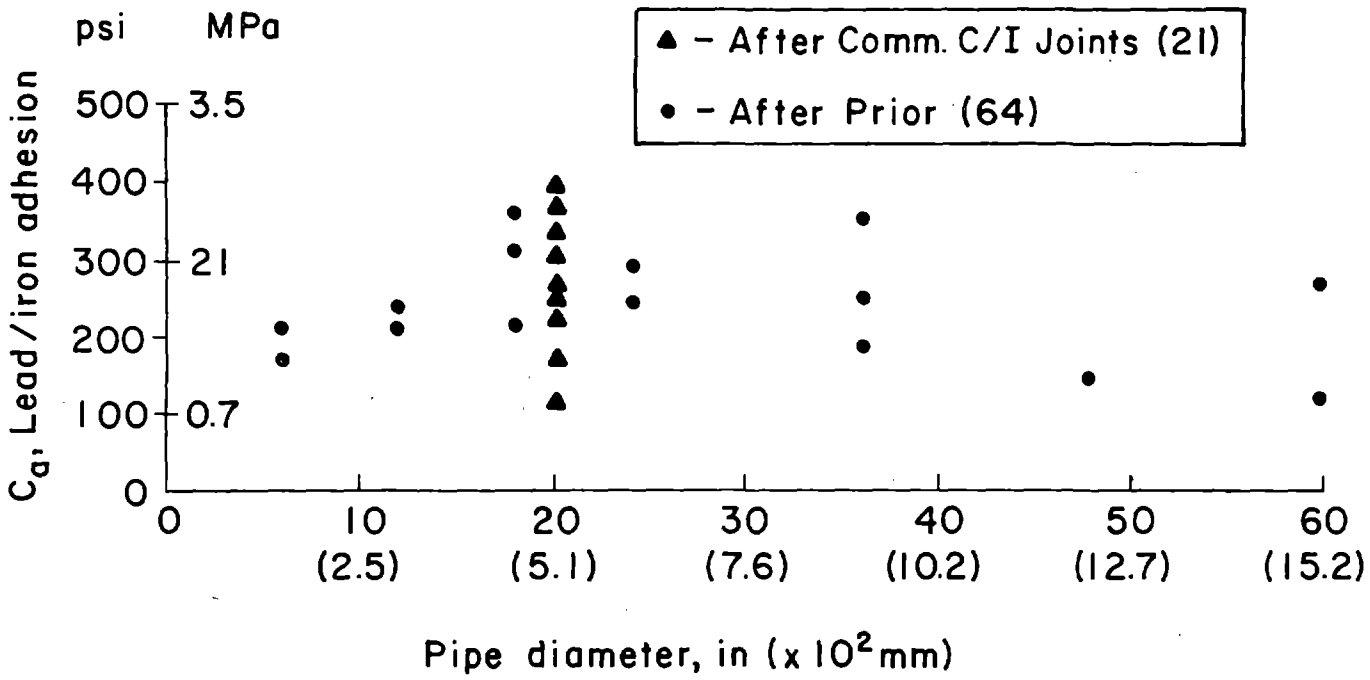

Figure 3.5 Lead-iron adhesion as a function of pipe diameter.

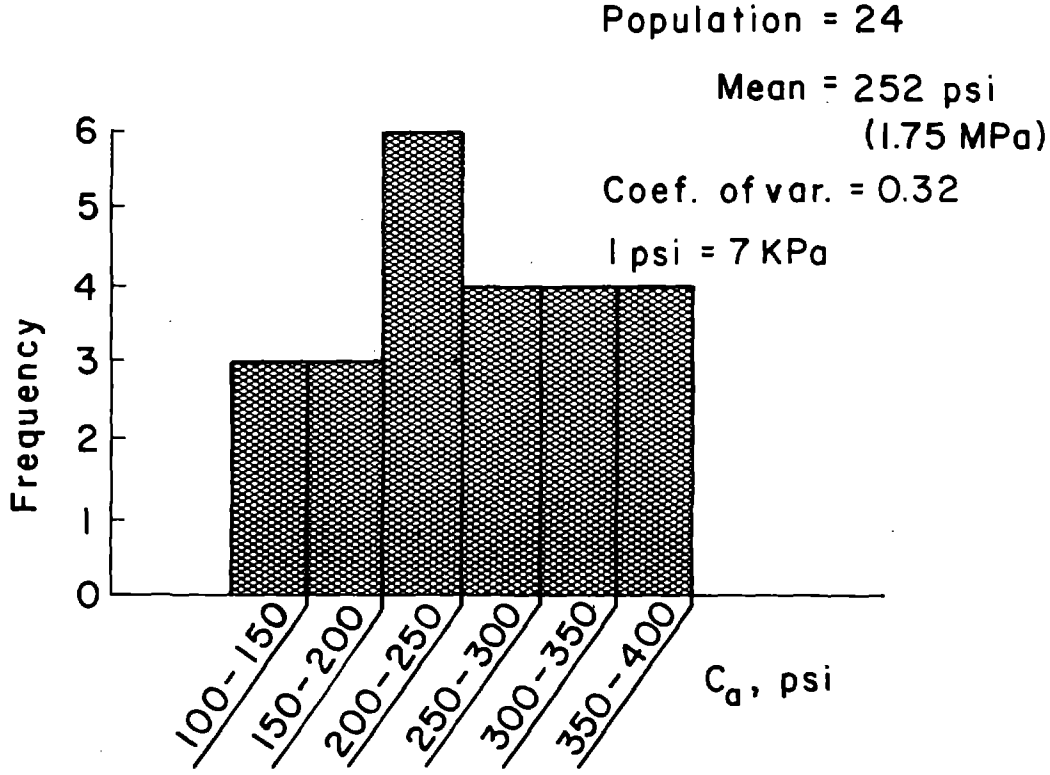

Figure 3.6 Frequency diagram of lead-iron adhesion values.

Knowing the adhesive strength, the pull-out resistance, P, can be calculated by means of the following expression:

$$P = \pi D \, C_a \, d_L \qquad (3.1)$$

where D is the outside diameter of the pipe.

Assuming the joint resists pure bending chiefly through the adhesive stresses at the coupling, a relationship can be derived between the moment corresponding to the first slip, M_C, and the adhesive strength:

$$M_C = 3/8 \, \pi D^2 \, C_a \, d_L \qquad (3.2)$$

Because the test observations generally confirm that first slip is associated with initial leakage, M_C may be regarded as a limiting value above which leakage will occur. Appendix A gives the complete derivation of this expression and develops additional relationships between pipe deformation and strength values.

Untrauer et al. (90) show that lead-caulked joints possess very little rotational restraint against bending. Hence, it is appropriate to model the response of lead-caulked joints to bending as that of a pinned connection. Other significant factors affecting the joint behavior include tolerable slip and pull-out resistance. Test data demonstrate that, after an initial period of leakage, the joints can sustain an axial slip from one to two inches (25 to 51 mm) without further loss of water (90). This laboratory behavior is corroborated by observations of deformed water mains in areas of fault creep (see Appendix B). Although the laboratory and field observations have shown that lead-caulked joints deformed substantially without continuous leakage, these observations should be regarded with caution. Due to the nonlinear, time dependent behavior of lead, the deflection of lead-jointed lines also will be non-linear and time

dependent. Hence, differential movements may be sustained without continuous leakage on the short term, which nevertheless may cause future leakage as adjustments to the imposed loading continue and as additional service and thermal stresses occur.

Table 3.2 summarizes published information on joint rotations and slip associated with leakage. Table 3.3 summarizes the values of joint rotation, maximum axial slip, and pull-out capacity that are used in this report to characterize lead-caulked coupling behavior.

3.4 Mechanical Couplings

Figure 3.7 shows several mechanical couplings in various states of deformation. As illustrated in the figure, the coupling achieves a leak-proof seal by means of a rubber gasket compressed by a special gland between the spigot and bell.

The coupling is flexible because it can accommodate axial slip and rotation with little bending or pull-out resistance. The maximum axial slip, S_L, that the joint can tolerate is shown in Figure 3.7b. Although the coupling is designed specifically to accommodate only the thermal contraction typical of most service conditions, it nonetheless can absorb a substantially larger movement provided that compression of the gasket is maintained and the spigot surface is relatively free of obstructions. The maximum slip is determined by the coupling geometry and distance remaining between the spigot end and bell hub when the pipe is installed. Typically, 1/8 in (3.2 mm) remains between the spigot and hub after installation. For most pipe sizes, this allows approximately 2.25 in (47 mm) of travel before the spigot end intercepts the gasket. The maximum rotation is limited by metal binding and controlled by both the ratio of the bell to spigot diameter and the

Table 3.2 Summary of published observations of joint rotation and slip associated with leakage.

Mode of Deformation	Description	Observed Value	Reference
Rotation	Laboratory tests on nominal 4 in (102 mm) pipe.	0.9°	Untrauer et al. (90)
Rotation	Field observations of nominal 12 in (0.3 m) pipeline; deformation adjacent to urban excavation.	0.4°	Maynard and O'Rourke (52)
Axial Slip	Laboratory tests on pipe with nominal diameters from 6 to 60 in. (0.15 to 1.5 m).	1 to 2 in. (25 to 51 mm)	Prior (64)

Table 3.3 Summary of mechanical characteristics of various pipe joints.

	Limiting Value		
Mode of Deformation	Lead-Caulked	Mechanical	Dresser Long
Rotation (deg)	0.5	5.0	7.0
Axial Slip (in)	1.0	2.25	6.0
Pull-Out Capacity	$\pi D\, C_a\, d_L$	0	0

Note: 1in = 25.4 mm

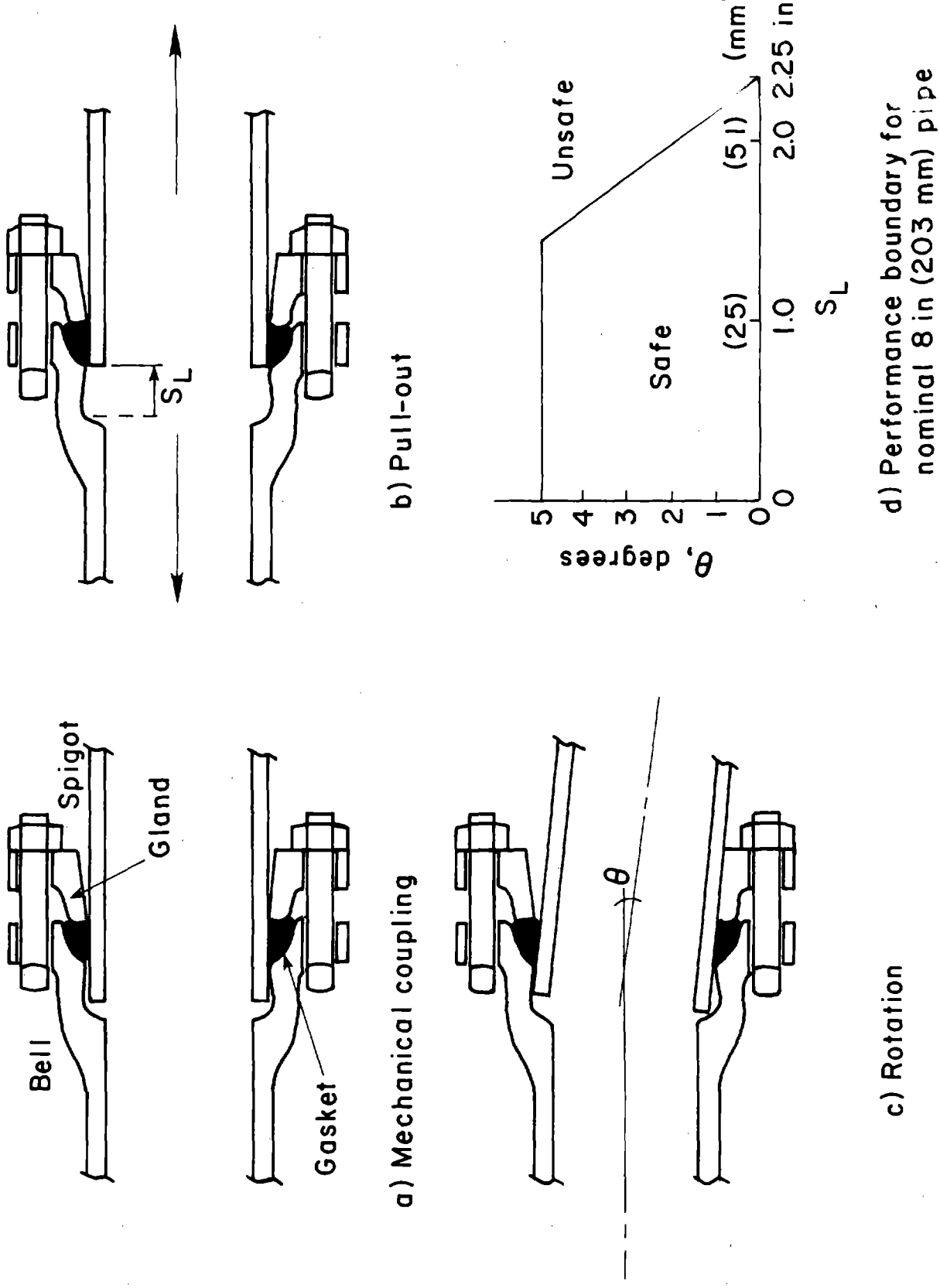

Figure 3.7 Cross-sectional view of mechanical couplings in various states of deformation.

inclination of the beveled surfaces at the interior of the bell. The maximum rotation varies inversely with the pipe diameter. For a nominal 8 in (203 mm) diameter main it is typically five degrees.

The maximum permissible rotation and axial slip are interrelated. Figure 3.7d shows the maximum rotation and slip for combined modes of deformation pertaining to an 8 in (203 mm) diameter pipe. This relationship may be regarded as the locus of points separating safe from unsafe performance.

Tests performed for the Cast Iron Pipe Research Institute (14) indicate that the pull-out capacity of mechanical joints is highly variable and, although it will depend on pipe surface texture, gasket compression, and gasket type, it is very low relative to the tensile capacity of the pipe. Table 3.3 summarizes the characteristics of mechanical couplings for 8 in diameter (203 mm) pipe.

3.5 Dresser Long Couplings

Typically, long couplings are used to join two pipes when the gap between the pipe end is larger than usual. If applied in areas of ground rupture, the long couplings could accommodate large ground displacements directed parallel to the pipeline.

Figure 3.8a shows a profile of a standard long coupling manufactured by Dresser Industries, Inc. (Style 40 Long Coupling). A leak-proof seal is maintained by means of a gasket compressed against the ends of the center ring. For center rings of 16 in (0.4 m) length, the maximum rotation at either end of the coupling is limited by metal binding and controlled by both the length of the pipeway and the ratio of the pipeway to pipe diameter. The long coupling for a nominal 8 in (203 mm) diameter pipe can accommodate up to 3.5 degrees of rotation at each end, or a total of 7 degrees of rotation across the coupling. The maximum slip is the amount of travel available to one of the pipes in the coupling. If the

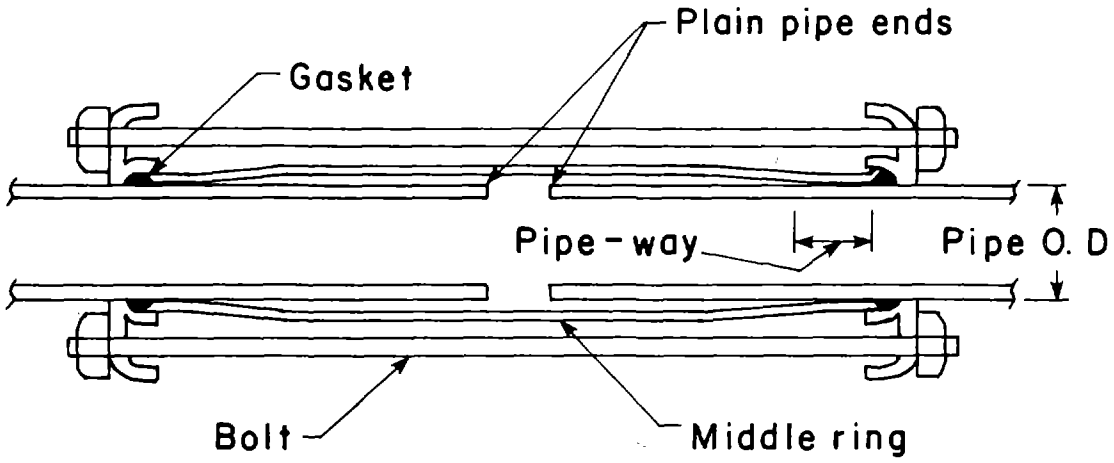

a) Long coupling

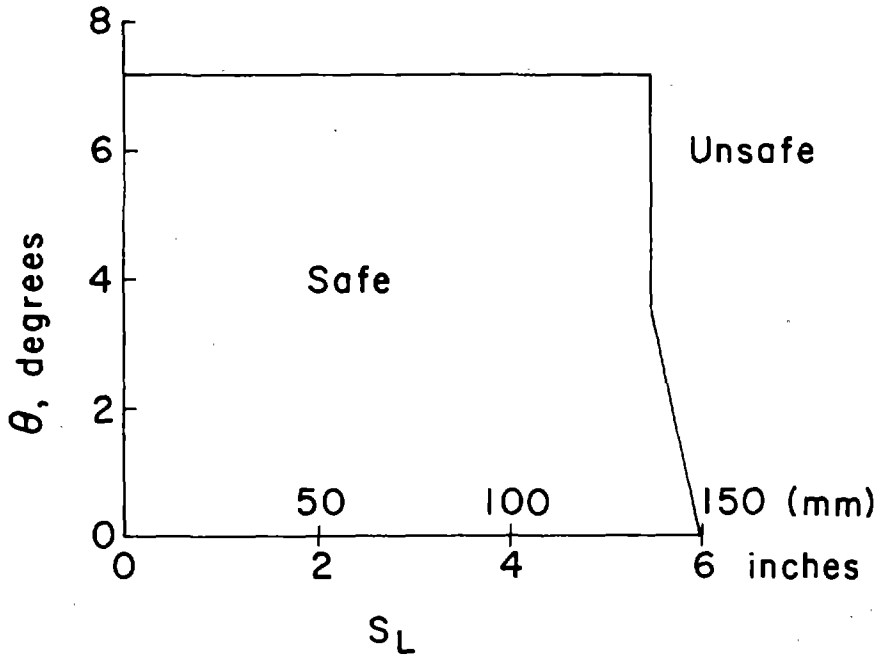

b) Performance boundary for long coupling

Figure 3.8 Cross-sectional view of Dresser Industries Style 40 Long Coupling and performance boundary.

pipes are initially separated by 2 in (51 mm) across the center of the coupling, the maximum axial slip is approximately 6 in (152)[2]. This limit is based on the conservative assumption that pull-out movement will be concentrated at only one side of the coupling.

Figure 3.8b shows the maximum rotation and slip for combined modes of deformation on a coupling joining 8 in (203 mm) diameter mains. As the pipe is pulled toward one end of the coupling, the maximum slip will be affected by the rotation at that end. Consequently, there is a break in the inclined portion of the performance boundary, which occurs at a rotation of 3.5 degrees.

Tests performed by Dresser indicate that the pull-out resistance is roughly 1000 lbs (4500 N) per inch of outside pipe diameter. As is the case for mechanical joints, the maximum pull-out load is very small relative to the tensile capacity of the line and can be disregarded during analysis. Table 3.3 summarizes the characteristics of Dresser long couplings.

[2]Dresser couplings are designed specifically to accommodate thermally-induced movements up to 3/8 in (10 mm). If axial slip exceeds this value, Dresser recommends the use of a special Style 63 expansion joints. Nevertheless, communication with engineering personnel at Dresser confirm that the long couplings can absorb movements consistent with their geometric limits provided that compression of the gasket is maintained and the spigot surface is relatively free of obstructions.

Dresser Style 63 expansion joints use a packing gland and stuffing box to form the seal at the joint. The packing consists of alternate rings of rubber and jute, wherein the jute serves as a lubricant reservoir to reduce wear on the rubber packing rings.

CHAPTER 4

ANALYTICAL MODELING OF BURIED PIPELINE PERFORMANCE

4.1 Modes of Pipeline Failure

When pipelines are deformed by differential ground movements, failure can occur in three ways: 1) failure of the pipe material, 2) excessive slip at a coupling, and 3) excessive rotation at a coupling. This chapter examines buried pipeline response to strike-slip faulting as a function of the three failure modes. The strength and performance characteristics developed in Chapter 3 are used to model pipe and coupling response to deformation. These are represented in finite element simulations that explore the relationships among the magnitude of fault displacement, the angle of intersection between the pipeline and fault, the pipe size, and the type and location of couplings.

4.2 Patterns of Fault Displacement

Frequently, surface faults are idealized as an abrupt planar movement for purposes of conceptualization and definition. Although surface ruptures can occur as large planar displacements, the patterns of ground movement associated with faulting commonly are complex and distributed throughout a zone extending to both sides of the fault centerline (44,61,71,86). Moreover, the character of the surface distortion can vary substantially along the same fault (16,56). Ground breakage patterns can include large planar displacements, pressure ridges, en echelon fractures, and antisymmetric warping (11,48,71).

Pipeline networks generally are vulnerable to all forms of fault movement as well as similar patterns of ground failure associated with secondary earthquake effects. Accordingly, one of the goals of this study is to represent

the pipeline response to widely different but characteristic displacement patterns at fault crossings. The patterns used include 1) abrupt, planar displacement and 2) distributed movements typical of fault creep. General characteristics of fault creep and observations of creep effects on buried pipelines are discussed in Appendix B.

To obtain detailed information on the distribution of fault creep, measurements were made of an offset fence at the Nyland ranch, approximately one mile north of San Juan Bautista, California. Figure 4.1 provides a plan view of the fence and USGS creepmeter station SJN. The creepmeter is located across the San Andreas fault, which intersects the fence at approximately a right angle. At the time of measurement, the total relative displacement of the fence along a distance parallel to the length of the creepmeter was approximately 10.5 in (267 mm). As the fence was constructed in 1940, the maximum displacement determined on the basis of the creep rate measured at station SJN would have been between 10 and 11.7 in (254 and 297 mm). Hence, the measured and inferred displacements are in reasonable agreement.

The measured displacements were modeled by means of a hyperbolic function of the form:

$$d = \frac{L}{1/a + L/b} \tag{4.1}$$

where d is the lateral displacement relative to the centerline of the fault zone, L is the distance from the center of the fault zone, and a and b are constants. This technique has been used elsewhere and is described in detail by Duncan and Chang (23).

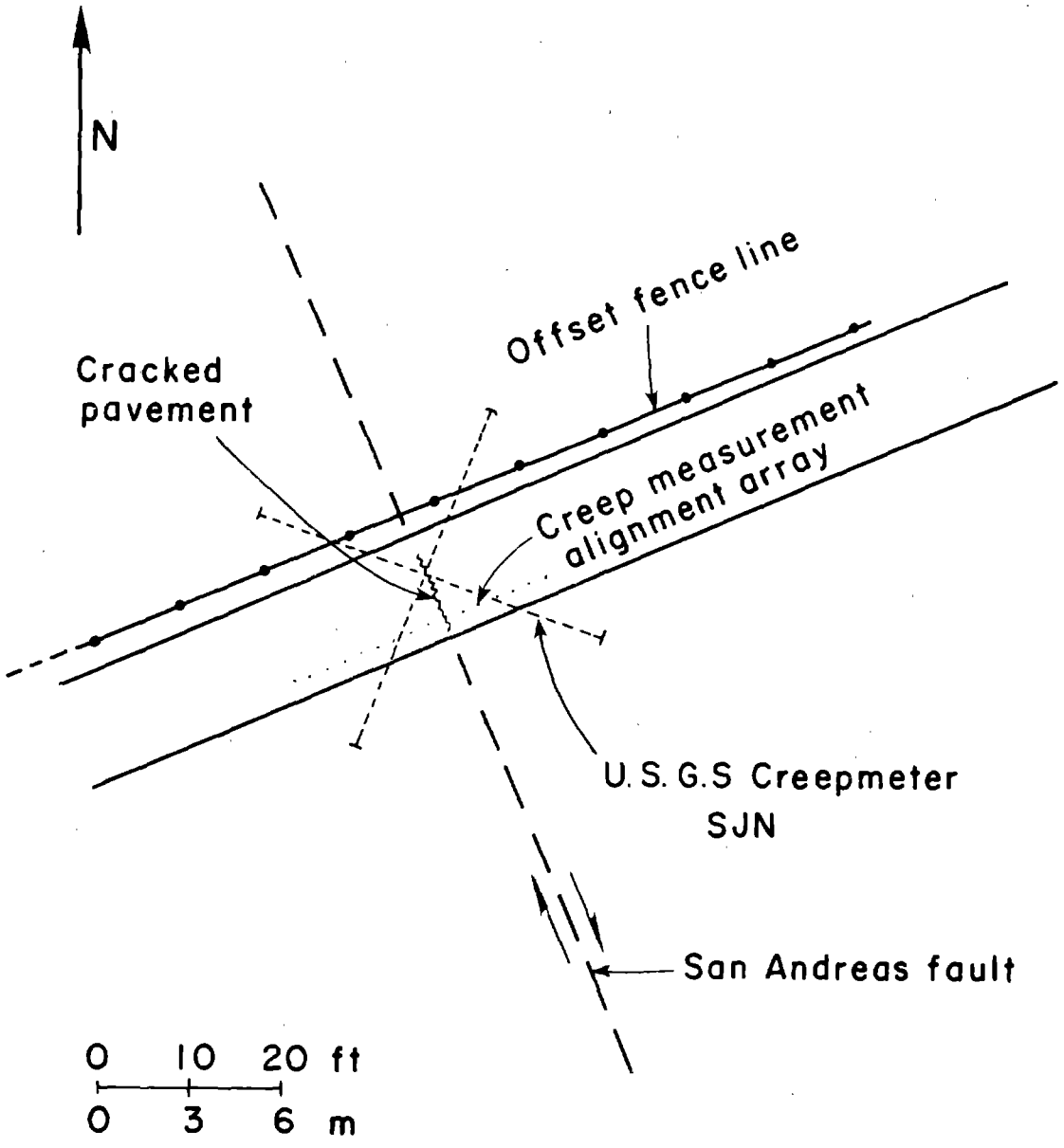

Figure 4.1 Offset fence and USGS creepmeter installation at Nyland Ranch near San Juan Bautista, CA.

Equation 4.1 also can be expressed in arithmetic form as:

$$\frac{L}{d} = \frac{1}{a} + \frac{L}{b} \tag{4.2}$$

Figure 4.2a shows the displacement data plotted in arithmetic form. Although some scatter in the data is apparent owing to variation in the initial alignment of the fence and disturbance at individual posts, there, nevertheless, is a consistent trend to the measurements. Furthermore, the hyperbolic function has two useful characteristics: 1) the y-intercept, 1/a, is the reciprocal of the maximum shear strain at the center of the fault zone and 2) the slope, 1/b, is the reciprocal of the ultimate fault displacement, or shift of one side of the fault relative to the center of the fault zone.

Using the measured displacements, an equation for the distribution of movement across the fault zone was developed:

$$d/d_{ult} = \frac{L}{168.3 + L} \tag{4.3}$$

where d_{ult} is the ultimate lateral displacement relative to the fault centerline, which is equal to 1/b, and L is expressed in inches. Figure 4.2b shows the normalized displacement as a function of distance from the center of the fault.

Equation 4.3 was used to represent fault movements for several cases of ultimate relative displacement. Pipeline response to both abrupt and distributed movements was then modeled by means of the finite element method.

4.3 Numerical Model of Pipeline Performance

Figure 4.3a shows a hypothetical buried pipeline crossing an active geologic fault. In the figure, β represents the angle between the fault and the pipeline. The free length between the fault and the point of effective fixity

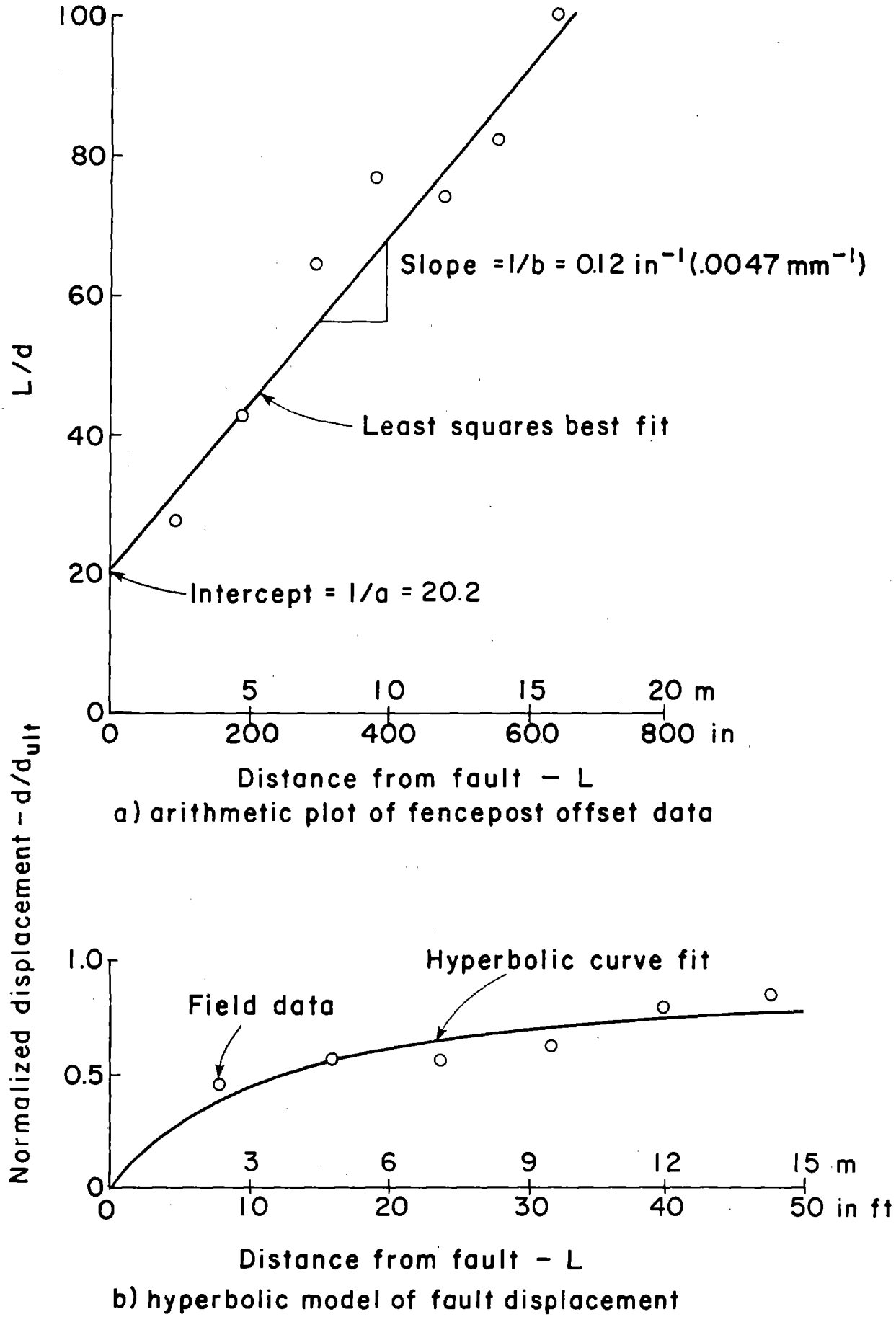

Figure 4.2 Representation of fault displacement by a hyperbolic curve fit.

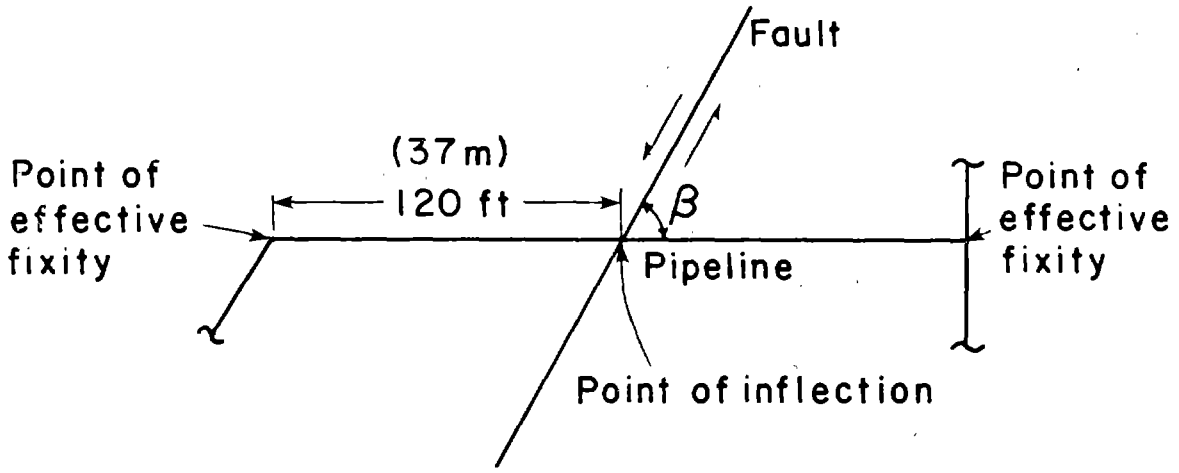

a) Pipeline / fault intersection

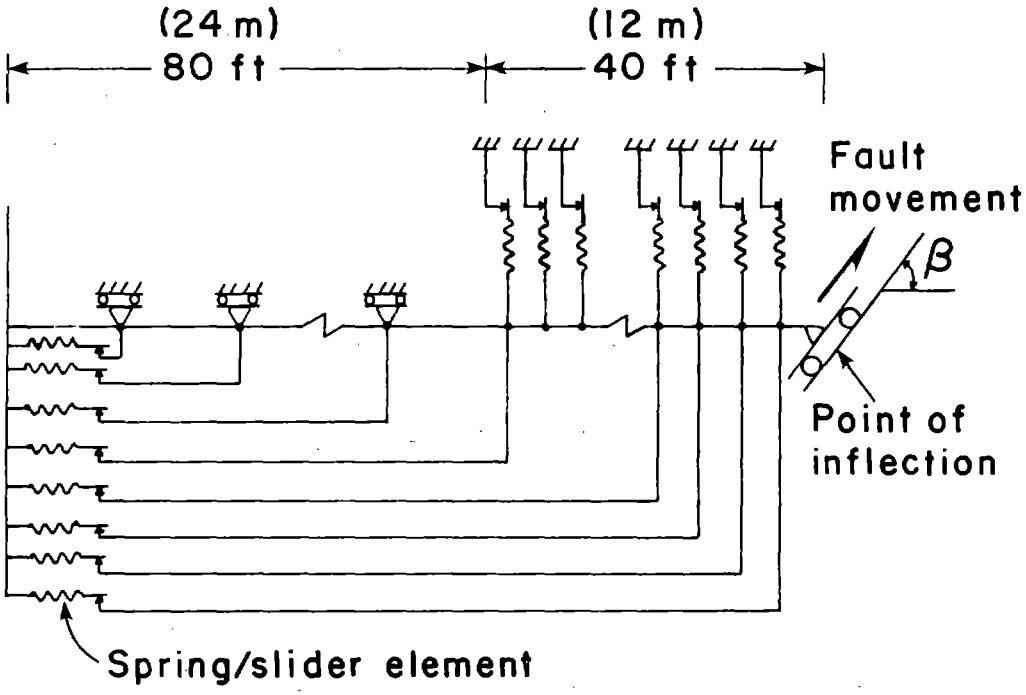

b) Finite element model

Figure 4.3 Plan view of hypothetical pipeline crossing a fault and finite element representation.

along the pipe, such as a bend or connection with another pipe, was selected as 120 ft (37 m).

Pipeline response to fault displacement was modeled with the finite element method by combining elastic pipe and spring-slider elements as shown in Figure 4.3b. The finite element program used was ANSYS, which is available through Swanson Analysis Systems, Inc.[3] Geometric nonlinearity was used in the pipe elements, and the fault displacement was assumed to occur entirely as strike-slip motion. Because the ground movements and pipeline response are antisymmetric about the center of the fault zone, the pipeline/soil interaction on only one side of the fault was modeled. Correspondingly, the input displacement at the fault centerline accounted for one-half the total relative displacement across the fault. As the inflection point of the pipeline occurs at the center of the fault zone, this point was modeled as a pinned connection. Abrupt fault movements were modeled by displacing the pinned end point a distance consistent with the magnitude and relative orientation of fault slip. Distributed fault displacements were modeled by means of Equation 4.3, from which fault movements were scaled according to distance from the fault centerline and used as boundary displacements of the spring-slider elements perpendicular to the pipeline.

Spring-slider elements were used to represent coupling behavior. The elements were connected to pins with zero rotational stiffness. Coupling rotations were monitored during the analyses and checked against maximum allowable rotation. The pull-out capacity for the lead-caulked joints was determined by Equation 3.1, assuming an adhesive strength of 252 psi (1.75 MPa) and a depth of caulked lead equal to 2.25 in (57 mm). Full resistance to pull-out was modeled after 1/8 in (3 mm) of displacement. The maximum slip for each type of joint was based on the values developed in Chapter 3.

---

[3]Swanson Analysis Systems, Inc., P.O. Box 65, Houston, PA, 15342

The soil reaction to lateral pipe displacement was represented on the basis of test data reported by Audibert and Nyman (5); these data show a curvilinear trend of soil resistance as a function of pipe displacement. This behavior was approximated in the analysis as a bilinear response of the spring-slider elements perpendicular to the pipeline. In addition, the angle of friction at the pipe/soil interface was estimated as two-thirds the soil angle of shearing resistance. The longitudinal resistance to movement was calculated as the product of the net horizontal force resisting lateral displacement and the tangent of the friction angle at the pipe/soil interface.

To model the soil as a continuum, the lateral spring spacings were 2 ft (0.6 m) at all points within 40 ft (12.2 m) of the fault. For most cases studied, this represents less than half the maximum spacing for conventional beam-on-elastic-foundation analysis (8).

4.4 Influence of Pipe Diameter

For a range of diameters, the pipeline response was analyzed in terms of the magnitude of abrupt fault displacement, distribution of pipe movement, and level of tensile stress. The cross-sectional dimensions of the pipe were chosen to be consistent with the American National Standard for cast iron pipe (14).

All pipelines were assumed to be buried at a depth, Z, of 3 ft (0.9 m) to the springline of the pipe. The unit weight, γ, of the backfill was assumed to be 120 pcf (0.019 MN/m^3). Following the recommendations of Audibert and Nyman (5), the ultimate load bearing capacity, q_u, acting against the pipe

was calculated as

$$q_u = \gamma Z N_q \qquad (4.4)$$

where N_q is the Brinch Hansen bearing capacity factor (33) and a function of both the angle of shearing resistance and the depth to diameter ratio for the pipe.

Figure 4.4 compares the assumed, normalized pressure/displacement relationship with that estimated on the basis of the data reported by Audibert and Nyman. The slope of the pressure/displacement response was chosen to give conservative values for virtually all levels of movement.

A continuous pipeline was analyzed. This type of line would represent pipes joined with bolted flange couplings. Although cast iron lines with bolted flange couplings are not common in buried pipeline systems, the continuous pipeline represents a reference condition of deformation, relative to which the performance of articulated pipelines can be compared.

Figure 4.5 shows the distribution of pipeline displacement at failure for nominal pipe diameters of 4, 8, and 24 in (102, 203, 610 mm). The pipeline deformations are in response to an abrupt fault offset, and the angle of pipeline/fault intersection is 90 degrees. The magnitudes of both the fault movement and the length along which the pipeline displacements are distributed increase with increasing pipe diameter. In addition, the location of pipeline failure occurs at successively greater distances from the fault as the diameter increases. The deformation, especially for the smaller diameters, is confined to a relatively small distance from the fault centerline. For the 8 in (203 mm) diameter pipe, little movement occurs beyond a distance 8 ft (2.4 m) from the fault centerline. For the 24 in (610 mm) diameter pipe, virtually no movement occurs beyond a distance of approximately 22 ft (6.7 m) from the fault centerline. The points of maximum

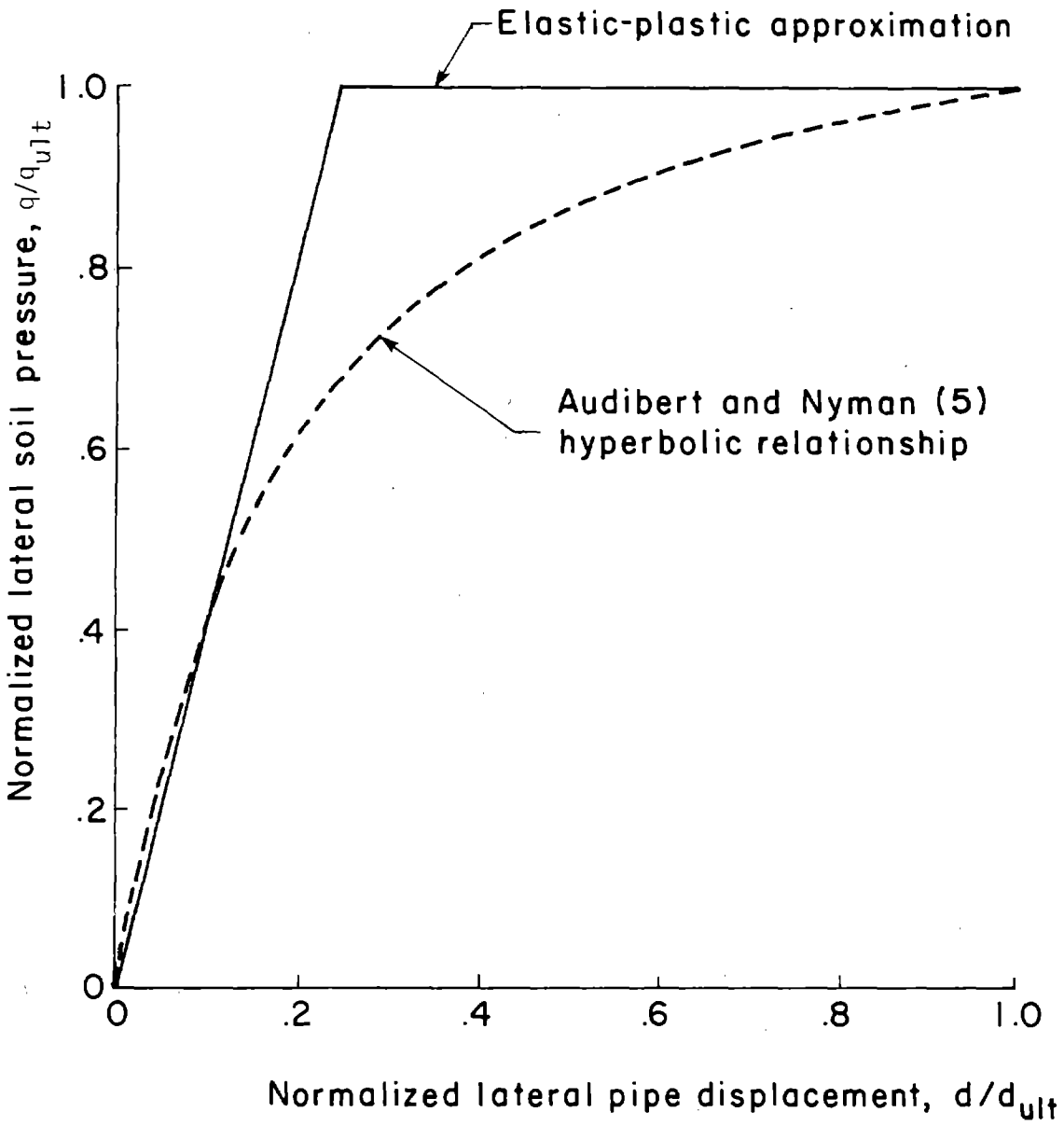

Figure 4.4 Hyperbolic pipe/soil pressure-displacement relationship and elastic-plastic approximation used in the finite element model.

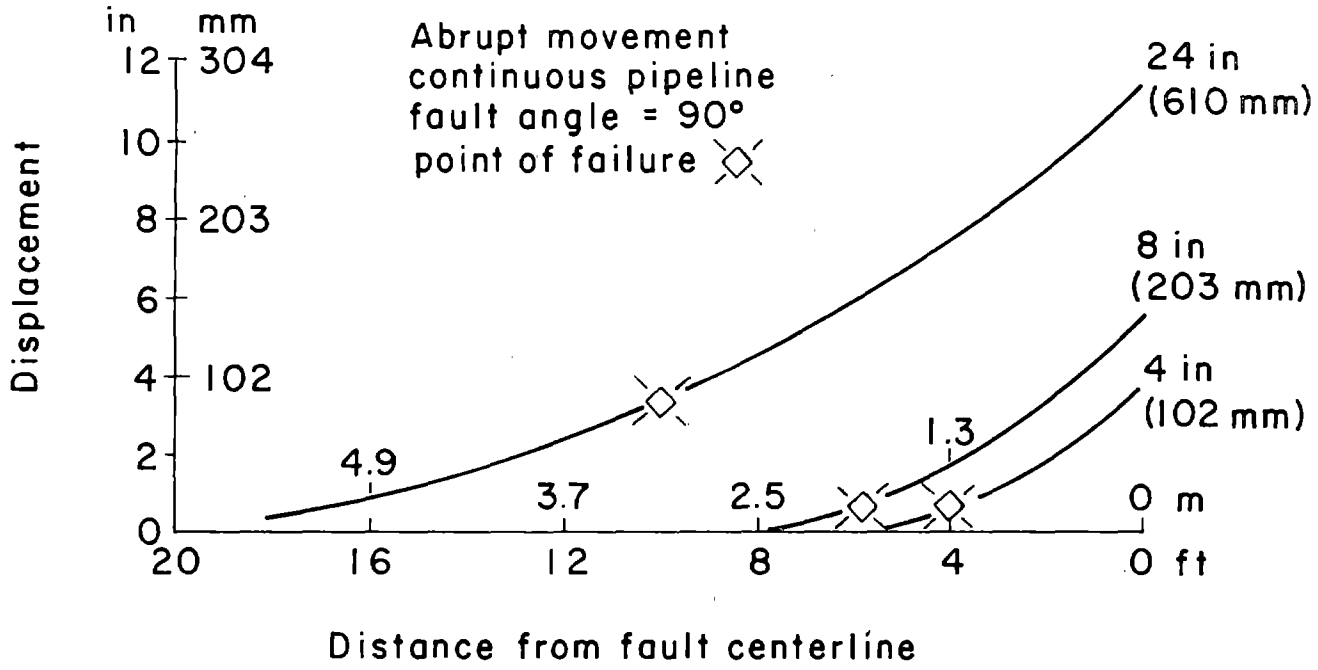

Figure 4.5 Plan view of pipe deformation at failure, for three pipe diameters, showing point of bending failure.

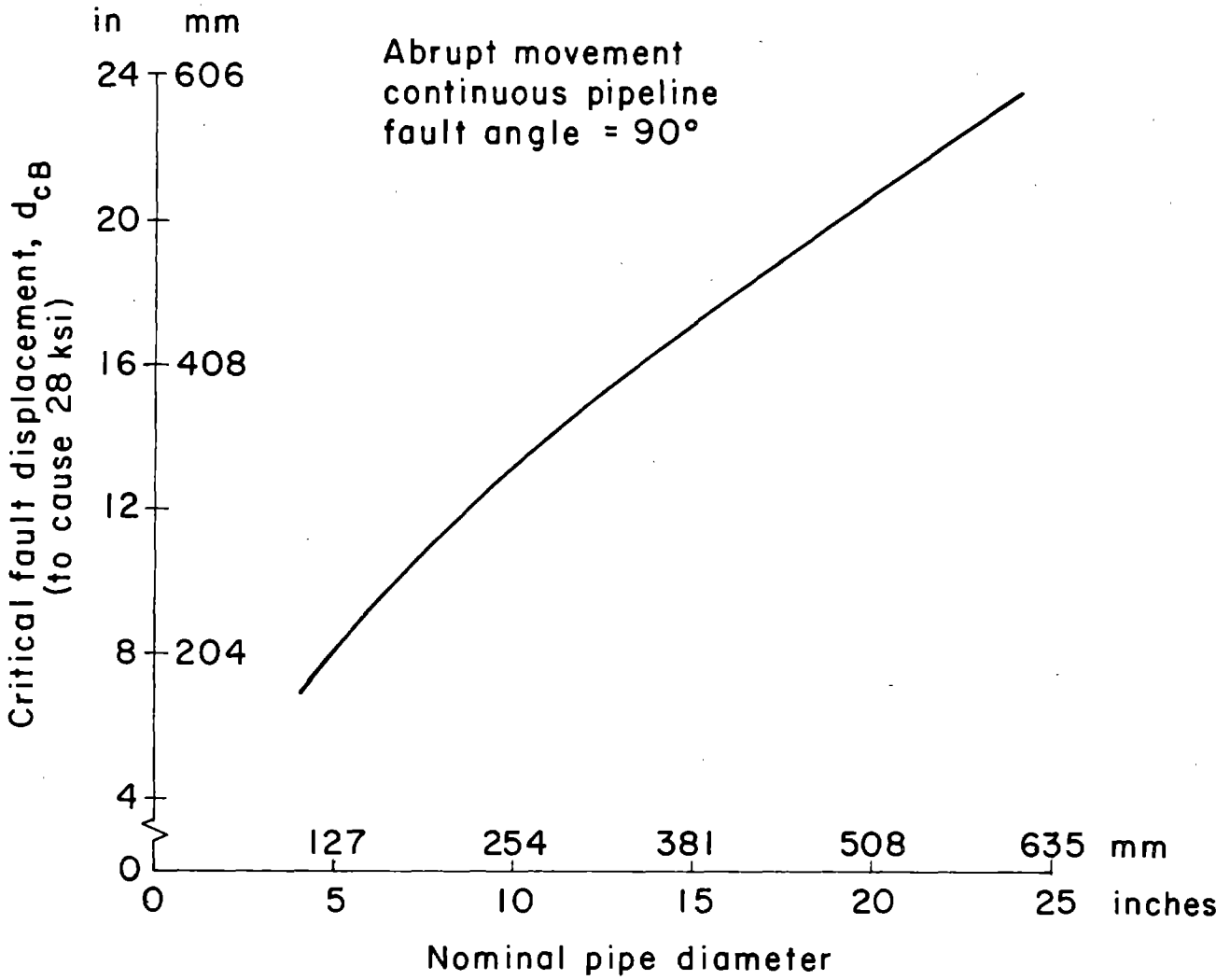

Figure 4.6 Fault displacement causing failure vs. pipe diameter for pipeline oriented vertically with fault.

curvature, or locations of failure, occur at approximately 6 and 10 ft (1.8 and 3.0 m) from the fault centerline for the 8 and 24 in (102 and 610 mm) diameter pipes, respectively.

Figure 4.6 shows the relationship between the critical fault displacement which initiates bending failure d_{cb}, and the pipe diameter. The critical fault displacement is defined on the basis of total fault offset. Hence, it is twice the maximum displacement for each line shown in Figure 4.5, where the movements on only one side of the fault are plotted. The plot shows that the critical fault displacement for bending failure, d_{cb}, can be estimated conservatively as being equal to the nominal diameter of the pipe.

4.5 Influence of Couplings

When couplings are used, the pipeline may behave as an articulated structure depending on the location of the couplings. Figure 4.7 shows the distribution of tensile stress as a function of distance from the fault centerline for a nominal 8 in (203 mm) diameter pipeline with mechanical couplings. The total fault offset is approximately the same for the three conditions shown. The fault movement is abrupt, and the angle of pipeline/fault intersection is 90 degrees. The stresses are indicated for three conditions of deformation, corresponding to coupling locations at 18, 12 and 6 ft (5.5, 3.7, and 1.8 m) from the fault centerline. Coupling locations at 18 and 12 ft (5.5 and 3.7 m) from the fault centerline have virtually no influence on the tensile stress because they lie outside the maximum length of continuous line distortion shown in Figure 4.5. When a coupling is located 6 ft (1.8 m) from the fault centerline. there is a dramatic decrease in tensile stress. This location corresponds to the point of maximum curvature for the continuous line shown in Figure 4.5. For this condition, bending of the pipeline is reduced as the coupling rotates to

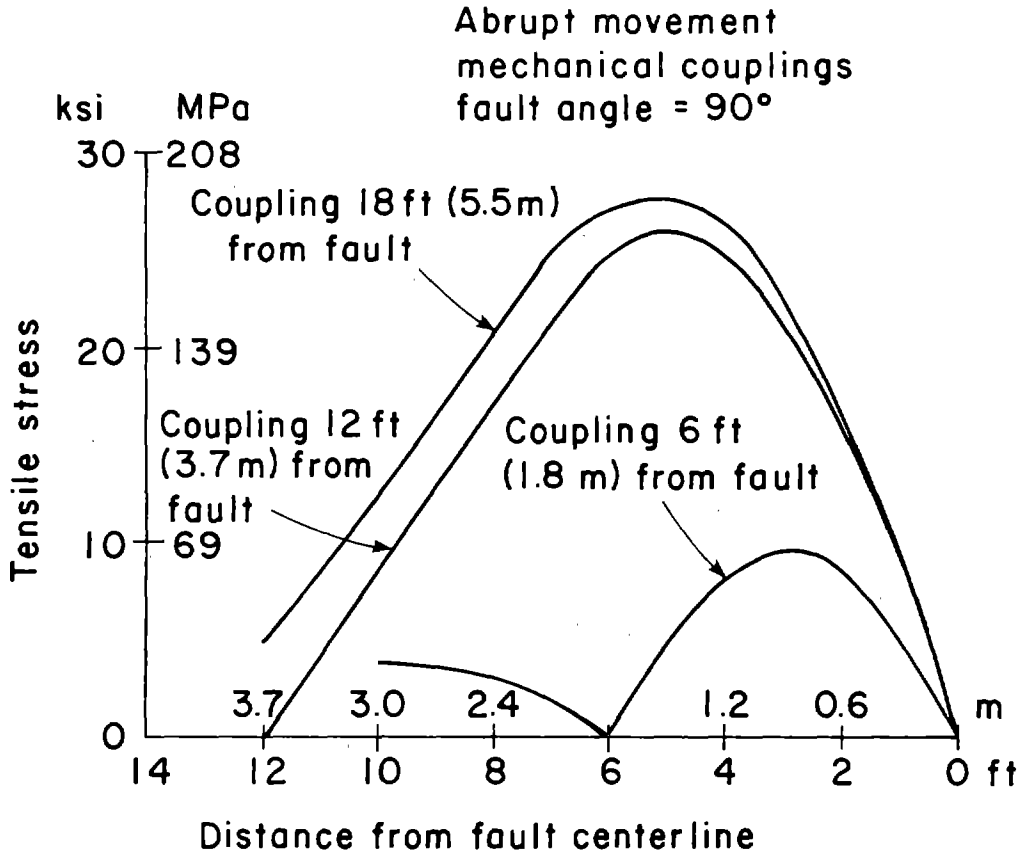

Figure 4.7 Distribution of stress for an 8 in. (203 mm) mechanically-coupled pipeline subjected to fault offset.

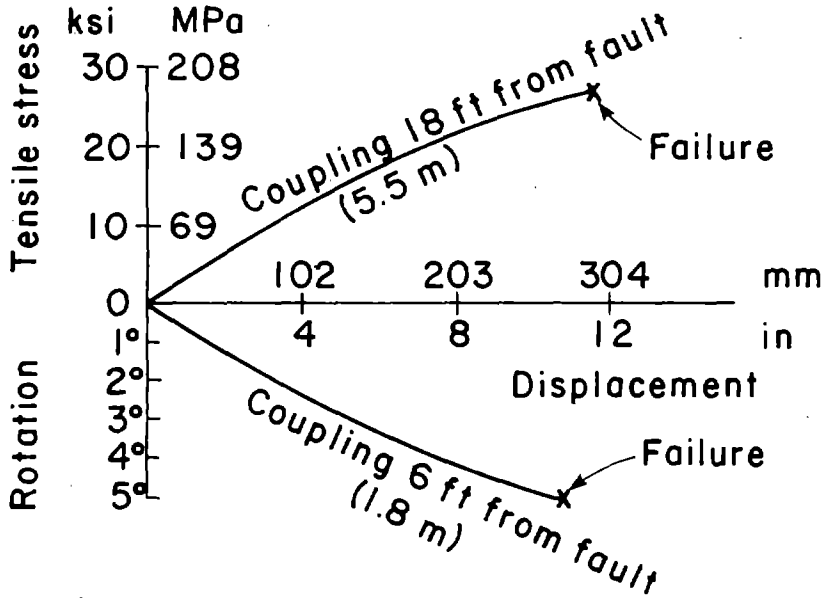

Figure 4.8 Distribution of pipe stress and joint rotation for two coupling locations.

accommodate the pattern of ground displacement. However, as rotation is concentrated increasingly at a single coupling, the pipeline is increasingly subject to failure by excessive rotation.

Figure 4.8 illustrates the modes of failure associated with various locations of mechanical couplings. When the coupling is located 18 ft (5.5 m) from the fault, the tensile stress in the pipe increases with increasing displacement until failure occurs at a critical fault displacement of approximately 11.5 in (0.3 m). When the coupling is located 6 ft (1.8 m) from the fault, the rotation of the coupling increases until the limit of rotation (5 degrees) is exceeded at a critical fault displacement of approximately 10.8 in (0.27 m).

4.6 Critical Fault Displacement and the Angle of Pipeline/Fault Intersection

This section examines the critical fault displacement, d_c, as a function of the angle of pipeline/fault intersection, β. The critical fault displacement is the relative movement across the fault which causes pipeline failure. This displacement is a general parameter which pertains to all angles of pipeline/fault intersection. The analyses were performed for an 8 in (203 mm) diameter pipe.

Figure 4.9 shows the critical fault displacement as a function of the pipeline/fault intersection for a cast iron line with lead-caulked joints. Individual pipe lengths of 12 ft (3.7 m) were used to model the pipeline performance. This length is typical of sand cast pipe, which constitutes many of the relatively old pipelines in service.

Analyses were performed for lines with couplings at distances of 6 ft and 12 ft (1.8 m and 3.7 m) from the fault. A location 6 ft (1.8 m) from

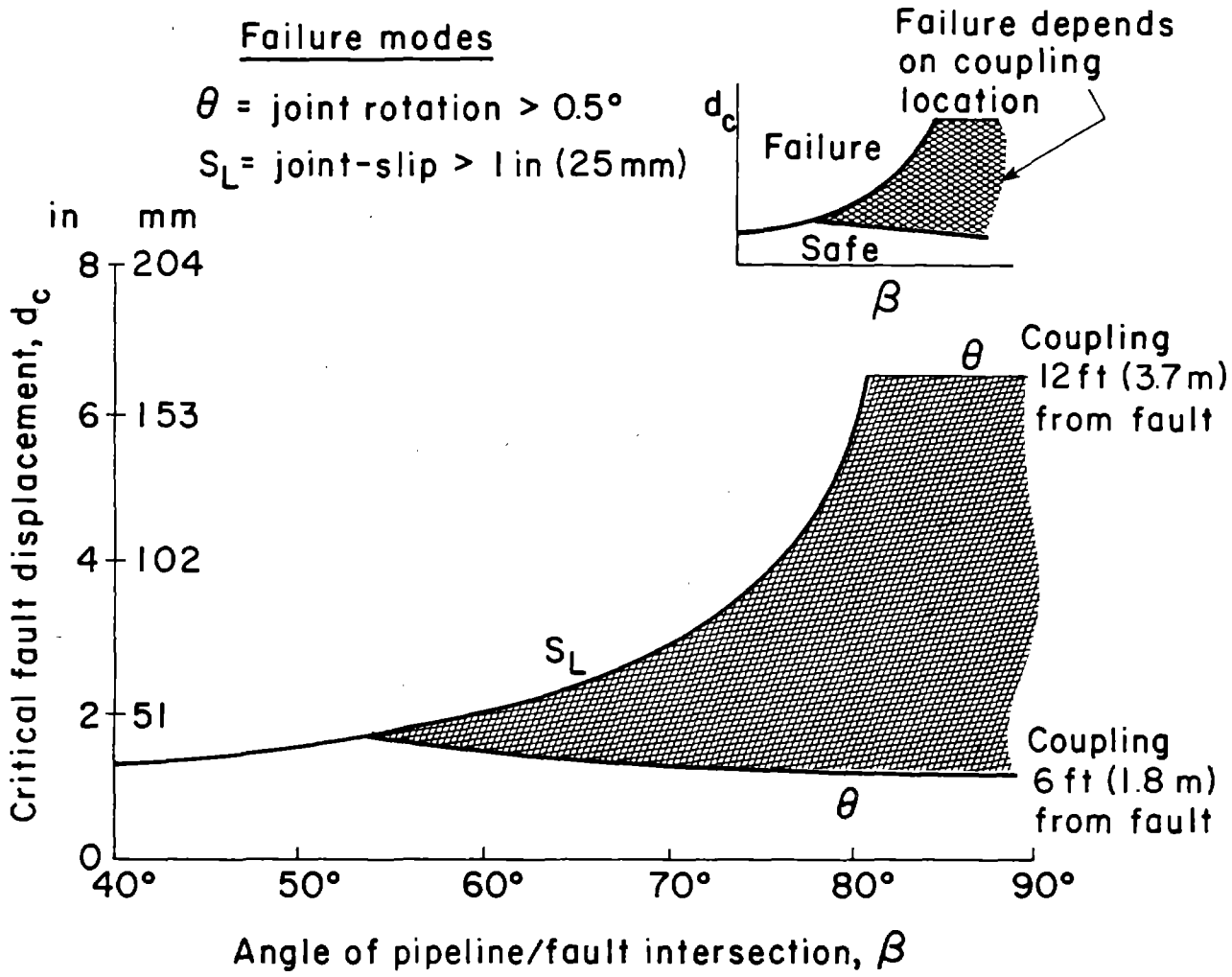

Figure 4.9 Critical fault displacement as a function of fault angle for cast iron pipeline with lead-caulked joints.

the fault will result in the maximum coupling rotation for a given fault movement, whereas a location 12 ft (3.7 m) from the fault will result in the minimum coupling rotation. Hence, these two conditions set an upper and lower bound on the critical fault displacement, provided that failure does not occur as coupling pull-out.

The analyses show that the lead-jointed pipeline will fail in only two modes: 1) joint rotation greater or equal to 0.5 degrees and 2) joint slip greater than or equal to one inch. The critical displacements for each of the individual failure modes are shown in the figure. When the plots for the individual failure modes are connected, they form a failure envelope, which is shown in the inset diagram of each figure. The shaded area of each figure corresponds to a zone in which pipeline failure will depend on the location of the couplings relative to the fault centerline. For angles of pipeline/fault intersection between 80 and 90 degrees, the pipeline response to fault movement is controlled by joint rotation and is particularly sensitive to the joint location. As the angle of pipeline/fault intersection decreases below 80 degrees, pipeline behavior is increasingly dominated by axial slip of the joints.

Figure 4.10 shows the critical fault displacement as a function of the pipeline/fault intersection for a pipeline with mechanical joints. Because an 18 ft (5.5 m) length is typical of commerically available pipe with mechanical couplings, this dimension was used to model the individual pipe lengths. Analyses were performed for lines with couplings at distances of 18, 12 and 6 ft (1.8, 3.7, and 5.5 m) from the fault centerline.

The analyses show that the mechanical-jointed pipeline can fail in three distinct modes: 1) tensile stress greater than or equal to 28 Ksi (194 MPa); 2) joint rotation greater than 5 degrees, and 3) joint slip greater than 2.25 in (57 mm). The limits on pipeline movement controlled by tensile stress and

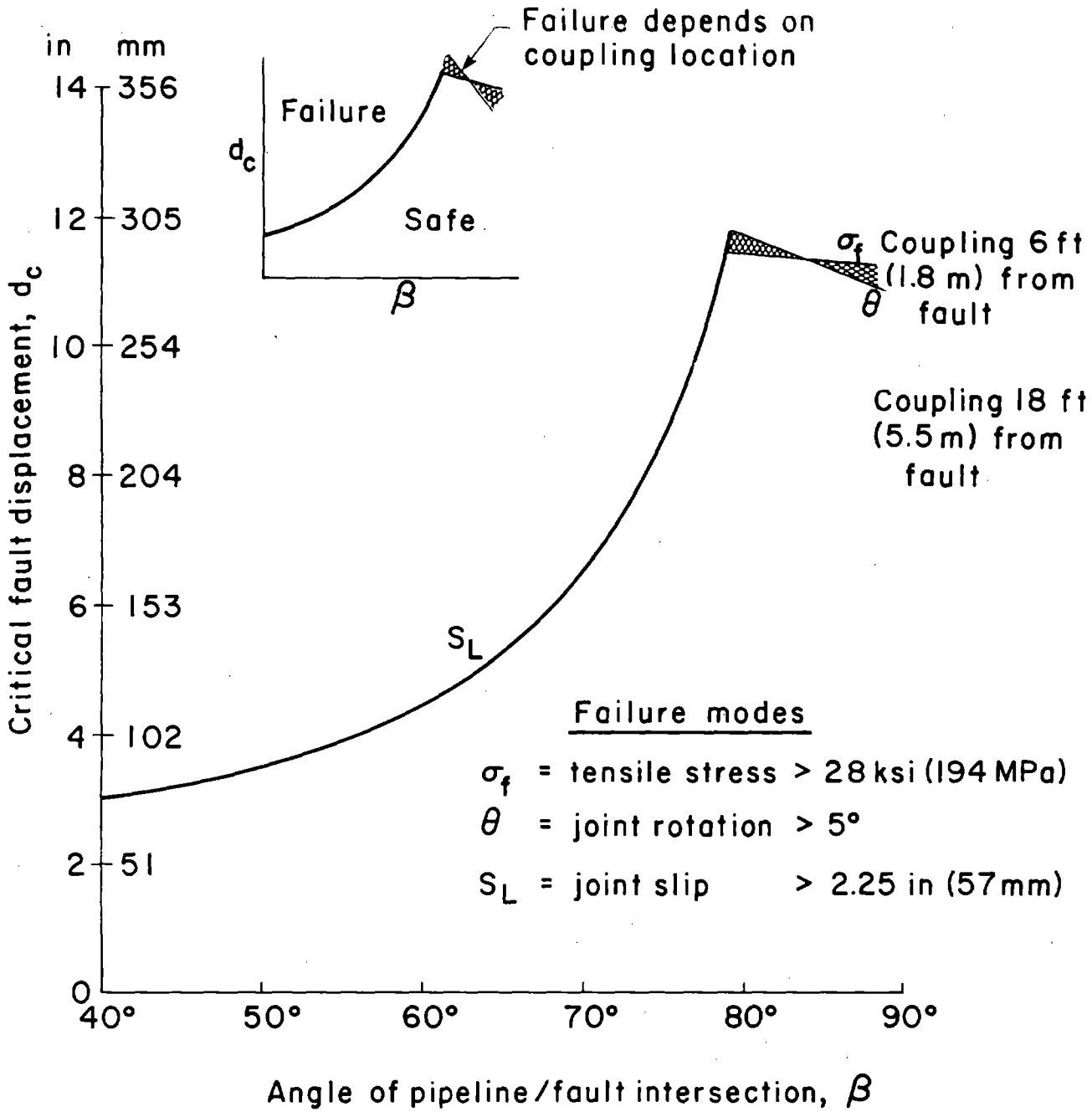

Figure 4.10 Critical fault displacement as a function of fault angle for cast iron pipeline with mechanical joints.

joint rotation are nearly the same. Hence the shaded area of the figure is relatively small. The most important mode of failure is axial slip at the coupling. For angles of pipeline/fault intersection less than about 79 degrees, axial slip controls the magnitude of critical fault displacement.

Because the mechanical couplings can accommodate a greater rotation than lead-caulked couplings, their capacity for fault displacement is from two to ten times higher for angles of pipeline/fault intersection larger than 70 degrees. Moreover, their response at high angles of pipeline/fault intersection is affected principally by bending failure.

Figure 4.11 shows the critical fault displacement as a function of the pipeline/fault intersection for a pipeline fitted with a Dresser long coupling at or very close to the fault centerline. Because a relatively large rotation is possible for the long coupling, the critical displacment even for the case of maximum possible rotation exceeds that for the condition of maximum tensile stress. Hence, the portion of the failure envelope controlled by tensile stress can be considered as a conservative bound on the magnitude of tolerable fault offset. Compared with the behavior of mechanically-jointed lines, the critical displacement for very high angles of pipeline/fault intersection does not change. However, the transition point from tensile failure to joint pull-out is displaced substantially to lower values of β. Because the long coupling can accommodate relatively large magnitudes of axial slip, the pipeline is able to sustain movement under conditions of tensile failure throughout a greater range of pipeline orientations relative to the fault.

Figure 4.12 shows the critical fault displacement as a function of the pipeline/fault intersection for a pipeline with a long coupling subjected to distributed fault movement. The pattern of movement was modeled with the hyperbolic function defined by Equation 4.3. The critical fault displacement is defined over a width of 30 ft (9 m) spanning both sides of the fault centerline.

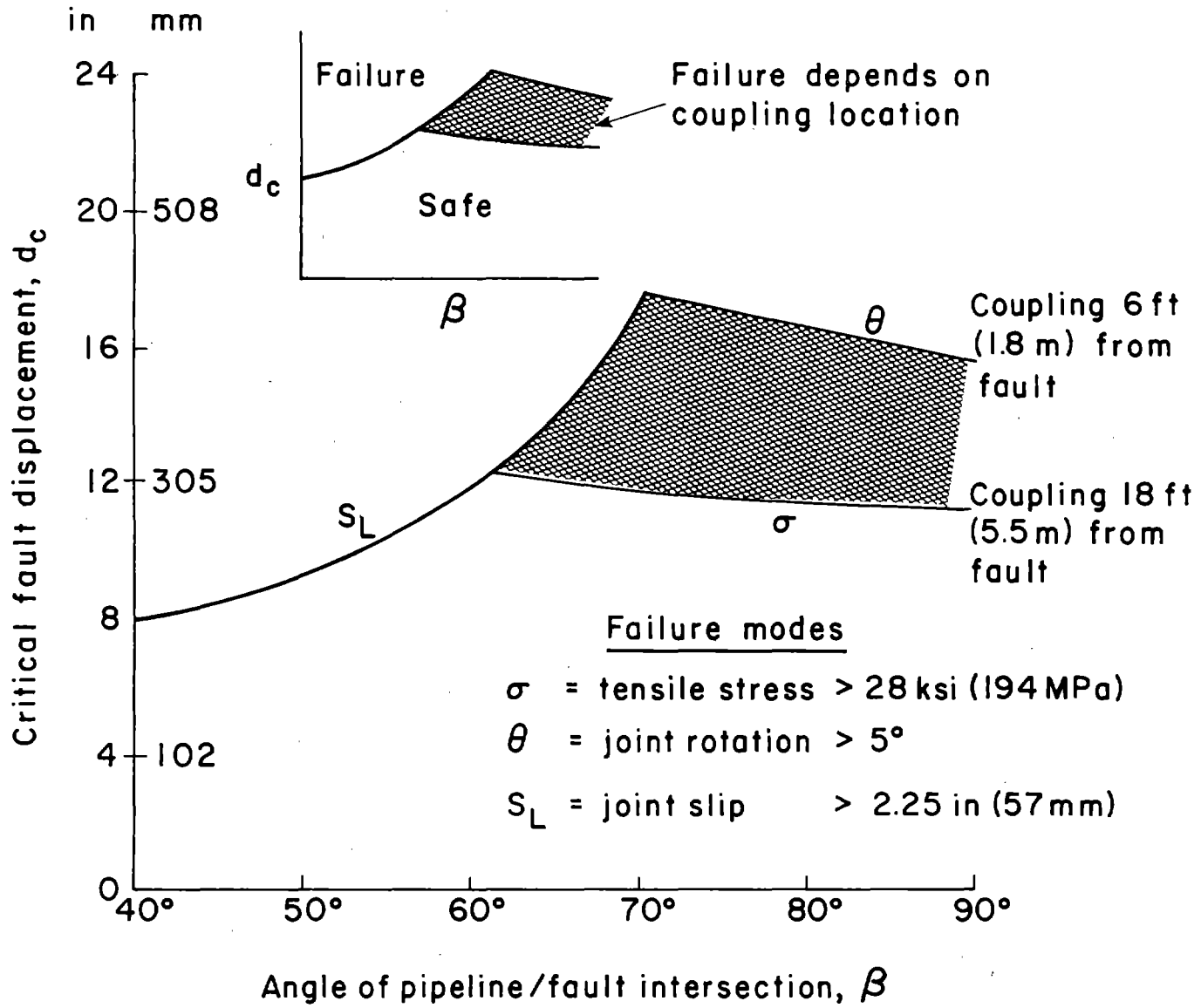

Figure 4.11 Critical fault displacement as a function of fault angle for cast iron pipeline with Dresser long couplings.

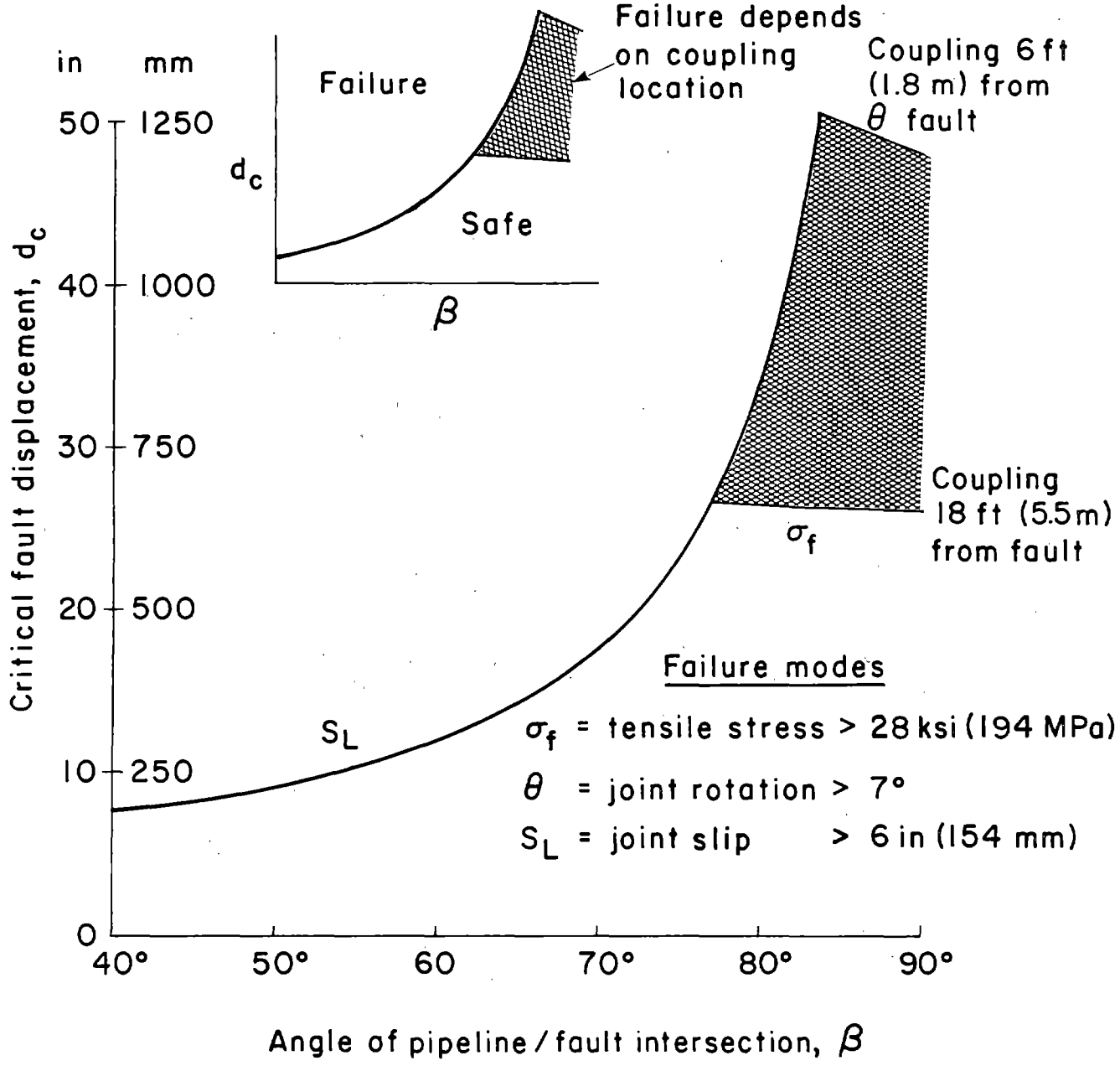

Figure 4.12 Critical fault displacement as a function of fault angle for cast iron pipeline with Dresser long couplings and distributed fault movement.

Compared with the response to abrupt fault movement, the distributed movement has a significant effect on the critical fault displacement. For angles of pipeline/fault intersection higher than approximately 78 degrees, the pipeline can sustain a distributed fault offset nearly three times that caused by an abrupt displacement. As the angle of pipeline/fault intersection decreases below 78 degrees, the pipeline is subject to pull-out at successively lower values of critical fault displacement. Below an angle of pipeline/fault intersection of 63 degrees, the critical fault displacements for both distributed and abrupt movement are the same.

4.7 Relationship between Bending and Pull-Out Failure.

For most combinations of pipe diameter, pipe length, and type of flexible coupling, the failure of cast-iron mains at high angles of pipeline/fault intersection can be determined conservatively on the basis of bending failure. Hence, the relationship between critical fault displacement and the angle of pipeline/fault intersection can be represented by two distinct curves: one determined by bending failure of the pipe - and the other by axial pull-out at a coupling.

At the critical fault displacement, d_c, the longitudinal extension S of the pipeline is closely approximated by

$$S = d_c \cos \beta + \frac{d_c^2 \sin^2 \beta}{4L} \qquad (4.4)$$

where β is the angle of pipeline/fault intersection and L is the distance on one side of the fault over which the pipeline displacement occurs.

The second term in Equation 4.4 is related to the geometric distortion that accompanies a purely transverse displacement. For typical values of d_c and L, the axial slip contributed by geometric distortion will be less than 5 percent of the allowable slip at a coupling. By neglecting the second term in

Equation 4.4 and substituting the allowable slip at the coupling, S_L, for S, a simple relationship between the critical fault displacement, allowable slip, and angle of pipeline/fault intersection is given by:

$$d_c = S_L \sec \beta \tag{4.5}$$

The critical fault displacement is defined solely on the basis of bending failure, as

$$d_c = d_{cb} \csc \beta \tag{4.6}$$

where d_{cb} is the critical fault displacement that causes bending failure at an angle of pipeline/fault intersection equal to 90 degrees. The relationship between d_{cb} and the nominal pipe diameter, D, is shown in Figure 4.5.

Substituting Equation 4.6 into Equation 4.5 yields

$$\tan \beta = \frac{d_{cb}}{S_L} \tag{4.7}$$

which defines the angle of pipeline/fault intersection corresponding to the transition point between pipeline failure caused by bending as opposed to failure caused by pull-out at a coupling.

Equations 4.5 and 4.6 can be used to develop a family of curves that define the critical fault displacement on the basis of failure by pull-out and bending, respectively. Using Equation 4.5, each curve is defined according to the allowable slip available with a particular type of coupling. In a similar manner, each curve is defined using Equation 4.6 according to the nominal pipe diameter.

Figure 4.13 illustrates how the relationship between critical fault displacement and the angle of pipeline/fault intersection can be developed for

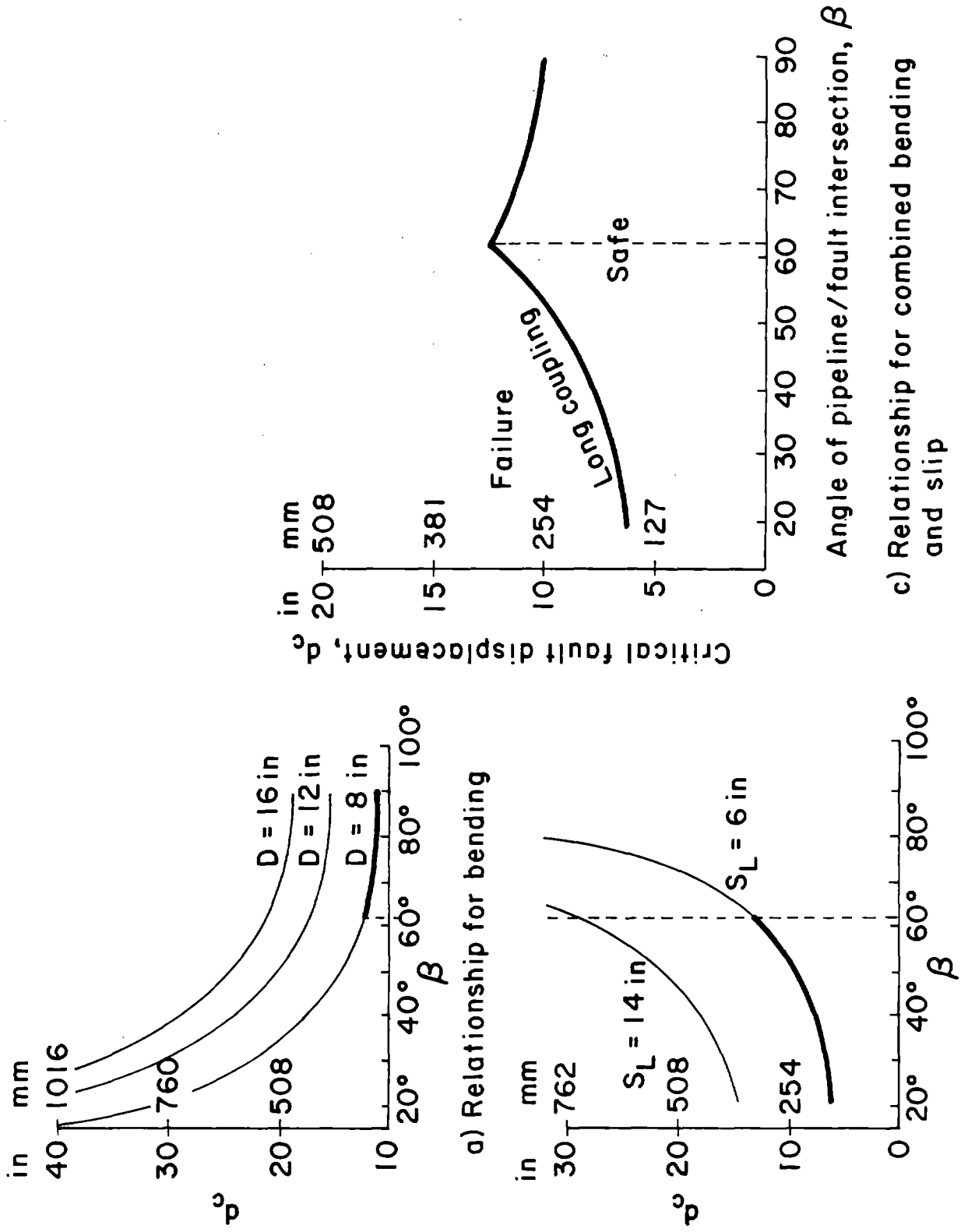

Figure 4.13 Relationship between critical fault displacement and fault angle for bending and pullout failure - Dresser long coupling.

an 8 in (203 mm) diameter pipeline with a long coupling located at or near the fault centerline. As determined from Figure 4.5, the critical fault displacement that causes binding failure is 11.6 in (295 mm). The allowable slip at the long coupling is 6 in (152 mm). Using Equation 4.7, the angle of pipeline/fault intersection that defines the transition point between failure by bending and coupling pull-out is 63 degrees. Accordingly, the portions of the curve corresponding to bending failure (Figure 4.13a) and pull-out failure (Figure 4.13b) are joined to construct the failure envelope shown in Figure 4.13c. This envelope is identical to the lower bound values shown in Figure 4.11, which were determined by the finite element simulations.

This general method can be extended to cover a variety of coupling types. For example, extra long, restrained couplings have been recommended by the Cast Iron Pipe Research Institute (15) as a protective measure against earthquake-induced ground movements. The restrained coupling allows axial slip, but prevents pull-out with a restraining gland attached on each side of the long coupling. Assuming that a long coupling is modified with restraining glands, the allowable axial slip at the coupling would be approximately 12 in (305 mm). Longitudinal components of movement in excess of 12 in (305 mm) would be transmitted to the mechanical coupling nearest the fault. Consequently, the total axial slip would be approximately 14 in (356 mm) before pull-out failure occurred at the mechanical joint. The allowable slip of 14 in (356 mm) is used both to plot the portion of the failure envelope controlled by coupling pull-out and to define the transition point between pull-out and tensile failure. This process is illustrated in Figure 4.14 which shows how the failure envelope is constructed for an 8 in (203 mm) diameter line.

A comparison of Figure 4.13 and 4.14 shows how the failure envelope changes as provision for increasingly greater magnitudes of axial slip is

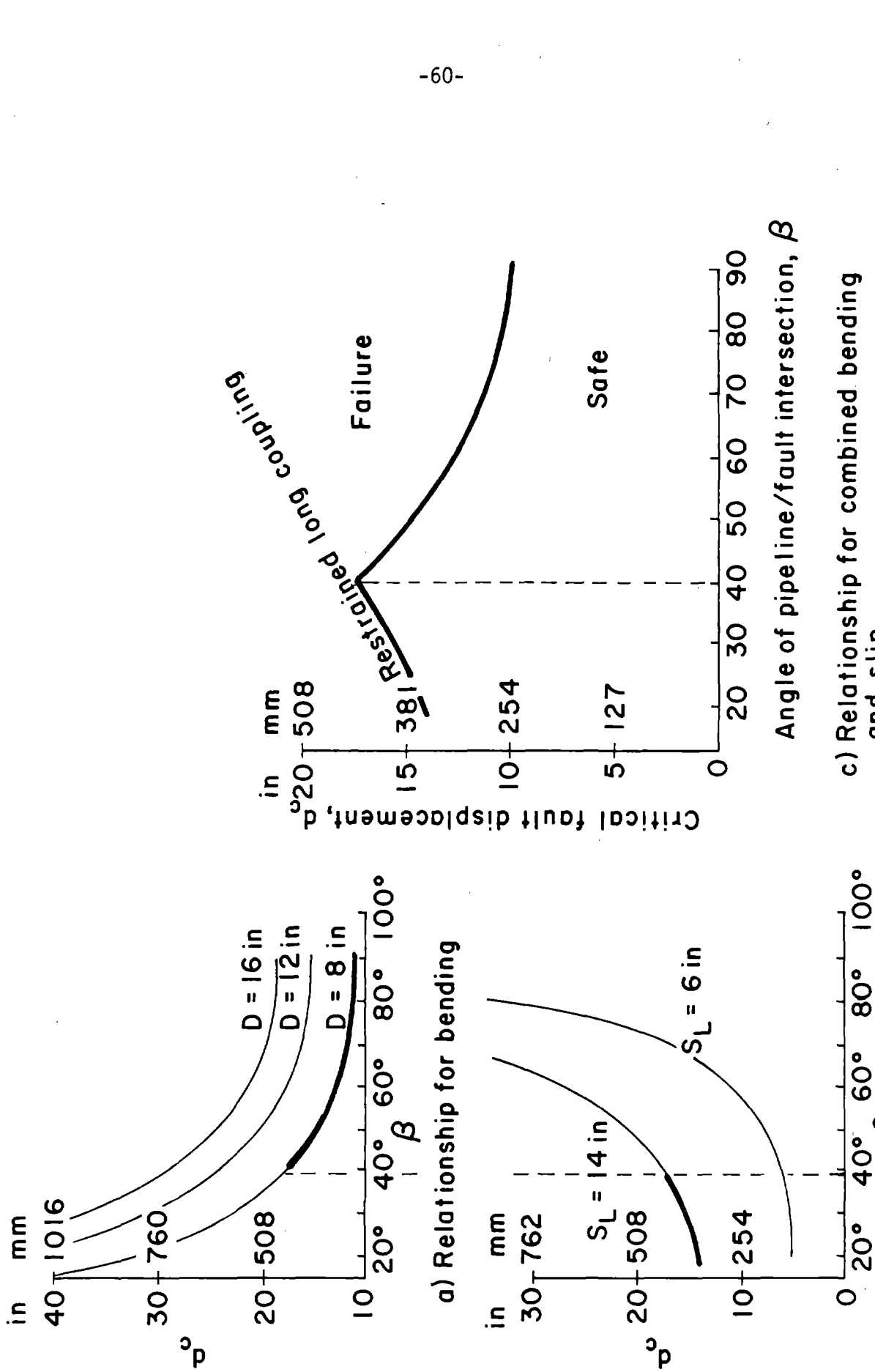

Figure 4.14 Relationship between critical fault displacement and fault angle for bending and pullout failure - Dresser long coupling with restraining gland.

incorporated in the line. In all cases, the optimum orientation of the pipeline relative to the fault occurs in the vicinity of the transition point. Accordingly, if the angle of pipeline/fault intersection is fixed, modification of the pipeline by installing special long couplings will only be justified if the pipeline is oriented at an angle less than the one that defines its current transition point.

4.8 Summary

The analytical procedures for modeling pipeline behavior described in this chapter are suitable for articulated lines made of various pipe lengths and coupling types. The analytical methods are sufficiently general to model a variety of pipe materials, provided that the stress/strain behavior is bounded either by the brittle failure or yield stress of the material.

The most important parameter affecting the response of jointed pipelines to fault displacement is the angle of pipeline/fault intersection. As the angle decreases, increasingly greater proportions of the fault displacement are transmitted to the pipeline as slip at the coupling nearest the fault. For pipelines joined with lead-caulked and mechanical couplings, failure is controlled principally by coupling pull-out at angles of pipeline/fault intersection less than about 80 degrees. The use of special, long couplings at or near the fault centerline will diminish the angle of pipeline/fault intersection below which failure will be controlled by coupling pull-out.

Pipeline response to abrupt strike-slip movement can be represented as a plot of the critical fault displacement versus the angle of pipeline/fault intersection for pipelines with flexible, gasketed couplings. This plot can be represented as two distinct curves: one determined by bending failure of the pipe and the other by axial pull-out at a coupling. The optimum orientation of the pipeline relative to the fault occurs at the angle associated with the transition point between failure by bending and coupling pull-out.

CHAPTER 5

CONCLUSIONS AND RECOMMENDATIONS FOR FUTURE RESEARCH

5.1 Conclusions

Earthquake records show that, in comparison to surface structures, pipeline systems are particularly vulnerable to local concentrations of permanent differential movements. Nevertheless, many pipelines typical of water and gas distribution systems can sustain relatively large displacements, depending on the pattern of imposed ground movement and the composition of the lines. For example, repair records in Hollister, California show a very low incidence of damage to water and gas mains crossing the Calaveras fault. This low level of damage exists, even though fault creep in Hollister occurs at a rate of approximately 0.4 in/yr (10 mm/yr) and that, since their installation, many of the lines have been subjected to between 15 and 20 in (381 and 508 mm) of total lateral offset.

The performance of typical distribution mains depends largely on pipeline construction and the pattern of imposed ground movements. The major parameters related to pipeline construction include the stress/strain behavior of the pipe material and the pull-out and rotational characteristics of the couplings. The most important parameters relating to ground movement include the distribution of displacement and, for lines crossing faults or other zones of abrupt displacement, the orientation of the pipeline relative to the strike of the movement zone.

Pipeline composition, particularly with regard to the type of couplings used, can have a significant effect on the ability of the line to sustain permanent differential movement. Records of repair along the Sylmar segment of the San Fernando fault zone show that cast iron mains with rubber gasket joints performed

substantially better than those with cement-caulked joints. In addition, lines composed of Mannesman steel, which are highly susceptible to internal corrosion, were far more heavily damaged than lines composed of cast iron or other types of steel.

The most important parameter affecting the response of jointed pipelines to strike-slip faulting is the angle of pipeline/fault intersection. For pipelines joined with lead-cualked and mechanical couplings, failure is controlled principally by coupling pull-out at angles of pipeline/fault intersection less than about 80 degrees. For angles of pipeline/fault intersection greater than 80 degrees, the pipeline performance is related closely to the type of coupling and to the location of the coupling relative to the fault centerline. At high angles of pipeline/fault intersection, analyses for cast iron mains show that pipelines with mechanical couplings can accommodate from two to ten times the magnitude of fault offset that can be sustained by pipelines with lead-cualked couplings.

The pattern of differential ground movements at fault crossings generally will fall within the two limiting conditions of: 1) abrupt, planar displacement, and 2) distributed movements typical of fault creep. Using a hyperbolic function to model distributed fault movement, analyses indicate that an 8 in (203 mm) diameter, cast iron pipeline can tolerate up to three times as much fault offset as the same line can accommodate when subject to abrupt, planar displacement.

Pipeline response to abrupt, strike-slip displacement can be represented as a plot of the critical fault displacement versus the angle of pipeline/fault intersection. Since the critical fault displacement is defined as the relative fault offset at which pipeline failure occurs, this plot represents a failure envelope. For pipelines with flexible, gasketed couplings, the relationship between the critical fault displacement and the angle of pipeline/fault intersection

can be represented as two distinct curves: one determined by bending failure of the pipe and the other by axial pull-out at a coupling. In all cases, the optimum orientation of the pipeline relative to the fault occurs at the transition point between failure by bending and coupling pull-out. Accordingly, if the angle of pipeline/fault intersection is fixed, modification of the pipeline by installing special long couplings will only be justified if the pipeline is oriented at an angle less than the one that defines its current transition point.

5.2 Recommendations for Future Research

There are four areas where future work can be directed to improve the current state of practice in Lifeline Earthquake Engineering with regard to both the analysis of pipeline performance and the development of earthquake resistant design. The areas are numbered and discussed as follows:

1. Earthquake-induced ground failure includes faulting, landslides, soil liquefaction, seismic compaction, and local lurching and squeezing of the soil. There is a need to characterize the patterns of ground movement typical of the various ground failure modes in a manner that is calibrated specifically to buried pipelines of different composition. Currently, there are many excellent published observations of pipeline response to permanent earthquake movements that can form a sound basis for summarizing movement patterns in terms of their potential for pipeline damage. Sources of unpublished information include the records of public utility companies regarding both earthquake repair and long-term maintenance in areas of fault creep.

2. The analytical procedures developed in this report can be used to model the performance of jointed pipelines in which the stress/strain behavior of the pipe is bounded either by the brittle failure or yield stress of the pipe material. These analytical procedures should be extended to cover the plastic deformation of pipe material such as steel and ductile iron. Of great importance

is the maximum curvature which develops in the pipe for high angles of pipeline/fault intersection. The analyses in this report show that the point of maximum curvature occurs within twelve feet of an abrupt, planar fault for most typical distribution lines. The provision for axial slip afforded by mechanical or Dresser couplings implies that the failure of jointed, ductile pipe at near vertical angles of pipeline/fault intersection will occur principally as bending and will be related to plastic hinge formation at the point of maximum curvature.

3. To date, the analyses of pipeline response to faulting have been performed for pipelines subject to extension. Nevertheless, strike-slip and reverse faulting can cause substantial compression. There is a great need to study pipeline response to strike-slip faulting in a compression mode. In many cases compressive strains are more damaging than tensile strains. In jointed pipelines, compressive strains may lead to severe stress concentrations at the bell ends of lead-caulked or mechanical couplings. Compressive slip at Dresser couplings will push the soil encrusted sides of the pipe into the gasket seal and, therefore, will be more likely to cause leakage than tensile slip.

4. The performance of articulated pipelines subject to both seismic shaking and permanent differential ground movements will be highly dependent on the response of the couplings. Consequently, there is a great need to characterize coupling behavior more reliably than is possible on the basis of existing data. Items that deserve special attention include 1) the short and long-term performance of pressurized lead and cement-caulked joints subject to combined extension and rotation, 2) the effect of scaling and surface deposits on the pull-out capacity of gasketed couplings for water mains, and 3) the behavior of gasketed couplings subject to bending after they become metal-bound.

REFERENCES

1. Allen, C. R. and J. M. Nordquist (1972), "Foreshock, Main Shock, and Larger Aftershocks of the Borrego Mountain Earthquake", U.S. Geological Survey Professional Paper 787, pp. 16-23.

2. Allen, C. R., M. Wyss, J. N. Brune, A. Gantz, and R. E. Wallace (1972), "Displacements on the Imperial, Superstition Hills and San Andreas Fault Triggered by the Borrego Mountain Earthquake", U.S. Geological Survey Professional Paper 787, pp. 87-104.

3. American Society for Metals (1978), Metals Handbook Ninth Edition, Vol. 1, American Society for Metals, Metals Park, Ohio 44073.

4. Angus, H. T. (1960), Physical and Engineering Properties of Cast Iron, B.C.I.R.A., Birmingham, England, p. 528.

5. Audibert, J. M. E. and K. J. Nyman (1977), "Soil Restraint Against Horizontal Motion of Pipes", Journal Geot. Engr. Div., ASCE, Vol. 103, No. GT10, pp. 1119-1142.

6. Bolt, B. A. (1975), "Earthquake Risk in Relation to Earthquake Characteristics", Bull. 196 California Div. of Mines and Geology, pp. 314-322.

7. Bonilla, M. G. (1959), "Geologic Observations in the Epicentral Area of the San Francisco Earthquake of March 22, 1957", Special Report 57, California Div. of Mines and Geology.

8. Boresi, A. P., O. M. Sidebottom, F. B. Seely and I. O. Smith (1978), Advanced Mechanics of Material, John Wiley and Sons, New York.

9. British Cast Iron Research Assoc. (1951), Typical Microstructure of Cast Iron, B.C.I.R.A., Alvechurch, Birmingham, England.

10. Brown, R. D. and R. E. Wallace (1968), "Current and Historic Fault Movement Along the San Andreas Fault Between Pacines and Camp Dix, California", Proc. Conf. on Geologic Problems of the San Andreas Fault System, Stanford University Publ., Geological Sciences, Vol. XI, pp. 22-41.

11. Brown, R. D., P. L. Ward, and G. Plafker (1973), "Geologic and Seismologic Aspects of the Managua, Nicaragua, Earthquakes of December 23, 1972", U.S. Geological Survey Professional Paper 838.

12. Buwalda, J. P. and P. St. Amand, "Geological Effects of the Arvin-Tehapachi Earthquake", Bulletin 171, Earthquakes in Kern County California during 1952, California Div. of Mines and Geology.

13. Cajina, A. (1977), "The Managua Earthquake and Its Effects on the Water Supply System", Proc. Earthquake Engr. Res. Inst. Conf., Oakland, CA, Vol. 2, pp. 768-790.

14. Cast Iron Pipe Research Assoc. (1978), Handbook: Ductile Iron Pipe, Cast Iron Pipe, 5th Edition, C.I.P.R.A., 1301 W 22nd St., Oak Brook, IL 60521, pp 103-140.

15. Cast Iron Pipe Research Assoc. (1976), "Earthquake and Other Geologic Hazards: Protective Design for Underground Pipe", Civil Engineering, ASCE, Sept. 1976, p. 35.

16. Clark, M. M. (1972), "Surface Rupture Along the Coyote Creek Fault", U.S. Geological Survey Professional Paper 787, pp. 55-86.

17. Cloud, W. K. (1959), "Intensity and Ground Motion of the San Francisco Earthquake of March 22, 1957", Special Report 57, California Div. of Mines and Geology.

18. Clough, G. W. and J. L. Chameau (1979), "A Study of the Behavior of the San Francisco Waterfront Fills under Seismic Loading", Final Report No. 35, Contract No. USGS-14-08-0001-16763, John A. Blume Earthquake Engineering Center, Stanford University.

19. Cluff, L. S. and G. A. Carver (1978), "Geological Observations, Managua, Nicaragua Earthquake of December 23, 1972", Reconnaissance Report, Earthquake Engineering Research Institute, pp. 5-20.

20. Coffin, C. L. (1950) "Stress Analysis of a 125-lb. Cast Iron Valve Assembly", Symposium on Testing of Cast Iron with SR-4 Type of Gage, ASTM Spec. Pub. No. 97.

21. Committee on Cast Iron Pipe Joints (1915), "Report of Committee on Cast Iron Pipe Joints", Proc. of American Gas Inst., Vol. 10, pp. 312-343.

22. Degenkolb, H. J. (1955), "Structural Observations of the Kern County Earthquake", ASCE Trans. Vol. 120, pp. 1280-1294.

23. Duncan, J. M. and C. Y. Chang (1970), "Non-linear Analysis of Stress and Strain in Soils", Journ. Soil Mech. Found. Div., ASCE, Vol. 96, No. SM6, pp. 1629-1654.

24. Durham, H. W. (1931), "Managua - Its Construction and Utilities", Engr. News Record, April 23, 1931, pp. 696-700.

25. Duryea, E., C. D. Marx, F. Riffle, A. L. Adams, and W. W. Harts (1907), "The Effects of the San Francisco Earthquake of April 18, 1906 on Engineering Constructions", Proc. ASCE, Vol. 33, No. 3, pp. 299-348.

26. Eckel, E. B. (1967), "Effects of the Earthquake of March 27, 1964 on Air And Water Transport, Communications and Utilities Systems in South-Central Alaska", U.S. Geological Survey Professional Paper 545-B, pp. B1-B27.

27. Eckel, E. B. (1970), "The Alaska Earthquake of March 27, 1964: Lessons and Conclusions", U.S. Geological Survey Professional Paper 546, pp. 1-57.

28. Erickson, M. A. (1950), "Stress Analysis of Automotive Cylinder Blocks", Symposium on Testing of Cast Iron with SR-4 Type of Gage, ASTM Spec. Pub. No. 97.

29. Fraser, G. D. (1964), "The Hebgen Lake, Montana, Earthquake of August 17, 1959: Intensity, Magnitude, and Ground Breakage", U.S. Geological Survey Professional Paper 435-F, pp. F31-F35.

30. Friedman, M., J. Handin, J. M. Logan, K. D. Min, and A. W. Stearns (1976), "Experimental Folding of Rocks Under Confining Pressure: Part III Faulted Drape Folds In Multilithologic Layered Specimens", Bull. Seismological Society of America, Vol. 87, pp. 1047-1066.

31. Gilbert, G. N. J. (1959), "An Evaluation of the Stress-Strain Properties of Flake Graphite Cast Iron in Tension and Compression", B.C.I.R.A. Journ., Vol. 7, No. 13, pp. 745-789.

32. Hadley, J. B. (1964), "Landslides and Related Phenomena Accompanying the Hegben Lake Earthquake of August 17, 1959", U.S. Geological Survey Professional Paper 435-K, pp. K197-K138.

33. Hansen, J. B. (1961), "The Ultimate Resistance of Rigid Piles Against Transversal Forces", Bulletin 12, Danish Geotechnical Institute, Copenhagen, Denmark.

34. Hansen, W. R. (1965), "Effects of the Earthquake of March 27, 1967 at Anchorage, Alaska", U.S. Geological Survey Professional Paper 542-A, pp. A1-A68.

35. Hardy, H. M. and T. D. Kuivinen (1950), "Strain Testing of Crankshafts, Engine Frames, and Cylinders", Symposium on Testing of Cast Iron with SR-4 Type of Gage, ASTM Spec. Pub. No. 97.

36. Heath, E. G. and F. B. Leighton (1973), "Subsurface Investigation of Ground Rupturing During San Fernando Earthquake, San Fernando, California Earthquake of February 9, 1971. U.S. Dept. of Commerce, Vol. III, pp. 165-172.

37. Hemborg, H. B. (1955), "Damage to Water Works Systems, Arvin-Tehachapi Earthquake", Bulletin 171, Earthquakes in Kern County California during 1952, California Div. of Mines and Geology.

38. Hillman, V. E. (1950), "Stress-Strain Studies of Cast Iron for Textile Machinery Parts", Symposium on Testing of Cast Iron with SR-4 Type of Gage, ASTM Spec. Pub. No. 97.

39. Housner, G. W. and P. C. Jennings (1972), "The San Fernando California Earthquake", Int'l. Journ. Earthquake Engr. and Structural Dynamics. Vol. 1, pp. 5-31.

40. Isenberg, J. (1978a) "The Role of Corrosion in the Seismic Performance of Buried Steel Pipelines in Three United States Earthquakes", Grant Report No. 6, Prepared for NSF, 1800 G. Street, Washington, D.C. 20550, Grant No. DRF 78-15049.

41. Isenberg, J. (1978b), "Seismic Performance of Underground Water Pipelines in The Southeast San Fernando Valley in the 1971 San Fernando Earthquake", Grant Report No. 8, Prepared for NSF, 1800 G. Street, Washington, D.C., 20550, Grant No. DRF 78-15049.

42. Johnson, A. E. (1979), "Stress Analysis of Gas Transmission Line 103 at the Calaveras Fault Crossing in Hollister, California", Pacific Gas and Electric Co., Dept. of Engr. Research, Report 463-79.

43. Johnson, J. B., (1889), "Cast Iron-Strength, Resiliance Tests, and Specifications", Transactions ASCE, Advance Copy, Vol. 21, pp. 1-31.

44. Kamb, B., L. T. Silver, M. J. Abrams, B. A. Carter, T. H. Jordan, and J. B. Minster (1971), "Pattern of Faulting and Nature of Fault Movement in the San Fernando Earthquake", The San Fernando, California, Earthquake of February 9, 1971, U.S. Geological Survey Professional Paper 733, pp. 41-54.

45. Kennedy, R. P., A. W. Chow, and R. A. Williamson (1977), "Fault Movement Effects on Buried Oil Pipeline", Journal of Transp. Engr. Div., ASCE, Vol. 103, No. TE5, pp. 617-633.

46. Kennedy, R. P., A. C. Darrow, and S. A. Short (1979), "Seismic Design of Oil Pipeline Systems", Journ. of Tech. Councils, ASCE, Vol. 105, No. TC1, pp. 119-134.

47. King, P. V. and J. M. Betz (1972), "Earthquake Damage to a Sewer System", Journ.of Water Pollution Control Federation, Vol. 44, No. 5., pp. 859-867.

48. Krinitzsky, E. L. (1974), "State of the Art for Assessing Earthquake Hazards in the United States: Fault Assessment in Earthquake Engineering", Miscellaneous Paper S-73-1, Report 2, U.S. Army Engineer Waterways Experiment Station.

49. Lawson, A. C. (1908), "The California Earthquake of April 18, 1906", Carnegie Institute of Washington, D.C., Publication No. 87.

50. Long, E. and W. George (1967), "Buttress Design for Earthquake-Induced Slides", Journ. of Soil Mech. and Found. Div., ASCE, Vol. 93, No. SM4, pp. 595-608.

51. Mahan, J. F., H. J. Dekenkolb, D. F. Maron, and K. V. Steinbrugge (1973), "Engineering Aspects, Managua, Nicaragua Earthquake of December 23, 1972", Reconnaissance Report, Earthquake Engineering Research Institute, pp. 27-214.

52. Maynard, T. R. and T. D. O'Rourke (1977), "Soil Movement Effect on Adjacent Public Facilities", Conference Preprint 3111, ASCE Annual Meeting, San Francisco, October.

53. McCulloch, D. S. and M. G. Bonilla (1970), "Effects of the Earthquake of March 27, 1964 on the Alaska Railroad", U.S. Geological Survey Professional Paper 545-D, pp. D1-D159.

54. McNorgan, J. D. (1973), "Gas Line Response to Earthquakes", Journal of Transp. Engr. Div., ASCE, Vol. 99, No. TE4, pp. 821-826.

55. Manefee, F. N. and A. E. White (1978), "A Study of Centrifugally-Cast and Sand-Cast Pipe", Dept. of Engr. Research, University of Michigan, No. 4.

56. Meyers, W. D. and W. Hamilton (1964), "Deformation Accompanying the Hebgen Lake Earthquake of August 17, 1959", U.S. Geological Survey Professional Paper 435-I, pp. I55-I98.

57. Moran, D. E. and C. M. Duke (1975), "An Engineering Study of the Behavior of Public Utility Systems in the San Fernando Earthquake of February 9, 1971", Bull. 196, California Div. of Mines and Geology, pp. 407-429.

58. Nason, R. D. (1971), "Instrumental Monitoring of Post-Earthquake Fault Movements (Afterslip)," U.S. Geological Survey Professional Paper 733, pp. 89-90.

59. Newmark, N. M. and W. J. Hall (1975), "Pipeline Design to Resist Large Fault Displacement", Proc. U.S. Nat'l. Conf. on Earthquake Engr., Ann Arbor, Mich., pp. 416-425.

60. O'Rourke, M. J. and L. R. Wang (1978), "Earthquake Response of Buried Pipelines", Grant Report No. 4, Prepared for NSF, 1800 G. Street, Washington, D.C., 20550, Grant No. ENV 76-14884.

61. O'Rourke, T. D. and C. H. Trautmann (1980), "Buried Pipeline Response to Permanent Earthquake Ground Movements", Pressure Vessels and Piping Conference, San Francisco, California, August 12-15, 1980, Paper No. 80-C2/PVP-78.

62. Plenard, E., (1964), "The Elastic Behavior of Cast Iron", Merchant, H.D. (Ed), Recent Research on Cast Iron: Gordon and Breach, New York.

63. Poulos, H. G. (1974), "Analysis of Longitudinal Behavior of Buried Pipes", Proc. Conf. on Analysis and Design in Geotechnical Engineering, ASCE, Austin, Texas, Vol. 1, pp. 199-223.

64. Prior, J. C. (1935), "Investigation of Bell and Spigot Joints in Cast Iron Water Pipes", Bull. 87, Ohio State University Engineering Experiment Station.

65. Radbruch, D. H. and M. G. Bonilla (1966), "Introduction: Tectonic Creep in the Hayward Fault Zone, California", U.S. Geological Survey Circular 525, pp. 1-3.

66. Radbruch, D. H. and B. J. Lennert (1966), "Damage to Culvert under Memorial Stadium, University of California at Berkeley", Tectonic Creep in the Hayward Fault Zone, California, U.S. Geological Survey Circular 525, pp. 3-6.

67. Richter, C. F. (1958), Elementary Seismology, W. H. Freeman and Co., Inc.

68. Schulz, S. S., R. O. Burford, and R. D. Nason (1975), "Catalog of Creepmeter Measurements in Central California for 1973 through 1975", U.S. Geological Survey Open-File Report 77-31.

69. Scott, N. H. (1973), "Felt Area and Intensity of San Fernando Earthquake", San Fernando, California, Earthquake of February 9, 1971, U.S. Dept. of Commerce, Vol. III, pp. 23-48.

70. Seismological Field Survey, NOAA (1972), "Intensity, Distribution and Field Effects, Strong-Motion Seismograph Records, and Response Spectra", U.S. Geological Survey Professional Paper 787, pp. 141-157.

71. Slemmons, D. C. (1977), "State-of-the-Art for Assessing Earthquake Hazards in the United States: Faults and Earthquake Magnitude", Miscellaneous Papers S-73-P, Report 6, U.S. Army Engineer Waterways Experiment Station.

72. Smalley, O., (1949), "Stress-Strain Tests on Rectangular Cast Iron Beams", "Symposium on Testing of Cast Iron with SR-4 Type of Gage", ASTM Spec. Pub. No. 97.

73. Smith, J. L. and R. B. Fallgren (1975), "Ground Displacement at San Fernando Juvenile Hall and the Sylmar Convertor Station", Bull. 196, California Div. of Mines and Geology, pp. 157-163.

74. Southern California Gas Company (1973), "Earthquake Effects on Southern California Gas Company Facilities", San Fernando, California, Earthquake of February 9, 1971, U.S. Dept. of Commerce, Vol. II, pp. 59-64.

75. Southern Research Institute (1957), "Holding Power of Mechanical Pipe Joints", Final Report No. 4 to Cast Iron Pipe Research Institute, 1301 W. 22nd. Street, Oak Brook, Ill. 60521.

76. Steinbrugge, K. V., V. R. Bush and E. G. Zacher (1959), "Damage to Buildings and Other Structures during the Earthquake of March 22, 1957", Special Report 57, California Div. of Mines and Geology.

77. Steinbrugge, K. V., W. K. Cloud, and N. H. Scott (1970), "The Santa Rosa, California, Earthquakes of October 1, 1969", U.S. Dept. of Commerce, Rockville, MD.

78. Steinbrugge, K. V., and D. F. Moran (1954), "An Engineering Study of the Southern California Earthquake of July 21, 1952 and Its Aftershocks", Bull. Seismological Society of America, Vol. 44, pp. 199-462.

79. Steinbrugge, K. V., E. E. Schader, H. C. Bigglestone, and C. A. Weers (1971), "San Fernando Earthquake February 9, 1971", Pacific Fire Rating Bureau, 465 California Street, San Francisco, CA.

80. Steinbrugge, K. V. and E. G. Zacher (1960), "Fault Creep and Property Damage", Bull. Seismological Society of America, Vol. 50, pp. 389-396.

81. Steinhardt, O. W. (1978), "Protecting a Power Lifeline against Earthquakes", Journ. of Tech. Councils of ASCE, Vol. 104, No. TC1, pp. 49-57.

82. Stearns, D. W. (1978), "Faulting and Forced Folding in the Rocky Mountains Foreland", Geological Soc. of Amer., Memoir 151, Laramide Folding Associated with Basement Block Faulting in the Western United States, ed. by V. Matthews III, pp. 1-37.

83. Subcommittee on Water and Sewerage Systems (1973), "Earthquake Damage to Water and Sewerage Facilities", San Fernando, California, Earthquake of February 9, 1971, U.S. Dept. of Commerce, Vol. II, pp. 75-193.

84. Sulton, D. I. (1931), "The Managua Earthquake", Military Engineer, Vol. 23, pp. 354-361.

85. Sylvester, A. G. and D. D. Pollard (1975), "Afterslip on the Sylmar Fault Segment", Bull. 196, California Div. of Mines and Geology, pp. 227-233.

86. Taylor, C. L. and L. S. Cluff (1977), "Fault Displacement and Ground Deformation Associated with Surface Faulting", Proc. Conf. on Current State of Knowledge of Lifeline Earthquake Engineering, ASCE, pp. 338-353.

87. Tocher, D. (1959), "Seismographic Results from the 1957 San Francisco Earthquakes", Special Report 57, California Div. of Mines and Geology.

88. Tocher, D. (1960), "Creep Rate and Related Measurements at Vineyard, California", Bull. Seismological Society of America, Vol. 50, pp. 397-404.

89. Ulrich, F. P. (1941), "The Imperial Valley Earthquakes of 1940", Bull. Seismological Society of America, Vol. 31, pp. 13-31.

90. Untrauer, R. E., T.-T. Lee, W. W. Sanders, Jr., and M. H. Jawad, (1970), "Design Requirements for Cast Iron Soil Pipe", Bull. 199, Iowa State University Engineering Research Institute, pp. 60-109.

91 U.S. Geological Survey Staff (1971), "Surface Faulting", The San Fernando, California, Earthquake, February 9, 1971, U.S. Geological Survey Professional Paper 733, pp. 55-76.

92. Witkind, I. J. (1964), "Structural Damage in the Hebgen Lake - West Yellowstone Area", U.S. Geological Survey Professional Paper 435-B, pp. B5-B11.

93. Witkind, I. J. (1964), "Reactivated Faults North of Hebgen Lake", U.S. Geological Survey Professional Paper 435-G, pp. G37-G50.

94. Yamashita, P. A. and R. O. Burford (1973), "Catalog of Preliminary Results from an 18-Station Creepmeter Network along the San Andreas Fault System in Central California for the Time Interval June 1969 to June 1973", U.S. Geological Survey Open-File Report, National Center for Earthquake Research, Menlo Park, CA.

95. Yerkes, R. F., M. G. Bonilla, T. L. Youd, and J. D. Sims (1974), "Geologic Environment of the Van Norman Reservoirs Area, Northern San Fernando Valley, California, U.S. Geological Survey Circular 691-A.

96. Youd, T. L. (1973), "Ground Movements in the Van Norman Lake Vicinity during San Fernando Earthquake", San Fernando, California, Earthquake of February 9, 1971, U.S. Dept. of Commerce, Vol. III, pp. 197-206.

97. Youd, T. L. and S. N. Hoose (1978), "Historic Ground Failures in Northern California Triggered by Earthquakes", U.S. Geological Survey Professional Paper 993, pp. 1-176.

98. Youd, T. L., R. F. Yerkes, and M. M. Clark (1978), "San Fernando Faulting Damage and Its Effect on Land Use", Proc. Conf. Earthquake Engineering and Soil Dynamics, ASCE, Vol. II, pp. 1111-1125.

APPENDIX A

THEORETICAL ANALYSIS AND DATA REVIEW FOR LEAD-CAULKED JOINTS SUBJECT TO BENDING

A.1 Theoretical Analysis

Figure A.1a shows a profile view of a lead-caulked coupling subjected to pure bending. The coupling resists bending by adhesion between the iron and lead along the outside surface of the spigot and by forces normal to the spigot, f_N, at the top and bottom of the coupling. For small rotations, the resisting moment contributed by the normal forces will be small relative to the bending resistance from adhesion. As the moment in the pipe, Mp, increases, the adhesive stresses will increase until the adhesive strength, C_a, is mobilized and slip along the pipe/lead interface occurs. Assuming the initial slip is related to the first occurrence of leakage, a lower bound for leakage can be determined as a function of the resisting moment from adhesion.

Neglecting the normal forces and assuming that rotation occurs about a point where the spigot end of one pipe bears against the hub wall of the other, the threshold moment for leakage at the coupling, M_c, is given by:

$$M_c = 2 \int_0^D \sigma_a \, y \, ds \qquad (A.1)$$

where σ_a is the adhesive stress per unit distance of circumference and y and ds are defined in Figure A.1c. As shown in Figure A.1b, the adhesive stress is distributed linearly and may be expressed as

$$\sigma_a = \frac{C_a \, d_L \, y}{D} \qquad (A.2)$$

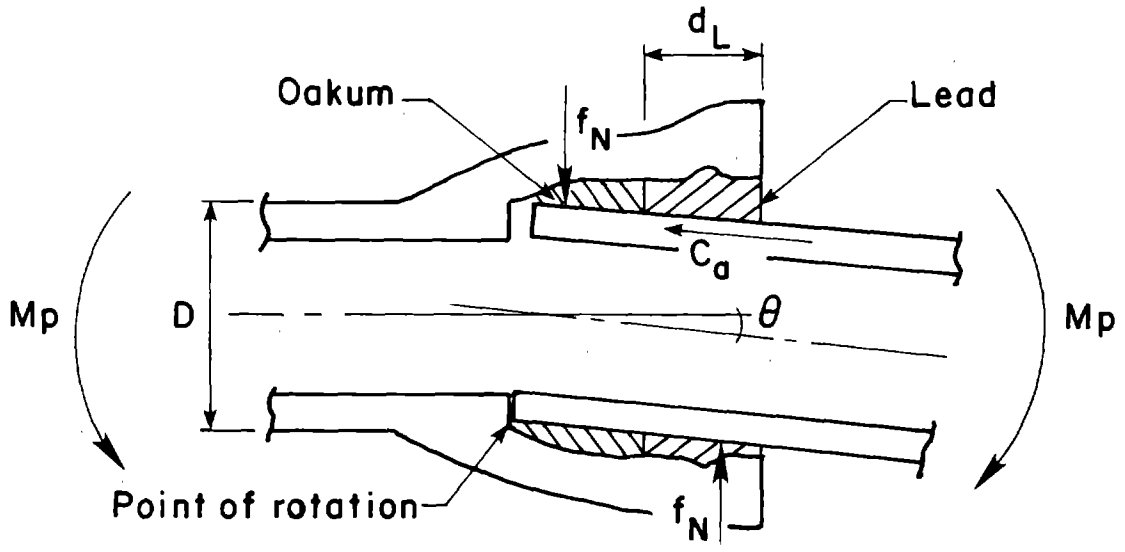

a) Lead-caulked joint subject to pure bending

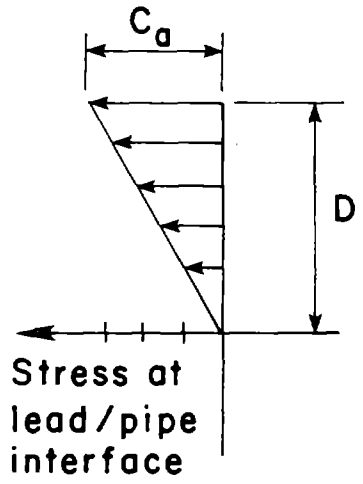

b) Stress distribution

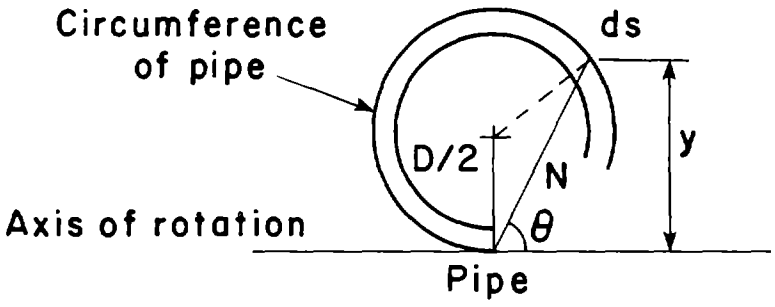

c) Polar geometry of pipe cross-section

Figure A.1 Cross-sectional view and analysis of lead-caulked joint subjected to pure bending.

where d_L is the depth of caulked lead and D is the outside pipe diameter. The dimension y is related to the diameter, D, as

$$y = D \sin^2 \theta \tag{A.3}$$

and

$$ds = D/2 \, d\theta \tag{A.4}$$

Substituting Equations A.2, A.3, and A.4 into Equation A.1 yields

$$M_c = D^2 C_a d_L \int_{-\pi/2}^{\pi/2} \sin^4 \theta \, d\theta \tag{A.5}$$

from which

$$M_c = 3/8 \, \pi D^2 C_a d_L \tag{A.6}$$

In some cases, it may be convenient to define the leakage threshold in terms of pipeline distortion. The bending moment in the pipe, Mp, is related to the pipe curvature, K, as

$$Mp = K EI \tag{A.7}$$

where E and I are the modulus of elasticity and moment of inertia, respectively, of the pipe. For thin-walled pipes the moment is given by

$$Mp = \frac{\pi K E t D^3}{8} \tag{A.8}$$

where t is the pipe wall thickness. Equating Mp and M_c yields

$$K_c = \frac{3\ C_a\ d_L}{D\ t\ E} \qquad (A.9)$$

where K_c is the critical curvature at which leakage starts.

In the absence of severe local restraint and abrupt ground movement, relatively flexible pipelines will deform as the ground deforms. Hence, equation A.9 can be used to relate the leakage threshold with the pattern of soil displacements.

The leakage threshold defined by equations A.6 and A.9 is likely to be a lower bound. Because lead-caulked couplings in water mains are frequently self-healing, the leakage caused by initial slip may not be permanent. Natural gas mains are more vulnerable to distortion, in part, because the oakum in the joints typically dries and shrinks after prolonged exposure to the gas. For gas mains, therefore, it will be prudent to use lower bound criteria.

A.2 Data Review

In a study of the design requirements for buried cast iron pipe, Untrauer et al.(90) subjected a series of lead-caulked, bell-and-spigot couplings to bending and measured the joint rotations and bending moments associated with leakage. For one group of nine tests on nominal four inch (102 mm) diameter, pipe, the average joint rotation and moment at first leakage were 0.9 degrees and 6270 in-lb. (12400 cm-N), respectively. The pipe was filled with water at a constant 5psi (35 KPa) internal pressure. The depth of caulked lead was approximately 0.9 to 1.0 in. (22.5 to 25.4 mm). Using an outside diameter typical of nominal 4 in. (102 mm) diameter pipe and the average adhesive strength determined in Chapter 3, Equation A.6 predicts a threshold moment of 6690 in-lb. (13200 cm-N). This is in excellent agreement with the measured value of 6270 in-lb.

Field measurements of ground movements adjacent to buried pipelines are shown in Figure A.2. These measurements were summarized by Maynard and O'Rourke (52) on the basis of vertical and horizontal displacement surveys adjacent to deep, braced cuts in Chicago.

Of special interest are the two curves, corresponding to cast iron water mains of 12 and 36 in (0.3 and 0.9m) diameter, whose movements are especially well defined. Although the magnitudes of deformation are largest near the central portion of the excavation, the maximum curvatures for both mains are essentially equal and concentrated near the edges of the cuts. The 12 in (0.3 m) diameter line was monitored continuously through the course of its deformation by the Water Distribution Division of the City of Chicago. Local exposures for visual inspection and continuous pressure testing were performed. Hence, the movements shown for the beginning of leakage are very reliable. Leakage eventually developed at the lead-caulked couplings with an especially high level of leakage near the location of maximum curvature. The absence of leakage in the 36 in (0.9m) diameter main is attributed more to the presence of mechanical joints, which retain their sealing capacity while deforming, than to the smaller magnitude of maximum movement.

The maximum curvature determined from the soil movements is approximately 4×10^{-4} ft^{-1} (1.3×10^{-3} m^{-1}). Using an outside diameter and pipe thickness typical of nominal 12 in (0.3m) diameter cast iron pipe, a 2.25 in. (57 mm) depth of caulked lead, and the adhesive strength and secant modulus of cast iron determined in Chapter 3, Equation A.9 predicts a critical curvature of 3.5×10^{-4} ft^{-1} (1.1 m^{-1}). This is in excellent agreement with the measured value.

The criterion for leakage also could be expressed as a rotation. This assumes that relative pipe rotation, as opposed to pipe flexure, is the dominant form of line distortion. From the displacement profile, the rotation

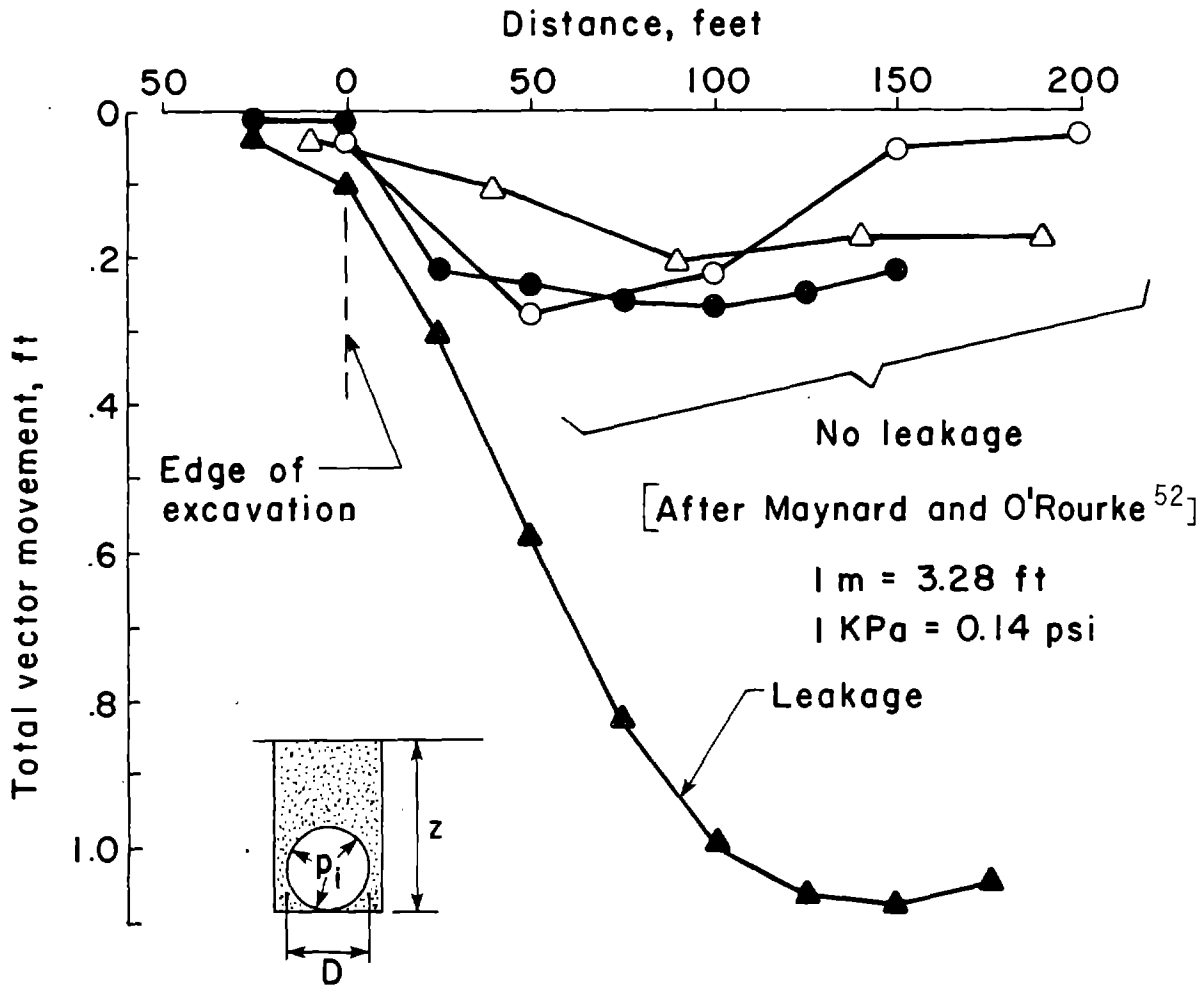

Symbol	Description	Geometry and pressure
▲	Water main, cast iron lead-caulked joints 1938	D = 12 in z = 7.0 ft p_i = 30 psi
△	Water main, cast iron lead-caulked joints pre 1900	D = 48 in z = 7.5 ft p_i = 45 psi
●	Water main, cast iron mechanical joints 1960	D = 36 in z = 5.5 ft p_i = 30-40 psi
○	Gas main, cast iron mechanical joints	D = 6 in z = 4.5 ft p_i = 0.25 psi

Figure A.2 Field observations of buried pipeline response to ground movements.

can be computed as the arc tangent of the change in slope of the plotted movements. The maximum rotation at which leakage was observed in the lead joints was approximately 0.4 degrees.

APPENDIX B

FAULT CREEP AND BURIED PIPELINE OBSERVATIONS IN AREAS OF FAULT CREEP

B.1 Rates of Fault Creep

Some faults exhibit slow, continuous or episodic movements with rates of displacement ranging from nearly zero to about 1.3 in/yr (33 mm/yr), as has been measured along the San Andreas fault (68, 94). Fault creep has been the subject of extensive study during the past two decades and has been discussed by many investigators, including Steinbrugge and Zacher (80), Tocher (88), Brown and Wallace (10), and Radbruch and Bonilla (65). Pipeline damage caused by fault creep has been reported by Steinbrugge and Zacher (80) and Radbruch and Lennert (66).

The USGS has monitored rates of fault creep at numerous locations in central California (68,94). Figure B.1 shows the locations of selected creepmeter stations operated by the USGS.

The USGS creepmeter is a wire extensometer with fixed end points on opposite sides of the fault. Under ideal conditions, measurements are accurate to $\pm$ 0.0001 in (0.003 mm) (94), but accuracy varies considerably with temperature and environmental effects.

Figure B.2 summarizes creep measurements taken at the creepmeter stations shown in Figure 5. Creep is plotted as a function of time, where time is referenced to the date of each creepmeter installation. In the vicinity of Hollister and San Juan Bautista, creep rates are approximately 0.3 to 0.4 in/yr (7.6 to 10.1 mm/yr).

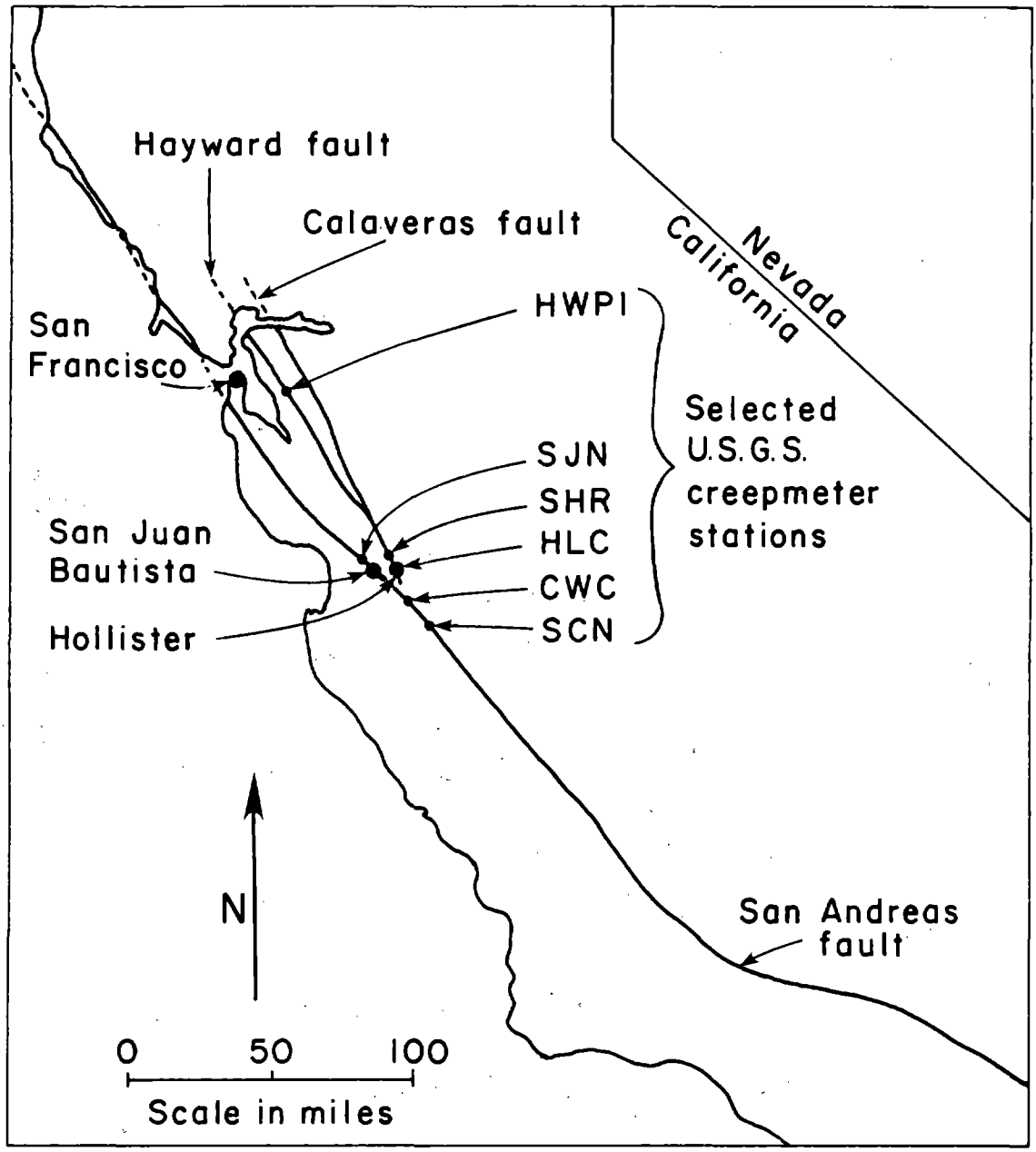

Figure B.1 Map showing locations of selected USGS creepmeter installations.

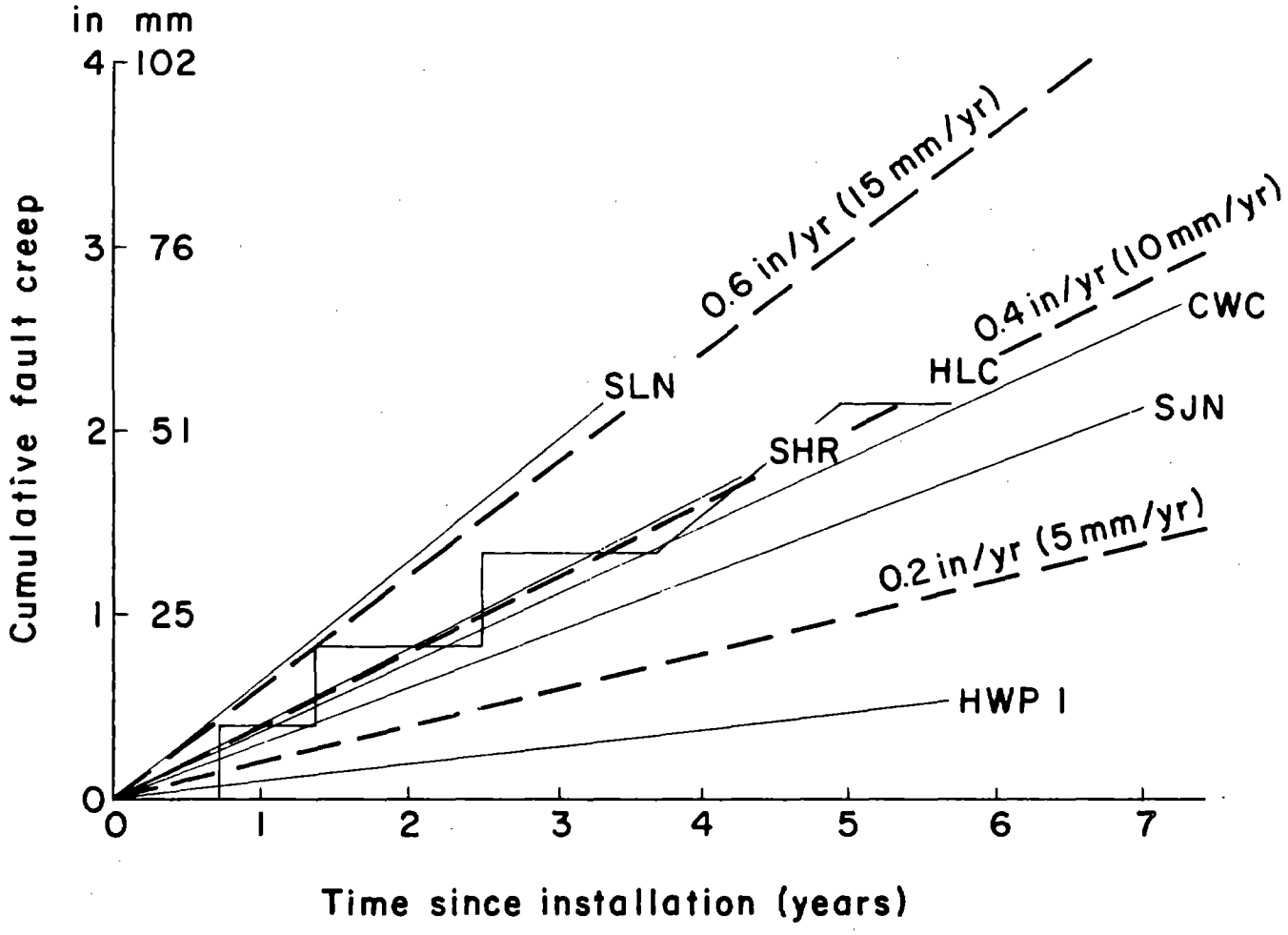

Figure B.2 Rates of fault creep at selected USGS creepmeter installations.

B.2 Pipeline Observations in Areas of Fault Creep

Because creep displacements accumulate slowly, their effect on buried pipelines is gradual. Nevertheless, when integrated over several decades, the total offsets they impose can be similar in magnitude to those associated with earthquakes.

In order to study the long term effects of creep on pipeline performance, field observations and records of pipeline repair were collected for the City of Hollister, California, which straddles the Calaveras fault. As shown in Figure B.2 the average creep rate measured on the main trace of the Calaveras fault in Hollister is approximately 0.4 in/yr (10 mm/yr). The creep occurs principally in events of accelerated displacement, each ranging from 0.2 to 0.4 in (5 to 10 mm). The episodic nature of the movement is shown in Figure B.1 as a step-wise acculumation of displacement.

Figure B.3 shows a plan view of a portion of the gas distribution system that crosses the main trace of the Calaveras fault in Hollister. Also shown is a 12-in (305 mm) diameter gas transmission line that crosses the fault near the northern boundary of the city. Most of the distribution system comprises either welded or coupled steel pipe. The pipelines are buried in sandy soil at depths of approximately 2.5 to 3 ft (0.75 to 0.91 m), and the operating pressure in the system is 40 psi (0.28 MPa). Most of the steel lines labeled in the figure were installed during the 1930's.

Since the Pacific Gas and Electric Company acquired the system in 1954, there have been no gas main repairs indicative of fault-induced damage. Visible bends in the mains have been observed by line foremen who work in the area. In addition, deformation of the 12-in (305 mm) diameter transmission line has been observed and recorded. The line, which was installed in 1930, is composed of continuous, welded steel and is buried at a depth of approximately 6 ft (1.8 m). In 1968, the line was excavated at its intersection with the

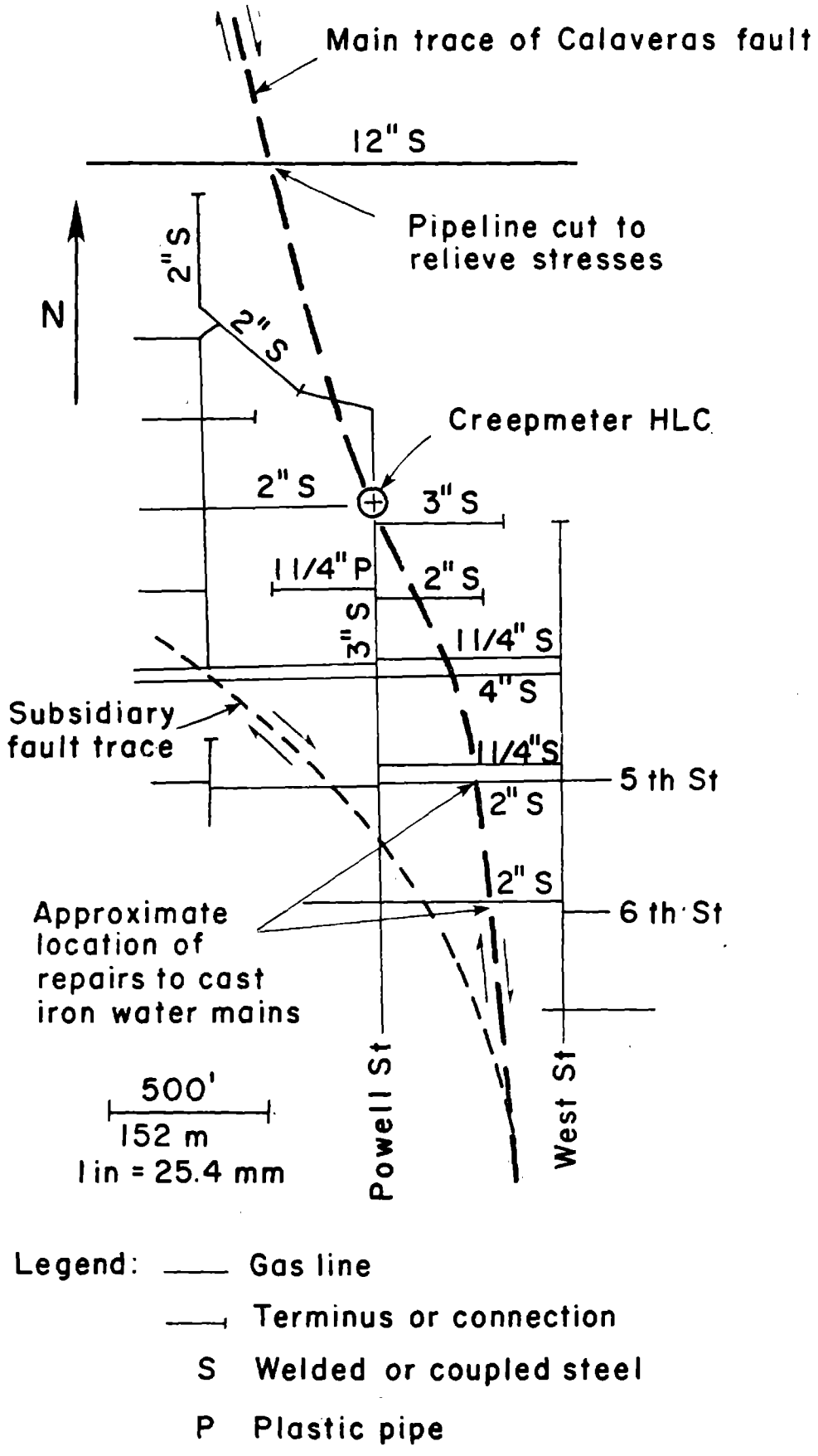

Figure B.3 Plan view of a portion of the gas distribution system in Hollister, CA, showing location of the Calaveras fault.

fault and cut to relieve the stress accumulated from fault creep since its installation. Upon cutting, the opposite ends of the line rebounded approximately 1 ft (0.3m). Since this time, the line has been instrumented and continuously monitored in the fault vicinity by the Pacific Gas and Electric Company (42).

There are no formal records of pipeline repair for the water distribution system in Hollister. Consequently, information on the deformation of water mains is limited to the field observations of city personnel who either supervised or conducted relatively recent repairs to the system. In 1976, couplings were replaced on two water mains in the vicinity of the fault. The approximate locations of the repairs are shown in the figure. Both lines are 4-in (102 mm) diameter cast iron mains, buried at a depth of approximately 3 ft (0.9m). Both lines contain lead-caulked, bell-and-spigot couplings. Although no leakage was noted at the time the lines were uncovered, severe rotation at the bell-and-spigot couplings was observed. At one location, for example, lead had been extruded from the coupling because of spigot rotation inside the bell.